Voltage-gated Na+ channels: Not just for conduction

by

Larisa Christine Kruger

A dissertation submitted in partial fulfillment
of the requirements for the degree of
Doctor of Philosophy
(Pharmacology)
in the University of Michigan
2016

Doctoral Committee:

Professor Lori L. Isom, Chair
Professor Miriam H. Meisler
Professor Jack M. Parent
Professor Leslie S. Satin

Table of Contents

List of Tables

List of Figures

Abstract:

Voltage-gated sodium channels (VGSCs), composed of a pore-forming α subunit and up to two associated β subunits, are critical for the initiation of the action potential in excitable tissues. VGSC β subunits, first cloned in 1992, modulate sodium current but also play non-conducting roles as cell adhesion molecules that allow them to function in the processes of neuronal migration, neurite outgrowth, pathfinding, and axonal fasciculation. Mutations in VGSC α and β genes are associated with diseases caused by dysfunction of excitable tissues such as epilepsy. *SCN1B-C121W*, the first epilepsy-associated sodium channel mutation identified, results in Genetic Epilepsy with Febrile Seizures plus (GEFS+). This mutation in *SCN1B*, which encodes the VGSC β1/β1B subunits, disrupts sodium current modulation and cell adhesive functions of β1 *in vitro*. The goal of my thesis research was to compare mice heterozygous for *Scn1b-C121W* (*Scn1b*$^{+/W}$) with mice heterozygous for the *Scn1b* null allele (*Scn1b*$^{+/-}$) to ask whether the C121W mutation results in loss-of-function *in vivo*. I found that *Scn1b*$^{+/W}$ mice were more susceptible than *Scn1b*$^{+/-}$ and *Scn1b*$^{+/+}$ mice to hyperthermia-induced seizures, a model for pediatric febrile seizures. Importantly, β1-C121W subunits are expressed at the neuronal cell surface *in vivo*. However, β1-C121W polypeptides are incompletely glycosylated and do not associate biochemically with VGSC α subunits. β1-C121W localization is restricted to the neuronal cell body in *Scn1b*$^{W/W}$ mice and is not detected at optic nerve nodes of Ranvier or axon initial segments in the cortex or cerebellum. These data, taken together with our previous results showing that β1-C121W cannot

participate in *trans* homophilic cell adhesion, lead to the hypothesis that *SCN1B-C121W* confers a deleterious gain-of-function. β1-C121W expression in brain may dilute the density of β1-WT subunits at the plasma membrane and thus effectively reduce the level of β1 functionality in neurons. In addition, β1-mediated *trans* homophilic cell-cell adhesion may be particularly disrupted in this mechanism, since WT-mutant or mutant-mutant β1 subunit pairs may be aligned, but not associated, in *trans* on adjacent axons, resulting in areas of aberrant adhesion and fasciculation.

Chapter 1. Voltage-gated Na+ channels: Not just for conduction

A version of this chapter up to the section on ”*SCN1B-C121W:* a GEFS+-associated VGSC mutation” has been accepted for publication by Cold Spring Harbor Protocols. Slight alterations have been added to make it more cohesive with the rest of the thesis.

Voltage-gated sodium channels (VGSCs) conduct inward current that depolarizes the plasma membrane and initiates the action potential (AP) in excitable cells, including neurons, cardiomyocytes, and skeletal muscle cells. Because of the intrinsic link between VGSCs and cellular excitability, it is not surprising that mutations in VGSC genes are linked with epilepsy, cardiac arrhythmia, neuropathic pain, migraine, and neuromuscular disorders (Table 1.1). The goal of this review is to provide an overview of critical discoveries in VGSC physiology and discuss the challenges of studying VGSCs in disease, including some of the exciting techniques to address these challenges. Finally, I will discuss what is known about a particular mutation in a VGSC gene and why we decided to do the studies presented in this thesis.

VGSC Discovery and Structure

In 1952, the Nobel Laureates Professor Alan Lloyd Hodgkin and Professor Andrew Fielding Huxley first recorded sodium current (I_{Na}) using their voltage-clamp technique on the squid giant axon. Their experiments showed three key features of I_{Na}: selective Na^+ conductance, voltage-dependent activation, and rapid inactivation (Hodgkin and

Huxley, 1952). The Hodgkin-Huxley model mathematically described voltage-dependent initiation of the AP by inward I_{Na}, followed by fast inactivation of I_{Na}, and simultaneous activation of outward I_K. Outward I_K was postulated to re-establish the charge balance across the plasma membrane (Hodgkin and Huxley, 1952). These results were supported by studies of peripheral motor neurons by Sir John Carew Eccles, who shared the Nobel Prize with Hodgkin and Huxley. Among other contributions, he identified deviations in membrane potential and APs due to injections of sodium into motor neurons (Coombs et al., 1955). In addition to this monumental discovery, refinement of the voltage-clamp technique opened the door for a plethora of research on membrane potential physiology.

In the 1960s, Dr. Bertil Hille and Dr. Clay Armstrong proposed the idea that I_{Na} and I_K are conducted through specific ion channels. At that time, many studies centered on performing voltage-clamp recordings of squid axon with sodium-free solutions containing organic cations (e.g. ammonium) to determine the size of the ion-conducting pore. The axon membrane became transiently permeable to these ions following depolarization, and this permeability was abolished by tetrodotoxin (TTX) (Larramendi et al., 1956; Lorente De No et al., 1957; Tasaki et al., 1965, 1966; Tasaki and Singer, 1966; Binstock and Lecar, 1969). Dr. Hille added to this body of work by using additional metal and many organic cations to develop a model of the narrowest region of the ion-conducting pore of the channel (Hille, 1971, 1972). Dr. Hille's model proposed a partial dehydration of Na^+ through interaction with a high-field-strength site at the extracellular end of the pore followed by rehydration in the lumen of the pore. This model is astonishingly close to what we now know to be true about VGSCs from crystal

Table 1.1 Tissue distribution and disease associations of VGSC genes

Gene symbol	**Type**	**Tissue distribution**	**Consequence of mutations**	**TTX sensitivity**
SCN1A	$Na_v1.1$	CNS, PNS, heart, DRG	DS, Familial Autism, FHM3, FS+, GEFS+, SUDEP	+
SCN2A	$Na_v1.2$	CNS, PNS, DRG	BFNIS, DS, EOEE, Familial Autism, GEFS, OS	+
SCN3A	$Na_v1.3$	CNS, PNS, heart, DRG	Unclear	+
SCN4A	$Na_v1.4$	Skeletal muscle, heart, DRG	PAM, PMC, HyperPP, HypoPP, SNEL	+
SCN5A	$Na_v1.5$	Skeletal muscle, heart, CNS, DRG	AF, AS, BS, DCM, LQTS, PCCD, SIDS, SSS, SUDEP	-
SCN8A	$Na_v1.6$	CNS, PNS, heart, DRG	EOEE; cognitive impairment, paralysis, ataxia, dystonia	+
SCN9A	$Na_v1.7$	DRG	CIP, IEM, PEPD, PPN	+
SCN10A	$Na_v1.8$	DRG	PPN	-
SCN11A	$Na_v1.9$	DRG	PPN	-
SCN1B	β1	CNS, PNS, heart, DRG, glia (oligodendrocytes, Schwann cells, astrocytes, radial glia)	AF, BS, DS, GEFS+, LQTS, PCCD, TLE	N/A
SCN2B	β2	CNS, PNS, heart, DRG	AF, BS	N/A
SCN3B	β3	CNS, PNS, heart, DRG	AF, BS, PCCD, SIDS, ventricular fibrillation	N/A
SCN4B	β4	CNS, PNS, heart, DRG	LQTS, SIDS	N/A
SCN1B	β1B	Fetal CNS, PNS, heart, DRG	BS, PCCD, epilepsy	N/A

AF, atrial fibrillation; AS, atrial standstill; BFNIS, benign familial neonatal-infantile seizures; BS, brugada syndrome; CIP, channelopathy-associated insensitivity to pain; CNS, central nervous system; DCM, dilated cardiomyopathy; DRG, dorsal root ganglia; DS, Dravet Syndrome; EOEE, early-onset epileptic encephalopathy; FHM3, familial hemiplegic migraine type 3; FS+, febrile seizures plus; GEFS+, genetic epilepsy with febrile seizures plus; HyperPP, hyperkalemic periodic paralysis, HypoPP, hypokalemic periodic paralysis; IEM, inherited erythromelaglia; LQTS, long QT syndrome; OS, Ohtahara syndrome; PAM, potassium-aggravated myotonia; PCCD, progressive cardiac conduction disease; PEPD, paroxysmal extreme pain disorder formally known as familial rectal pain syndrome; PMC, Paramyotonia congenital; PNS, peripheral nervous system; PPN, painful peripheral neuropathies; SIDS, sudden infant death syndrome; SNEL, severe neonatal episodic laryngospasm; SSS, sick sinus syndrome; SUDEP, sudden unexplained death in epilepsy; TLE, temporal lobe epilepsy

structure information (Payandeh et al., 2011; McCusker et al., 2012; Zhang et al., 2012). Dr. Armstrong and Dr. Francisco Bezanilla developed signal averaging techniques to detect the movement of ‘gating charges’ (Armstrong and Bezanilla, 1973, 1974) corresponding to what we now understand to be the movement of voltage sensors, which respond to changes in membrane potential. Remarkably, without having any of the knowledge that we possess today about nucleotide/amino acid sequence and crystal structures, these early studies made many accurate predictions about VGSC structure and the functions of various channel domains.

While early physiological studies provided evidence for the existence of a VGSC, the biochemical proof that tetrodotoxin/saxitoxin (STX) receptors were also ion-conducting did not yet exist. Membrane protein purification techniques were being established, but they required an extraordinarily large amount of time and biological starting material compared to today’s techniques. Photoaffinity labeling of STX receptors with a scorpion toxin derivative by Dr. William Catterall’s group identified a family of VGSC proteins that were designated α and β subunits (Beneski and Catterall, 1980). Purification of VGSC protein to theoretical homogeneity was challenging due to the difficulty of solubilizing a high molecular weight, highly lipophilic membrane protein and the large amount of biological starting material required. Again, the Catterall lab was the first to overcome these challenges and purify VGSCs from rat brain (Hartshorne and Catterall, 1981, 1984; Hartshorne et al., 1982). This work was closely followed by purification of VGSCs from rat and rabbit skeletal muscle (Barchi, 1983; Kraner et al., 1985), and from chicken heart (Lombet and Lazdunski, 1984). Reconstitution of purified VGSCs in a lipid bilayer membrane allowed observation of Na^+ flux and confirmed that a functional VGSC

protein had been purified (Hartshorne et al., 1985). The evolution of VGSC purification methods is discussed in detail in (Catterall, 1992). Purification from rat brain revealed that VGSCs are heterotrimers, composed of a single α subunit and two non-pore-forming β subunits, β1 and β2 (Hartshorne and Catterall, 1981). We now know that there are more than two VGSC β subunits. Subsequent homology cloning and heterologous expression studies showed that each VGSC α is associated at the plasma membrane with a non-covalently linked β1 or β3 subunit and a covalently linked β2 or β4 subunit (Morgan et al., 2000; Yu et al., 2003).

To clone the first VGSC α subunit cDNA, researchers from Dr. Shosaku Numa's group took on the arduous task of purifying brain VGSCs and obtaining partial amino acid sequence by N-terminal Edman degradation as well as through cleaved peptides from the α subunit. They then generated and screened multiple cDNA libraries based first on predicted degenerate cDNA sequences and then on cloned sequences. Assembly of the cloned VGSC cDNA fragments revealed what we now know to be *Scn1a* (Noda et al., 1984). Heterologous expression of the cloned cDNAs gave a functional channel, which we now recognize as $Na_v1.1$.

VGSC β subunits are required to recapitulate physiological expression of I_{Na} in Xenopus oocytes

Early cloning of $Na_v1.2$ cDNA and its expression in oocytes resulted in I_{Na} that inactivated more slowly than I_{Na} recorded from neurons. Co-injection of low-molecular weight rat brain mRNA was required for recapitulation of physiological I_{Na} in terms of rates of activation and inactivation, and voltage dependence (Auld et al., 1988; Krafte,

1990). Cloning and expression of the VGSC β1 and β2 subunits showed that they mimicked the effects of low molecular weight mRNA on α subunit expression in oocytes (Isom et al., 1992, 1995b). Co-expression of $Na_v1.2$ + β1 in oocytes resulted in a larger I_{Na} that activated and inactivated more rapidly and had a negative shift in the voltage-dependence of inactivation compared to α alone. Co-expression of $Na_v1.2$ with both β1 and β2 further increased I_{Na} density (Isom et al., 1995b). As discussed by Calhoun and Isom, when expressed in heterologous systems, β subunits in general increase I_{Na} density, shift the voltage-dependence of current activation and inactivation, and accelerate the rates of activation and inactivation. However, the magnitude of current increase and direction of the shifts in activation and inactivation are dependent upon the particular heterologous cell line and the identities of the β and α cDNAs expressed (Calhoun and Isom, 2014). Importantly, heterologous expression systems cannot replicate the native cellular milieu, especially the multi-protein VGSC complexes that are known to form in specific subcellular domains of neurons and cardiac myocytes (Calhoun and Isom, 2014). For example, in *Scn1b null* ventricular myocytes, peak and persistent sodium current is increased, mediated by increased $Na_v1.5$ expression, with no effect on channel kinetics and voltage dependence (Lopez-Santiago et al., 2007). Furthermore, loss of *Scn1b* also results in increased TTX-S current and *Scn3a* expression in ventricular myocytes (Lin et al., 2015). However, in the dorsal root ganglia, critical neurons for peripheral pain sensation, *Scn1b* deletion causes a depolarizing shift in the voltage dependence of VGSC inactivation and *decreased* persistent I_{Na+} (Lopez-Santiago et al., 2011). As heterologous expression systems

cannot accurately replicate these cell types, *in vivo* and transgenic mouse models offer more appropriate methods for studying the functional roles of VGSC subunits.

Mechanistic Insights on VGSC Structure and Function

VGSC α subunits are highly evolutionarily conserved. Each α subunit is composed of 4 homologous domains, each containing six transmembrane helices (S1-S6), which come together in pseudo-tetrafold symmetry to form the ion-conducting pore (Figure 1.1). As discussed earlier, long before the emergence of crystal structures, much of VGSC structure and function was inferred through studies modeling gating and using site-specific antibodies and toxins during electrophysiological recordings.

The sliding-helix model of VGSC voltage-dependent activation was proposed in the 1980's by Dr. Catterall (Catterall, 1986a,b). The S4 segments of each domain, which serve as voltage sensors, contain arginine residues at every third position, which pair with negatively charged residues in nearby transmembrane segments. Upon membrane depolarization, these residues change ion-pair partners, causing each S4 helix to rotate or slide outward, pushing a single arginine residue in each of the four segments out, and generating gating current that activates, or opens, the channel pore (Payandeh et al., 2011). Data from potassium channel structures prompted the paddle model as an alternate mechanism of voltage-dependent activation (Jiang et al., 2003), however, the solving of multiple prokaryotic α subunit crystal structures demonstrated the validity of the sliding helix model for VGSCs (Payandeh et al., 2011; Vargas et al., 2012).

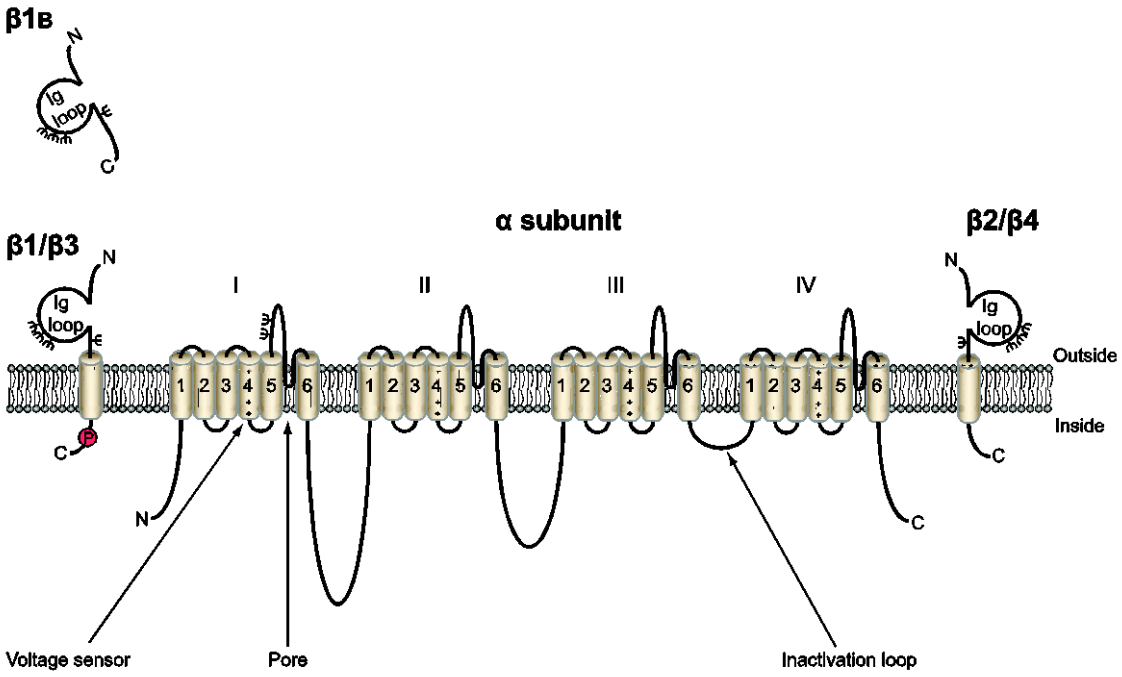

Figure 1.1 VGSC α and β subunit topology.

The pore-forming α subunit is composed of four homologous domains (I-IV), each with six transmembrane segments. The fourth segment in each domain contains the voltage-sensing domain of the channel. The inactivation loop between domains III and IV contains the IFM domain required for channel inactivation. Up to two β subunits may be associated with VGSCs. β1 and β3 subunits associate non-covalently, while β2 and β4 subunits associate via a disulfide link. *Reprinted with permission from Brackenbury and Isom, 2011, copyright Frontiers Media SD*

Another critical property of VGSCs is voltage-dependent inactivation, which occurs in spite of an on-going depolarizing pulse. Early studies identified the intracellular loop between domains III and IV as the inactivation gate (Figure 1.1). This was proposed to "swing" into the pore in a voltage-dependent manner, physically blocking ion conduction, and effectively inactivating the pore (Vassilev et al., 1988, 1989). A short amino acid sequence in the inactivation gate, IFM, was identified as critical to the process of inactivation. Mutation of these three residues to glutamine resulted in a non-inactivating channel (West et al., 1992; Kellenberger, 1997). These studies, combined with a three-dimensional NMR structure of the inactivation gate (Rohl et al., 1999), helped form the current understanding of the molecular basis for fast inactivation of VGSCs.

Recent crystal structures of bacterial VGSCs have led to a more detailed understanding of the pore and selectivity filter. The membrane re-entrant P-loop, located between transmembrane helices S5 and S6 of each domain that line the pore, was identified as the target for the pore-blocking TTX, suggesting its close location to the pore (Noda et al., 1989; Terlau et al., 1991). The crystal structure of a bacterial VGSC showed that the 4 P-loops together form a ring of glutamates, located near the extracellular end of the pore (Payandeh et al., 2011). As predicted in 1992, these highly-conserved glutamates form a high-field-strength site critical in determining ion selectivity of the channel (Heinemann et al., 1992). These residues stabilize multiple ionic occupancy states, preferentially conducting hydrated Na^+ through the pore (Payandeh et al., 2011). In contrast, potassium channels conduct dehydrated K^+ (Doyle et al., 1998).

Capturing crystal structures of bacterial VGSCs in different activation states has provided new insights and biochemical modeling tools. A closed-pore conformation of the *Arcobacter* channel (Na_vAb), crystallized within a lipid-based bicelle, offered the first VGSC 3D structure (Payandeh et al., 2011). A putatively inactive Na_vRh channel from the marine bacterium *Rickettsiales* showed significant differences from Na_vAb and supplied new information about conformational rearrangements required for inactivation (Zhang et al., 2012). Finally, the apparently open conformation of the Na_vM structure from the marine bacterium *Magnetococcus* presented further insights into channel gating and selectivity (McCusker et al., 2012).

Despite the wealth of information provided by these prokaryotic VGSC structures, crystallization of a eukaryotic VGSC is the essential next step. While prokaryotic VGSCs are homotetramers, mammalian VGSC α subunits are single polypeptides containing 4 non-identical domains. Further, the extensive extracellular and intracellular loops of mammalian channels are not present in their prokaryotic orthologs. Thus, major gaps in the field include the crystal structure of a mammalian α subunit and the co-crystal structure of an α subunit associated with β subunits. This information will be critical in fully understanding mammalian VGSC structure.

VGSC Diversity

Originally, VGSC α subunit proteins were named according to the tissue from which they were purified. For example, brain type II, rat II, and R-II are all outdated terms for $Na_v1.2$ (Catterall et al., 2005). To date, nine VGSC α proteins ($Na_v1.1$-1.9) and five β

proteins (β1-4 and β1B), encoded by *SCN(X)A* and *SCN1B-SCN4B* genes, respectively, have been identified in mammalian genomes.

A BLAST search of the cDNAs encoding β1 and β2 in 1995 revealed important, and unexpected, new information. Both proteins contained areas of homology to known cell adhesion molecules (CAMs) of the immunoglobulin (Ig) superfamily, e.g. contactin and myelin P0. This led to the hypothesis that β1 and β2 function as CAMs in addition to channel modulators (Isom et al., 1995b). We now know that all five β subunit proteins contain an extracellular Ig domain and have CAM function, as discussed later in this review. β1-4 (encoded by *SCN1B-SCN4B*) are type 1 transmembrane proteins with an extracellular N-terminus (containing the Ig domain) and an intracellular C-terminus (Isom et al., 1992, 1995b; Morgan et al., 2000). By contrast β1B, a splice variant of *SCN1B*, is secreted. Retention of intron 3 results in generation of an alternate C-terminal domain that does not contain a transmembrane region (Patino et al., 2011). Recently, the three-dimensional crystal structures of the human Ig domains of β3 and β4 were solved. β3 formed a trimer when crystalized (Namadurai et al., 2014). In contrast, the β4 Ig domain was monomeric in crystal form (Gilchrist et al., 2013). While this could represent a physiological difference in homophilic interactions, it could also be due to removal of 31 amino acids at the β4 N-terminus to facilitate crystallization (Gilchrist et al., 2013). Comparisons of these structures will give new insights into the function of β subunits, but the co-crystal structure of α and β subunits remains the next frontier.

VGSC α- and β-subunits are highly expressed in central and peripheral neurons, cardiac myocytes, skeletal muscle, and some non-excitable cells (Maier et al., 2004; Patino and Isom, 2010; Brunklaus et al., 2014), including breast cancer cells (Fraser et al., 2005), astrocytes, and oligodendrocytes. Adapted from (Patino and Isom, 2010; Catterall, 2012; Brunklaus et al., 2014), Table 1.1 shows the gene name, known tissue expression, and diseases associated with mutations for each VGSC subunit. VGSC expression is developmentally regulated. For example, $Na_v1.3$, β3, and β1B are most prevalent in embryonic and neonatal rodent brain. This expression profile then changes such that $Na_v1.1$, $Na_v1.2$, $Na_v1.6$, β1, β2, and β4 are predominant in the adult brain, albeit distribution is not equivalent across brain regions (Kazen-Gillespie et al., 2000; Catterall et al., 2005; Patino et al., 2011).

VGSC subcellular localization is critical for normal physiological functions. In neurons, VGSCs are concentrated at the axon initial segment (AIS), where the AP is initiated, and nodes of Ranvier in myelinated axons, which are critical for saltatory conduction. In cardiomyocytes, VGSCs are differentially localized at intercalated disks and transverse tubules. Reviews that discuss this in more detail include (Bao and Isom, 2014; Calhoun and Isom, 2014).

Despite their high sequence similarity, each VGSC α subunit has subtle differences in biophysical properties and pharmacological sensitivities, as summarized in (Catterall et al., 2005; Kwong and Carr, 2015). Many of the agents that target α subunits are toxins, including TTX, STX, μ-conotoxins, and their derivatives such as 4,9-anhydro-TTX which

preferentially blocks $Na_v1.6$ (Rosker et al., 2007; Kwong and Carr, 2015). VGSCs are canonically separated into TTX-sensitive (TTX-S) and TTX-resistant categories (TTX-R), which are blocked by nanomolar or micromolar concentrations of TTX, respectively (Catterall et al., 2005). Interestingly, mutation of a single residue changes TTX sensitivity (Noda et al., 1989). Modulation of I_{Na} by these toxins [reviewed by (Gilchrist et al., 2014)] can be affected by β subunit expression. For example, expression of β1 and β3, but not β2 or β4, tend to increase the rate of association and binding affinity of μ-conotoxins for VGSCs. However, modulation of I_{Na} by STX or TTX was unaffected by β subunit expression (Isom et al., 1995a; Zhang et al., 2013). *In vivo,* a combination of electrophysiology and toxicology are used to infer which VGSCs contribute to aspects of endogenous I_{Na}. Although challenging, *in vivo* studies are crucial, as heterologous results can be difficult to translate to *in vivo* physiological and pathophysiological mechanisms.

Postranslational Modifications of α and β subunits

VGSC α subunits are heavily glycosylated, although the extent of glycosylation varies between subunits (Bennett, 2002). 40-50% of these added carbohydrate residues are sialic acid moieties such that each channel contains approximately100 sialic acid residues (Miller et al., 1983; Roberts and Barchi, 1987). Differential glycosylation of VGSC subunits can affect channel gating, putatively due to the local negative charge of sialic acid residues. In general, when α subunits are less glycosylated, channel gating occurs at more depolarized voltages (Recio-Pinto et al., 1990; Bennett et al., 1997; Zhang et al., 1999; Tyrrell et al., 2001). For example, $Na_v1.9$ expressed in neonatal

dorsal root ganglia (DRG) neurons is more glycosylated than in adult DRG, suggesting developmental regulation of glycosylation. This may account for developmental differences in gating of persistent I_{Na} attributed to $Na_v1.9$ (Tyrrell et al., 2001). Voltage-dependent activation and inactivation of $Na_v1.4$, but not $Na_v1.5$, shifts when expressed in cells incapable of sialylation, indicating not all VGSCs are affected equally (Bennett, 2002). Glycosylation accounts for about one-third of the molecular weights of β subunits. Mature β subunits contain three to four N-linked glycosylation sites in the Ig domain (Isom et al., 1992; McCormick et al., 1998) all of which are exposed in the β3 crystal structure (Namadurai et al., 2014). Sialic acid residues in these sites affect β1- and β2-mediated modulation of I_{Na} and channel surface expression (Johnson et al., 2004; Johnson and Bennett, 2006). Critically, VGSC glycosylation varies developmentally and between cell types; e.g., neonatal and adult myocytes have distinct differences in glycogen expression, as do atrial and ventricular myocytes (Stocker and Bennett, 2006). Therefore, tissue-specific variations in β subunit processing likely include altered sialylation/glycosylation and may contribute to differential modulation of I_{Na} by β subunits between cell types (Zhang et al., 1999; Bennett, 2002).

β1 can be phosphorylated on intracellular tyrosine residue (Y) 181 (Malhotra et al., 2002, 2004). Tyrosine phosphorylation regulates β1-mediated recruitment of ankyrin to points of cell-cell contact (Malhotra et al., 2002) and likely occurs via fyn kinase, a src family kinase (Brackenbury et al., 2008; Nelson et al., 2014). Receptor tyrosine phosphatase β interacts with the intracellular domain of β1 and may modulate β1 phosphorylation (Ratcliffe et al., 2000). In cardiac myocytes, non-phosphorylated β1

localizes at the t-tubules with ankyrinB while phosphorylated β1 localizes at intercalated disks with connexin-43, N-cadherin, and $Na_v1.5$ (Malhotra et al., 2004). Therefore, the phosphorylation state Y-181 regulates β1 association with cytoskeletal proteins, as well as its subcellular localization.

β subunits are substrates for sequential proteolytic cleavage by BACE1 (β-secretase) and γ-secretase, similar to amyloid precursor protein. BACE1 cleavage releases the extracellular domain (ECD), followed by a γ-secretase-mediated cleavage event to release the C-terminal fragment (CTF) (Wong et al., 2005). These cleaved peptides may have important physiological functions. For example, the β2-CTF translocates to the nucleus and promotes *Scn1a* mRNA and protein expression when heterologously expressed in cultured neurons (Kim et al., 2005, 2007). Consistent with this proposed mechanism, total and surface expression of $Na_v1.1$ in acutely dissociated hippocampal neurons is significantly reduced in BACE1 null mice compared to wildtype (Kim et al., 2011). The physiological importance of BACE1 and γ-secretase cleavage of the other β subunits is not understood. As β1B can act as a CAM, it is possible that the β1-ECD, which contains the identical Ig loop domain, functions as a ligand for cell adhesion (Patino et al., 2011). γ-secretase activity, and thus formation of the β1-CTF, is critical for β1-mediated neurite outgrowth *in vitro* (Brackenbury and Isom, 2011). Determining whether these functions occur *in vivo* represents a critical next step in our understanding of post-translational processing of VGSCs.

β subunits are multifunctional

Effects on surface expression

Co-expression of β subunits with α results in increased I_{Na} density, in part due to promotion of α cell surface expression. Following post-translational processing, α subunits are stored in an intracellular pool associated with the plasma membrane (Schmidt et al., 1985; Schmidt and Catterall, 1986). Concomitant with plasma membrane insertion, α and β2 covalently associate via a disulfide bond (Chen et al., 2012). *Scn2b* null mice on the C57BL/6 x 129SV background have a 50% reduction in hippocampal I_{Na} density and level of surface α subunits (Chen et al., 2002). However, a second study of *Scn2b* null mice congenic on the C57BL/6 background saw no change in hippocampal I_{Na} (Uebachs et al., 2010), suggesting genetic background influences on β2 function. The effect of β2 on channel surface expression may also depend on the particular α subunit. *Scn2b* null small-fast DRG neurons have reduced TTX-S I_{Na}, but unchanged TTX-R I_{Na} (Lopez-Santiago et al., 2006). A *Scn2b*-linked Brugada syndrome mutation results in decreased surface $Na_v1.5$ protein compared to WT (Riuró et al., 2013). Thus, modulation of α subunit surface expression by β2 may contribute to disease mechanisms. This is not unique to β2; β1 and β1B also promote VGSC surface expression [reviewed in (Calhoun and Isom, 2014)].

Effects of β4 on resurgent INa

Resurgent I_{Na} is the transient opening of VGSCs during recovery from inactivation following the AP. This specialized current is an important adaptation for high-frequency firing neurons, such as cerebellar Purkinje neurons (Raman and Bean, 1997). For this

to occur, a 'blocking protein,' putatively the ICD of β4, must bind to open channels during depolarization and unbind upon repolarization, shortening the typical refractory period and producing a resurgent I_{Na}. Without β4 expression, resurgent current is lost from cerebellar Purkinje neurons, but is rescued by a β4 ICD peptide (Grieco et al., 2005). This same β4 peptide is sufficient to invoke resurgent I_{Na} in $Na_v1.7$-expressing HEK cells (Theile and Cummins, 2011). With β4 knockdown in cerebellar granule neurons, resurgent I_{Na} is decreased, but is rescued by the β4 peptide (Bant and Raman, 2010). Other β subunits may also contribute to modulation of resurgent I_{Na}, as *Scn1b* null cerebellar granule neurons have reduced resurgent I_{Na} (Brackenbury et al., 2010).

Cell adhesion and neurite outgrowth

β subunits are multifunctional. They play critical roles in neurite outgrowth, migration, and maintenance of nodes of Ranvier. β subunits are CAMs and, as such, recruit other signaling proteins to the VGSC complex. Most is known about the CAM interactions of β1 and β2, which participate in *trans*-homophilic adhesion, via the Ig loop, with β1 or β2 molecules on adjacent cells (Malhotra et al., 2000). β1 or β2 *trans*-homophilic adhesion recruits the cytoskeletal protein ankyrin to points of cell-cell contact (Malhotra et al., 2000). Ankyrin recruitment is abolished by phosphorylation of β1-Y181 (Malhotra et al., 2002). β1-β1 *trans*-homophilic adhesion promotes neurite outgrowth via a pathway requiring fyn kinase, the CAM contactin, γ-secretase activity, and localized I_{Na} (Brackenbury et al., 2008, 2010; Brackenbury and Isom, 2011). Because β1B contains the identical Ig loop, it similarly promotes neurite outgrowth of neurons expressing β1 (Patino et al., 2011). Together, these properties may contribute to neuronal

development *in vivo*; *Scn1b* null mice have neuronal pathfinding dysfunction and differences in subcellular localization of α subunits at axon initial segments (Chen et al., 2004; Brackenbury et al., 2008).

β1, and likely β1B, interacts with other CAMs and extracellular matrix proteins, including contactin, neurofascin-186, NrCAM, N-cadherin, and tenascin-R (Ratcliffe et al., 2001; Kazarinova-Noyes et al., 2001; Malhotra et al., 2004; McEwen and Isom, 2004; Patino et al., 2011). Some of these interactions affect β1-modulation of α surface expression. For instance, coexpression of NF186 or contactin with $Na_v1.2$ and β1 increases $Na_v1.2$ surface expression compared to $Na_v1.2$ and β1 alone, although NF186 and contactin have no impact on $Na_v1.2$ expression in the absence of β1 (Kazarinova-Noyes et al., 2001; McEwen and Isom, 2004). Heterophilic interactions with tenascin-R, an extracellular matrix protein secreted by oligodendrocytes during myelination, repels cells expressing β1 or β2 and therefore may play a role in restricting VGSCs to nodes of Ranvier in myelinated axons (Xiao et al., 1999). The cell adhesive properties of β1 and β1B have likely clinical relevance, as most known *SCN1B* epilepsy mutations are located in or near the Ig loop domain [reviewed in (O'Malley and Isom, 2015)].

Much less is known about the CAM functions of β3 and β4. Studies of β3 homophilic adhesion give conflicting results: the β3 Ig domain appears to interact with full-length β3 when expressed heterologously (Yereddi et al., 2013), yet another group reported that β3 expression could not induce aggregation of *Drosophila* S2 cells, unlike β1 and β2 (McEwen et al., 2009). β3 and β1 likely do not associate, as β3 does not interact with a

peptide containing the β1-ECD (McEwen and Isom, 2004). β4 did not promote neurite outgrowth of cerebellar granule neurons, but this observation does not preclude other CAM interactions (Davis et al., 2004).

Pathophysiological Roles of VGSCs

Mutations in VGSC genes are associated with many types of genetic epilepsy, peripheral neuropathy, long QT syndrome, neuromuscular disorders, and other diseases associated with dysfunction of excitable tissues. Recent reviews discuss the complex pathophysiological mechanisms of sodium channelopathies associated with pain and cardiac disease (Dib-Hajj et al., 2010; Adsit et al., 2013; Bao and Isom, 2014; O'Malley and Isom, 2015). Here, we will focus on the role of VGSCs in the genetic epilepsies and cancer as examples of disease resulting from aberrant or loss of VGSC function in mammals.

Epilepsy

Epilepsy results from an imbalance between excitation and inhibition in the brain. Over 2 million Americans have epilepsy, which can be caused by genetic mutations or brain injury (Hirtz et al., 2007). Epilepsy significantly impacts the quality of life for both patients and caregivers due to the unpredictability of seizures and the risk of co-morbidities including cognitive decline, intellectual disability, developmental delay, and Sudden Unexpected Death in Epilepsy (SUDEP).

Mutations in genes encoding VGSC α and β subunits are associated with epilepsies with a wide range of phenotypic severities, including genetic epilepsy with febrile

seizures plus (GEFS+), an inherited epilepsy with a wide range of phenotypes, and Dravet Syndrome (DS), one of the most devastating pediatric epileptic encephalopathies. An intriguing discussion of the complex mechanisms underlying DS was published recently (Chopra and Isom, 2014). In 1998, the first VGSC mutation associated with epilepsy was identified in *SCN1B* in a patient with GEFS+. This initial mutation, *SCN1B-C121W,* is the focus of this thesis and is discussed in further detail later. However, GEFS+ is incompletely penetrant and family members with the same *SCN1B* mutation presented with a wide range of epilepsy severities (Wallace et al., 1998), a now familiar characteristic of the genetic epilepsies. Since this initial discovery, a large number of mutations in *SCN1A, SCN2A, SCN8A*, and *SCN1B* (Escayg et al., 2000; O'Malley and Isom, 2015) have been implicated in multiple types of epilepsy (see Table 1.1, reviewed in part by (Shi et al., 2012; Steinlein, 2014; Wagnon and Meisler, 2015)). Over 1200 mutations have been identified in *SCN1A* alone (Meng et al., 2015). Identifying the pathophysiological mechanisms underlying DS is of particular importance, as traditional antiepileptic drugs (AEDs) often aggravate seizures in DS patients and development of new therapeutics to help these patients is especially critical. While 70-80% of DS patients have an identified heterozygous *de novo SCN1A* mutation (Marini et al., 2011), homozygous mutations in *SCN1B* have been also been reported (Patino et al., 2009; Ogiwara et al., 2012).

Studies of DS *SCN1A* mutations have shown that a majority result in loss-of-function (Meng et al., 2015). Studies of *Scn1a+/-* null mice and knockin mice expressing human mutations have led to the "interneuron hypothesis," suggesting that selective I_{Na} loss in GABAergic interneurons causes epilepsy via loss of inhibitory tone (Yu et al., 2006).

However, this has become controversial (Chopra and Isom, 2014; Isom, 2014). More recent studies of DS patient derived induced pluripotent stem cell (iPSC) neurons showed either that both inhibitory and excitatory (Liu et al., 2013) or excitatory neurons (Jiao et al., 2013) are hyperexcitable compared to non-epileptic controls. These studies suggest that *SCN1A* haploinsufficiency may result in compensatory upregulation of other VGSC α subunits. Adding further complexity, *Scn1a*$^{+/-}$ mice show strain-dependent seizure severity and survival. On the 129S6/SvEvTac background, *Scn1a*$^{+/-}$ mice have a mild phenotype and normal survival. In contrast, *Scn1a*$^{+/-}$ F1 generation C57BL/6J x 129 mice have severe epilepsy and premature lethality (Mistry et al., 2014). Acutely dissociated hippocampal GABAergic interneurons from F1.*Scn1a*$^{+/-}$ mice showed decreased I_{Na} compared to 129.*Scn1a*$^{+/-}$ and wild-type mice. However both 129.*Scn1a*$^{+/-}$ and F1.*Scn1a*$^{+/-}$ mice showed increased I_{Na} in hippocampal pyramidal neurons (Mistry et al., 2014). It is postulated that 129.*Scn1a*$^{+/-}$ mice may have a milder phenotype due to preservation of GABAergic interneuron excitability. Hyperexcitability of both inhibitory and excitatory neurons may lead to seizures in DS via increased network excitability or synchronization of firing.

Scn1b null mice also model DS; they experience spontaneous seizures and early lethality. At least one DS *SCN1B* mutation causes β1 to be retained intracellularly, preventing surface expression and thus function (Patino et al., 2009). *Scn1b* null mice have differences in neuronal pathfinding that are observed prior to seizure onset (Brackenbury et al., 2013). Thus, *SCN1B*-liked DS mutations may alter neuronal excitability by affecting α-subunit surface expression/function as well as by altering neuronal development via changes in cell adhesion.

A major concern for epilepsy patients and their families is the risk of SUDEP. Research suggests that a “perfect storm” of seizures, cardiac arrhythmias, respiratory dysfunction, or autonomic dysfunction contributes to SUDEP (Kalume, 2013; Massey et al., 2014)(Auerbach et al., 2013). Heterozygous *Scn1a-R1407X* knock-in GEFS+/DS mice, as well as *Scn1b* null DS mice, have increased transient and persistent I_{Na} in cardiac myocytes, which may provide substrates for cardiac arrhythmias and contribute to SUDEP (Lopez-Santiago et al., 2007; Auerbach et al., 2013). Fully understanding the mechanisms underlying SUDEP will be essential to epilepsy treatment.

One of the greatest challenges in epilepsy research is the need for novel AEDs. Even with optimal treatment, 20-30% of all epilepsy patients are pharmacoresistant, defined as being unresponsive to at least two different, tolerated AEDs (Kwan et al., 2010, 2011). Even in non-refractory patients, AEDs treat disease symptoms rather than preventing disease progression and often have intolerable side effects. A major goal of studying epilepsy-associated VGSC mutations is to further understand epileptogenesis (how a brain becomes epileptic) to inform new AED discovery.

Emerging roles for VGSCs in cancer

An exciting area of research is the role of VGSCs in non-excitable cells, including multiple cancer cell types. Almost two decades ago, researchers observed that cancer cell lines with higher VGSC expression have increased cell motility and metastatic potential. Furthermore, the invasive capacity of these cells could be reduced by incubation with TTX (Grimes et al., 1995; Laniado et al., 1997). Since then, both α and β subunits have been detected in many cancer cell lines and in some patient biopsies.

VGSC α subunits are expressed in some cervical, ovarian, breast, and colon tumors *in vivo* (Fraser et al., 2005; House et al., 2010; Gao et al., 2010; Hernandez-Plata et al., 2012), while, some prostate, breast, cervical, and lung cancers express β subunits [reviewed in (Patel and Brackenbury, 2015)]. Studies have identified both positive and negative associations between VGSC expression and metastatic potential. $Na_V1.5$ expression in breast cancer cells correlates positively with increased risk of recurrence and metastasis (Fraser et al., 2005; Yang et al., 2012), and a similar trend has been described for colon, prostate, and ovarian cancers. However, there is an inverse correlation between α expression and clinical grade in glioma and no correlation in lung cancer cell lines (Schrey et al., 2002; Onganer and Djamgoz, 2005; Roger et al., 2007). Expression of α subunits can potentiate lateral motility, adhesion, process extension, and other cellular behaviors associated with metastasis (Brackenbury, 2012). It is not clear how increased expression of the pore-forming α subunits potentiates invasive changes in the tumor cells. Three potential models have been proposed: increased Na+ influx enhances H+ efflux thus activating pH-dependent extracellular matrix degradation and invasion; regulation of an “invasion gene network,” particularly by *SCN5A*; and increased intracellular Ca2+ which enhances formation of invasive projections [reviewed in (Brackenbury, 2012)].

SCN1B and *SCN2B* expression are associated with metastatic potential in prostate cancer cells (Diss et al., 2008; Jansson et al., 2012). However, studies of the invasive potential of *SCN1B*-expressing breast cancer *in vitro* have been contradicted by *in vivo* studies. β1 expression is associated with less invasive breast cancer cell lines (Chioni

et al., 2009), however, in a mouse model of breast cancer, overexpression of β1 increased tumor growth, metastasis, and angiogenesis (Nelson et al., 2014). β1 *trans*-homophilic adhesion mediates process outgrowth from breast cancer cells (Nelson et al., 2014), thus it is proposed that β1 promotes metastasis by a mechanism similar to β1-mediated neurite outgrowth.

New frontiers and novel techniques

The list of pathogenic VGSC gene mutations is growing rapidly. The explosion of whole genome sequencing has led to multi-institution efforts such as the NINDS funded Epi4K Project (www.epi4k.org), with the goal of sequencing the genomes of 4000 patients with epilepsy, and the England Department of Health funded 100,000 Genomes Project (http://www.genomicsengland.co.uk/) (Kearney, 2014; Siva, 2015). However even with familial genetic information in hand, determining whether mutations are causative and understanding their pathophysiology are not simple tasks. A given patient can have mutations in several genes, which may be causative, benign, or modify another mutation. A single causative mutation may result in a wide range of phenotypes among individuals, for example, DS and GEFS+ patients may express the same *SCN1A* or *SCN1B* mutation. Genetic background is critical. *Scn1a+/-* mouse models of DS have phenotypes of varying severity depending on genetic background (Yu et al., 2006; Miller et al., 2014). This issue can now be addressed directly with the induced-pluripotent stem cell (iPSC) technique. Patient iPSCs, usually derived from a skin cell biopsy, can theoretically be differentiated into any cell type, including cardiomyocytes, and specific neuronal subtypes (Parent and Anderson, 2015). With this remarkable technique, we

now have the opportunity to study disease-causing mutations in human cells within the context of the patient's unique genomic background (Takahashi et al., 2007). Furthermore, endogenous genes that may contribute to pathology remain present. Brain organoids made from human iPSC-derived cells with a mutation in a gene involved in pluripotent cell maintenance were used to model microcephaly, providing proof-of concept for use of organoids to model other neurological diseases (Lancaster et al., 2013). Another advantage of iPSCs is the opportunity to perform drug screening on differentiated human cells, alongside animal models, thus providing insight into toxicity and species-specific effects prior to clinical trials [reviewed in (Ko and Gelb, 2014)]. Patient-derived iPSC cells are critical for precision medicine approaches. For instance, AED effectiveness or toxicity may be optimized on patient-derived iPSC-neurons prior to patient treatment. As the iPSC technique is further refined and developed, it will provide additional, critical tools in therapeutic development.

Another challenge to the field is the non-specificity of clinically available VGSC-targeted drugs. There are 6 different potential sites for small molecule targeting on VGSCs, as demonstrated by the wide variety of toxin binding sites. However, most of the current anti-arrhythmic, anti-epileptic, and analgesic VGSC drugs on the market, e.g. lamotrigine, phenytoin, and lidocaine, target the 'local anesthetic' site located in domain IVS6 (Kwong and Carr, 2015). This site is highly conserved between α subunits, thus these drugs have little selectivity for specific VGSCs and often cause adverse effects. Development of VGSC agents that target other binding sites remains an important task. While, in most cases, toxins cannot be used directly for therapeutics, they can greatly inform drug design; small molecules can be developed that preserve beneficial effects

while reducing harm. Drugs targeting specific toxin binding sites may allow more selective blockade of specific α subunits to treat disease such as neuropathic pain, cardiac arrhythmias, epilepsies, and perhaps even cancer (Stevens et al., 2011; Xiao et al., 2014).

Transgenic zebrafish are an economical and rapid vertebrate system that can be used to screen small molecule libraries and FDA-approved drugs for novel applications. Zebrafish with mutations in *scn1Lab,* the gene orthologous to *SCN1A*, have spontaneous seizures that are resistant to many AEDs and appear to model DS. Dr. Peter de Witte's group showed DS zebrafish responded to fenfluramine (Zhang et al., 2015). Dr. Scott Baraban used locomotion tracking in mutant zebrafish to monitor behavioral seizures in a drug screen, which was validated using diazepam, valproate, and stiripentol, AEDs effective in some DS patients. Out of 320 compounds tested, clemizole, an FDA-approved antihistamine, suppressed spontaneous seizures *in vivo* (Baraban et al., 2013). This approach can be adapted for screening potential therapeutics for any monogenic epilepsy, especially if combined with the CRISPR/Cas9 technique. Discovered in 2010 as a bacterial defense mechanism against phages (Deveau et al., 2010), the CRISPR/Cas9 system has since been adapted to easily and quickly introduce heritable genetic mutations in mice, rats, zebrafish, and rabbits (Li et al., 2013; Chang et al., 2013; Yang et al., 2014a). Compared to zinc-finger nucleases and transcription activator-like effector nucleases (TALENs), CRISPR/Cas creates double-stranded DNA breaks in a sequence-specific manner at sites complementary to a 'single-guide RNA.' Because these are easy to design, the CRISPR/Cas9 system vastly improves the precision, speed, and accuracy of creating transgenic cell lines

(including iPSCs) and animal models for single gene mutations (Yang et al., 2014b). These and other cutting edge techniques will allow us to discover novel disease mechanisms and therapeutics for diseases linked to VGSC mutations for another six decades (Catterall, 2012).

SCN1B-C121W: a GEFS+-associated VGSC mutation

Prevalence of SCN1B-C121W

The first VGSC gene mutation associated with epilepsy was a heterozygous *SCN1B-C121W* mutation, associated with the mild epilepsy syndrome GEFS+ (Wallace et al., 1998; Scheffer et al., 2007). This cysteine to tryptophan mutation at residue 122, encoded by c.363C>G (alternatively labeled as c.387C>G if the signal sequence is included) has been reported by six studies to date (Table 1.2)(Wallace et al., 1998, 2002; Haider et al., 2005; Scheffer et al., 2007; Dibbens et al., 2010; Carvill et al., 2014). A majority of these studies report the presence of the mutation in Australian families with hereditary epilepsy. One study looking at 123 unrelated patients with idiopathic generalized epilepsies in Kuwait found three of these individuals carried c.363C>G in *SCN1B*. These patients also experienced febrile seizures (Haider et al., 2005)[1]. In total, 54 individuals with *SCN1B-C121W* have been reported, 9 of which were unaffected carriers. The remaining patients have a spectrum of heterogeneous epilepsy phenotypes (Table 1.2). Many of these patients have febrile seizures and other milder

[1] This study concluded that this mutation was not the cause of the patients' epilepsy symptoms on the rationale that there were only 2% of their patient population that carried this mutation. However, this frequency is in agreement with (or a little higher) than the incidence of GEFS+ patients with *SCN1B*-C121W mutations. A study of these patients' families to see if there was a history of epilepsy within the other family members who also carried the *SCN1B-C121W* mutation would further elucidate whether *SCN1B-C121W* contributed to the idiopathic generalized epilepsies and febrile seizures seen in these Kawaitian patients.

seizure phenotypes. Surprisingly, one proband with DS has been reported to be heterozygous for *SCN1B-C121W*, with no mutations in other known epilepsy genes (Carvill et al., 2014). Although the proband's mother and grandmother are also heterozygous for *SCN1B-C121W*, the mother has febrile seizures and the grandmother has no epilepsy phenotype (Carvill et al., 2014). This recent report further supports the hypothesis that while *SCN1B-C121W* contributes to epilepsy in these patients, genomic and epigenomic background and environmental factors may also play important roles in determining the phenotypic severity of an individual.

Table 1.2 Reports of Patients with SCN1B-C121W

Reference	Starting screen	# Families	# individuals with mutation	Diagnoses	Location of patients
(Wallace et al., 1998)		1	18	Unclassified seizures (1), FS+ (6), FS (6), myoclonic ataxic epilepsy (1), FS and absences (1), Unaffected (3)	Australia
(Wallace et al., 2002)		1	16	FS (6), FS+ (6), FS & partial epilepsy (1), GTCS (1), unaffected (4)	Australia
(Haider et al., 2005)	123 unrelated patients with idiopathic generalized epilepsy		3	IGE with FS (3)	Kuwait
(Scheffer et al., 2007)	402 probands with seizure disorders	2*	13	FS (7), FS+ (1), TLE (1), TLE & FS+ (1), TLE & FS (2), unaffected (1)	Australia
(Dibbens et al., 2010)	Patients with GEFS+, looking for HCN2 mutations	N/a	1	FS, included in (Wallace et al., 1998)	Australia
(Carvill et al., 2014)	13 DS patients, negative for *SCN1A* mutations (parents were also sequenced when possible)	1	3	DS (1), FS(1), unaffected (1)	Not reported
*these two families and the families from (Wallace et al., 1998, 2002) share a haplotype – suggesting a founder mutation					

Although the term “GEFS+” was used previously to describe a spectrum of seizure disorders, this terminology has rapidly changed. Advances in genetic testing and seizure classifications are creating subdivisions within clinical diagnoses once considered indistinguishable. As exome sequencing initiatives like Epi4K (Epi4K Consortium, 2012) have implicated more genes associated with epilepsy syndromes, the field is debating whether epilepsies with similar phenotypes but different genetic origins have converging pathophysiological mechanisms or not. The answer to this question could impact which therapies are effective for patients. Therefore, although I refer to *SCN1B-C121W* as a GEFS+-associated mutation, in clinical practice, this refers to a very heterogeneous patient population.

Heterologous studies of SCN1B-C121W

A majority of the literature studying *SCN1B-C121W* has focused on heterologous over expression and, similar to other studies of VGSC physiology, these findings are mostly dependent on cell type and VGSC α subunit expressed. I have summarized studies that compare effects of β1 and β1-C121W in Table 1.3. I will discuss how some of the differences observed between β1 and β1-C121W modulation of VGSC α subunits may contribute to altered Na^+ current. In addition, the pathophysiological mechanisms proposed from these *in vitro* studies may not be applicable to neurons *in vivo*. A major difference is that most *in vitro* studies have a single VGSC α subunit expressed, while *in vivo* changes in a single VGSC α subunit may result in compensatory changes in other channels.

Table 1.3 Heterologous results of β1 or β1-C121W expression

	Effect from β1-WT expression	Effect from β1-C121W expression	VGSC α subunit	Cell line	Reference
Biotinylation of surface proteins	Both present at the surface		N/A	1610	(Patino et al., 2011)
β1 trans-homophilic adhesion	aggregation of cells	no aggregation of cells	N/A	*Drosophila* S2 cells	(Meadows et al., 2002)
Saxitoxin binding of VGSC α	both ↑ surface α expression		$Na_v1.2$	1610	(Meadows et al., 2002)
Coimmunoprecipitation with VGSC α	both associate		$Na_v1.3$	CHO	
	both associate		$Na_v1.2$	1610	
	both associate		$Na_v1.1$	HEK	(Aman et al., 2009)
Sodium current density	both ↑ current density similarly		$Na_v1.4$	HEK	(Tammaro et al., 2002)
	↑ current density	less ↑ current density	$hNa_v1.1$-M1841T*	tsA-201	(Rusconi et al., 2007)
VGSC α mRNA expression	↑ $Na_v1.3$, ↑ $Na_v1.6$	↑ $Na_v1.3$, ↓ $Na_v1.6$	endogenously express $Na_v1.1$, $Na_v1.2$, $Na_v1.3$, $Na_v1.6$	GH3	(Baroni et al., 2013)
	↑ $Na_v1.2$, ↑ $Na_v1.4$, ↑ $Na_v1.6$, ↓ $Na_v1.5$	↑ $Na_v1.2$, ↑ $Na_v1.6$	endogenously express $Na_v1.5$	H9C2	
VGSC α protein expression	↑ total VGSC α expression	no increase in total VGSC α expression	endogenously express $Na_v1.1$, $Na_v1.2$, $Na_v1.3$, $Na_v1.6$	GH3	
	↑ $Na_v1.2$, ↑ $Na_v1.6$	↑ $Na_v1.3$, ↓ $Na_v1.6$			
	↑ total VGSC α expression		endogenously express $Na_v1.5$	H9C2	
	↑ $Na_v1.2$, ↑ $Na_v1.4$, ↑ $Na_v1.6$, ↓ $Na_v1.5$	↑ $Na_v1.2$, ↑ $Na_v1.6$			
Slow inactivation constant	↓	no effect	$Na_v1.2$	Xenopus oocytes	(Wallace et al., 1998)
	↓	no effect	$Na_v1.4$ or $Na_v1.2$	Xenopus oocytes	(Moran and Conti, 2001)
	β1-WT + β1-C121W coexpression – intermediate effect on slow inactivation				
Recovery from inactivation	lengthens recovery	no effect	$Na_v1.3$	CHO	(Meadows et al., 2002)
			$Na_v1.2$	1610	
	hastens recovery	no effect	$Na_v1.4$	HEK	(Tammaro et al., 2002)

	Effect from β1-WT expression	Effect from β1-C121W expression	VGSC α subunit	Cell line	Reference
Voltage-dependence of inactivation	no effect	shifted to more negative voltages	endogenously express $Na_v1.1$, $Na_v1.2$, $Na_v1.3$, $Na_v1.6$	GH3	(Baroni et al., 2013)
	shifted toward more positive voltages		endogenously express $Na_v1.5$	H9C2	
	no effect		$Na_v1.3$	CHO	(Meadows et al., 2002)
	no effect		$Na_v1.2$	1610	
Voltage-dependence of activation	no effect		$Na_v1.2$	1610	(Meadows et al., 2002)
	no effect		$Na_v1.3$	CHO	
	no effect	no effect	endogenously express $Na_v1.1$, $Na_v1.2$, $Na_v1.3$, $Na_v1.6$	GH3	(Baroni et al., 2013)
	shifted toward more positive voltages		endogenously express $Na_v1.5$	H9C2	
Fraction of channels available at subthreshold membrane potentials†	~10mV shift in availability curve to more negative voltages.	No shift	$Na_v1.3$	CHO	(Meadows et al., 2002); (Lucas et al., 2005)
	β1-WT + β1-C121W coexpression – same shift as β1-WT alone				
Frequency-dependent rundown	~60% decline	only 20-30% decline	$Na_v1.2$	1610	(Meadows et al., 2002)
	~60% decline	only 20-30% decline	$Na_v1.3$	CHO	
	β1-WT + β1-C121W coexpression – same decline as β1-WT alone				
At elevated temperatures (34˚C)	Compared to WT, β1-C121W caused ↓use-dependent inactivation, ↑ persistent current, ↑ window current, delayed onset of inactivation, and accelerated recovery from inactivation		$Na_v1.2$	CHO	(Egri et al., 2012)
Drug sensitivity	sensitive to phenytoin	less sensitive to phenytoin	$Na_v1.3$	CHO	(Lucas et al., 2005)
	sensitive to lacosamide at RT and 34˚C	not sensitive to lacosamide at RT and 34˚C	$Na_v1.2$	CHO	(Abdelsayed et al., 2013)
Coimmunoprecipitation with β4	associates with β4		n/a	HEK	(Aman et al., 2009)
Modulation of β4 effect on resurgent sodium current ‡	reduction in persistent current	no reduction in persistent current	$Na_v1.1$ + β4	HEK	(Aman et al., 2009)

	Effect from β1-WT expression	Effect from β1-C121W expression	VGSC α subunit	Cell line	Reference
* $hNa_v1.1$-M1841T is a trafficking-deficient GEFS+ mutant † To test this, cells are held at a long conditioning pulse of various potentials, followed by a test pulse. ‡ Resurgent current occurs as Na+ channels are blocked by a blocking particle, postulated to be β4, at positive voltages, during depolarization, and then become unblocked during repolarization. To measure this, we step to a positive voltage, to stimulate an AP, and then then step back down to different voltages. Then we can measure the extent of resurgent current seen when you step back down. This is generally higher with presence of β4 or a β4 peptide, although it does depend on the cell type and VGSC α subunit expressed.					

It is important to remember, as discussed earlier in this chapter, that epilepsy mutations may not affect inhibitory and excitatory neurons in the same manner *in vivo.* VGSC α subunit expression varies between different subpopulations and these cell types may be differentially affected by an epilepsy mutation. Epilepsy results from an imbalance between excitation and inhibition, so overall increased excitation, decreased inhibition, or a combination of both can contribute to network hyperexcitability. This does not mean that in an epileptic brain all excitatory neuronal populations will be hyperexcitable and all inhibitory neuronal populations will be hypoexcitable. Recall that recent studies of DS patient derived induced pluripotent stem cell (iPSC) neurons showed that both inhibitory and excitatory neurons are hyperexcitable compared to non-epileptic controls (Liu et al., 2013).

β1 and β1-C121W modulation of sodium channels and I_{Na}

An important function of β1 is to promote sodium channel cell surface expression. β1-C121W is expressed at the cell surface in heterologous cells, including *Xenopus* oocytes, *Drosophila* S2 cells, and transfected fibroblasts, and co-immunoprecipitates with some VGSC α subunits, including $Na_v1.1$, $Na_v1.3$, and $Na_v1.4$ (Meadows et al., 2002; Aman et al., 2009; Patino et al., 2011). β1-C121W is capable of promoting sodium channel cell surface expression and increasing sodium current density, similar to β1-WT, in some systems (Tammaro et al., 2002; Meadows et al., 2002). However, while β1-WT was reported to increase cell surface expression of a trafficking-defective *SCN1A* GEFS+ mutant protein, $hNa_v1.1$-M1841T, β1-C121W only had a partial effect on promoting the cell surface expression of this mutant (Rusconi et al., 2007). Therefore *SCN1B-C121W* has the potential to aggravate other epilepsy-associated mutations.

β1 expression can also modulate mRNA and protein expression of VGSC α subunits. This is postulated to occur through sequential cleavage of β1 by BACE and γ-secretase, leading to nuclear translocation of the β1 intracellular domain and its subsequent modulation of gene expression (Kim et al., 2005, 2007, 2011; Wong et al., 2005). For example, in both a rat pituitary cell line (GH3) and a rat cardiac myocyte cell line (H9C2), total VGSC protein expression and I_{Na} density was increased with WT-β1 cDNA transfection. In contrast, β1-C121W expression increased VGSC protein expression in H9C2 but not in GH3 cells (Baroni et al., 2013). When specific VGSC α subunit expression was examined, β1 and β1-C121W had differing effects. β1-WT increased, but β1-C121W decreased, $Na_v1.6$ mRNA and protein expression, in GH3 cells (Baroni et al., 2013). β1-WT overexpression in H9C2 cells induced expression of $Na_v1.2$, $Na_v1.4$, and $Na_v1.6$ mRNA and protein but decreased $Na_v1.5$ mRNA and protein. In contrast, β1-C121W expression induced $Na_v1.2$ and $Na_v1.6$ expression, but did not affect $Na_v1.5$ in the same cell line (Baroni et al., 2013). These results emphasize how β1 and β1-C121W modulation of VGSCs are cell-type and VGSC α subunit specific.

In general, β1-WT, but not β1-C121W, reduced the slow inactivation component of sodium current (Wallace et al., 1998; Moran and Conti, 2001). *SCN1B-C121W* abolishes the modulatory effects of β1 on sodium current recovery from fast inactivation (Tammaro et al., 2002; Meadows et al., 2002). We previously observed lengthening of recovery from inactivation with β1 expression. Therefore, since β1-C121W does not have this effect in some cell types, channels are available sooner after an action potential, which could lead to a more excitable phenotype (Meadows et al., 2002).

Voltage-dependence of activation and inactivation are not different with β1-C121W expression compared to β1 expression (Meadows et al., 2002; Baroni et al., 2013). However, the voltage-dependence of inactivation is shifted to more negative voltages when β1-C121W was expressed in GH3 cells compared to β1-WT (Baroni et al., 2013). Depending on the neuronal cell type, these changes in channel inactivation ranges and voltage dependence of inactivation could lead to changes in excitability. For example, in pyramidal neurons, a negative shift in sodium channel voltage-dependence of inactivation could lead to hyperexcitability because more channels will be available for activation at a given potential compared to cells expressing β1-WT. However, as this cell type originates from rat heart, this may not have relevance for the GEFS+ phenotype of *SCN1B-C121W* patients.

There are several other notable differences seen between β1-WT and β1-C121W, which could contribute to overall network hyperexcitability and a seizure phenotype. β1-WT, but not β1-C121W, negatively shifts the availability of channels at subthreshold membrane potentials. Therefore, more $Na_v1.3$ channels were available at subthreshold voltages when co-expressed with β1-C121W, which could increase sodium current amplitude (Meadows et al., 2002; Lucas et al., 2005). Furthermore, β1-C121W failed to increase frequency-dependent rundown over time compared to β1-WT (Meadows et al., 2002).

Modulation of β4 effect on resurgent sodium current

As discussed previously, β4 is critical for resurgent Na+ current,[2] and β1 is capable of modulating the effects of β4 on resurgent current. We have previously hypothesized that β4 acts like the "gas" – promoting resurgent current, while β1 acts as a "brake" – reducing resurgent current. Like β1, β1-C121W associates with β4 (Aman et al., 2009), but β1-C121W is unable to reduce persistent current, unlike β1-WT. Therefore increased persistent current, and thus a prolongation of Na+ current, could contribute to altered neuronal firing patterns (Aman et al., 2009).

Does β1-C121W have dominant-negative effects?

Since GEFS+ patients are heterozygous for *SCN1B-C121W*, it is possible that β1-C121W acts in a dominant-negative function by associating with VGSC α subunits and preventing them from trafficking and/or being modulated by β1-WT. When both β1-WT and β1-C121W were co-expressed with $Na_v1.4$ in oocytes, an intermediate rate of inactivation was measured compared to either β subunit alone, suggesting that β1-C121W antagonizes β1-WT in this system (Moran and Conti, 2001). However, CHO cells expressing $Na_v1.3$ + β1-WT + β1-C121W and $Na_v1.3$ + β1-WT had a similar negative shift in the $V_{1/2}$ of channel availability and an increase in frequency-dependent

[2] Resurgent current occurs as Na+ channels are blocked by a blocking particle, postulated to be β4, at positive voltages, during depolarization, and then become unblocked during repolarization. To measure this, we step to a positive voltage, to stimulate an AP, and then then step back down to different voltages. Then we can measure the extent of resurgent current seen when you step back down. This is generally higher with presence of β4 or a β4 peptide, although it does depend on the cell type and VGSC α subunit expressed.

rundown. In the same study, β1-C121W was unable to modulate these properties of $Na_v1.3$ (Meadows et al., 2002). Therefore, β1-C121W appears to have dominant-negative effects in some models, but not others. Altogether, these data from heterologous systems emphasizes the importance of *in vivo* studies for clarifying the pathophysiological impact of *SCN1B-C121W.*

Disruption of trans-homophilic cell adhesion by *SCN1B-C121W*

The immunoglobulin domain of β1 shares homology with other cell adhesion molecules including myelin P_0. The β1 Ig loop contains a single, intramolecular, disulfide bond between Cys121 and Cys45. Therefore, upon the discovery of *SCN1B-C121W* this mutation was hypothesized to abolish this disulfide bond and disrupt homophilic adhesion. In 2012, Barbieri and colleagues used 2D-diagonal SDS-PAGE analysis to confirm the disruption of a disulfide bond in the Ig loop by the *SCN1B-C121W* mutation (Barbieri et al., 2012). We have shown evidence of disrupted β1-mediated homophilic adhesion by the *SCN1B-C121W* mutation in *Drosophila* S2 cells (Malhotra et al., 2000; Meadows et al., 2002). S2 cells have no endogenous cell adhesion molecules so heterologous expression of homophilic cell adhesion molecules results in cellular aggregation. When expressed in S2 cells, β1-WT, but not β1-C121W, induces high affinity cellular aggregation (Malhotra et al., 2000; Meadows et al., 2002). These results suggest β1-C121W is incapable of *trans*-homophilic adhesion. β1- and β1B-mediated *trans*-homophilic adhesion promote neurite outgrowth in cultured neurons (Patino et al., 2011). Therefore, p.C121W may result in neuronal pathfinding and fasciculation defects similar to what we have reported in *Scn1b*-null mice (Brackenbury et al., 2008). Decreased dendritic arborization in subicular neurons of mice homozygous for *Scn1b*-

C121W (Reid et al., 2014) may be due to the loss of β1-mediated *trans*-homophilic adhesion. Although β1-C121W cannot interact homophilically with other β1-C121W molecules (Malhotra et al., 2000; Meadows et al., 2002), to date no studies have determined whether β1-C121W is capable of interacting with β1-WT. As GEFS+ patients are heterozygous for *SCN1B-C121W,* this is an important question for understanding how *SCN1B-C121W* affects neuronal development.

Effects on potassium channels

Several investigators have found evidence that β1 modulates potassium channels, summarized in Table 1.4. Marrioneau et al. (2012) immunoprecipitated Kv4.2 and found a β1 extracellular peptide associated via mass spectroscopy and proteomic analysis (Marionneau et al., 2012). β1 co-localizes with Kv1.2 at axon initial segments in the mouse brain (Nguyen et al., 2012). Heterologously co-expressed FLAG-tagged β1 and Kv1.2 associate as assessed by co-immunoprecipitation. β1 modulates K+ current when co-expressed with Kv1 or Kv7 channels in *Xenopus* oocytes (Nguyen et al., 2012). However, β1 does not appear to modulate Kv3 channels. Using P_0-β1 chimeras, the authors showed that the external Ig domain was critical for β1-mediated acceleration of Kv1.3 activation. β1-C121W was unable to modulate Kv1.3 activation (Nguyen et al., 2012). In contrast, β1 and β1-C121W both slowed Kv1.1 deactivation (Nguyen et al., 2012). Together, this evidence suggests that studies of *SCN1B* mutations need to consider that potassium currents, not just sodium currents, may be altered.

Table 1.4 Heterologous effects of β1 on K+ channels

	Effect from β1-WT expression	Effect from β1-C121W expression	Cells/tissue	Reference
Coimmunoprecipitation	associates with K_v4.2, as identified by mass spectrometry	not tested	mouse brain	(Marionneau et al., 2012)
	β1-EYFP associates with K_v4.2	not tested	HEK	
	β1-V5 associates with K_v1.2-flag, K_v7.2-flag	not tested	HEK	(Nguyen et al., 2012)
Modulation of K+ current	modulates Kv1 and Kv7, but not Kv3 channels accelerated Kv1.3 activation slows Kv1.1 deactivation	did not accelerate Kv1.3 activation slows Kv1.1 deactivation	HEK	(Nguyen et al., 2012)

Effect on drug sensitivity and excitability at higher temperatures

Of therapeutic interest is whether *SCN1B-C121W* alters the pharmacological sensitivity of sodium channels in patients. *In vitro,* $Na_v1.3$ channels were less sensitive to phenytoin and $Na_v1.2$ channels were less sensitive to lacosamide when co-expressed with β1-C121W, compared to β1-WT (Lucas et al., 2005; Abdelsayed et al., 2013).

Due to the febrile seizure phenotype in many GEFS+ patients (Wimmer et al., 2010), one study has examined whether β1-C121W has altered current modulatory effects compared to β1-WT at 34˚C, a temperature which is closer to physiological temperatures than the 22-25˚C most *in vitro* studies use. At this elevated temperature, CHO cells expressing $Na_v1.2$ and β1-C121W had decreased use-dependent inactivation, increased persistent current and window current, and delayed onset of, and accelerated recovery from, fast inactivation compared to cells expressing $Na_v1.2$ and β1-WT (Egri et al., 2012). This study did not repeat these studies at 22-25˚C to determine if the differences with β1-C121W expression was specific to their model or the elevated temperatures they used. Thus, β1-C121W appears to lack a protective effect against increased excitability at elevated temperatures. However, although CHO cells are mammalian in origin, they have distinctly different protein expression and physiology from neurons so this result may not apply to neurons *in vivo.*

In vivo effects of SCN1B-C121W

A knock-in *Scn1b-C121W* mouse model of GEFS+ was reported in 2010 (Wimmer et al., 2010). Heterozygotes ($Scn1b^{+/W}$), which model GEFS+, and homozygotes ($Scn1b^{W/W}$) from this model are more sensitive to thermally-induced seizures (Wimmer

et al., 2010). In addition *Scn1b*$^{W/W}$ mice experience spontaneous seizures, beginning around post-natal day 14, and early lethality by post-natal day 21, similar to *Scn1b* null mice and are thus thought to model the severe epileptic encephalopathy, Dravet Syndrome (Chen et al., 2004; Wimmer et al., 2010). Researchers have been interested in confirmation or rejection of previous heterologous results regarding β1-C121W function. As most of these *in vitro* results were done with only β1-WT or β1-C121W present, most studies of this mouse model have focused on comparing *Scn1b*$^{W/W}$ and *Scn1b*$^{+/+}$. In Table 1.5, I summarized the *in vivo* findings regarding *Scn1b-C121W*. I will focus on describing those studies that are most relevant to the experiments that I have performed.

Establishing how p.C121W results in changes in neuronal excitability is critical to understanding the mechanisms underlying epileptogenesis and/or seizure phenotype. For example, an epilepsy-causing mutation may alter the balance between excitatory and inhibitory signals by causing hyperexcitability of excitatory neurons and/or hypoexcitability of inhibitory neurons. Some studies suggest that epilepsies can be caused by “interneuronopathies” or dysfunction of the inhibitory neurons, as these models show decreased excitability in inhibitory neurons, thus disrupting the excitatory/inhibitory balance (Yu et al., 2006; Ogiwara et al., 2007; Oakley et al., 2011). Interestingly, evidence suggests that smaller sub-populations of neurons, such as the parvalbumin-positive interneurons, or layer II/III cortical pyramidal neurons for example, can each be modulated differentially by ion channel mutations and play critical roles in epilepsy. Therefore, determining not only how p.C121W alters neuronal excitability, but

which neuronal populations are affected is key to understanding the mechanisms underlying *SCN1B-C121W*-linked epilepsy.

β1 sub-cellular localization *in vivo*

Another important consideration is whether β1-C121W can localize to the appropriate subcellular domains of neurons *in vivo*. The two neuronal subcellular domains most often considered for VGSC α and β subunit localization are the axon initial segment and the nodes of Ranvier. Virally expressed β1-C121W-EGFP in a wildtype mouse appeared to localize to the AIS in many brain regions. However the data did not suggest AIS surface localization (Wimmer et al., 2010). In contrast, the same group later reported that *Scn1b*$^{W/W}$ mice have no β1-positive AIS domains in the subiculum (Wimmer et al., 2015). Although changes in β1 expression *in vitro* resulted in altered sodium channel expression (Baroni et al., 2013), as discussed above, Wimmer et al. reported no difference in $Na_v1.1$, $Na_v1.2$, and $Na_v1.6$ distribution along the AIS in the hippocampus of *Scn1b*$^{W/W}$ mice (Wimmer et al., 2010). Here, we sought to build on these previous studies to compare β1 localization in *Scn1b*$^{+/W}$, *Scn1b*$^{+/-}$, and *Scn1b*$^{W/W}$ brains, using *Scn1b*$^{-/-}$ brains as negative controls. β1 localization in *Scn1b*$^{+/W}$ mice has not been reported previously. This experiment is critical to understand the mechanism of GEFS+, in which patients express one WT and one mutant *SCN1B* allele. In addition, we compared β1 and β1-C121W localization in the cortex, which is relevant to epilepsy, and in the cerebellum, which may be relevant to co-morbid effects of epilepsy syndromes.

Table 1.5 In vivo results from Scn1b-C121W mice

	***Scn1b*$^{+/+}$ mice**	***Scn1b*$^{+/W}$ mice**	***Scn1b*$^{W/W}$ mice**	**Tissue**	**Reference**
Immunohistochemistry of β1	virally expressed β1-C121W-EGFP appears to traffic to AIS			pyramidal CA3 neurons in hippocampus; pyramidal neurons in the subiculum; layer 2/3 pyramidal neurons in primary somatosensory cortex; Purkinje cell in the cerebellum	(Wimmer et al., 2010)
	~95% AIS are β1+	~50% AIS are β1+	0% AIS are β1+	mouse subiculum	(Wimmer et al., 2015)
$Na_v1.1$, $Na_v1.2$, and $Na_v1.6$ distribution along the AIS	no differences between *Scn1b*$^{+/+}$ and *Scn1b*$^{W/W}$			molecular layer of the hippocampus	(Wimmer et al., 2010)
Dendritic arborization	↓ in *Scn1b*$^{W/W}$ neurons compared to *Scn1b*$^{+/+}$			subicular neurons	(Reid et al., 2014)
Intrinsic bursts in response to current injections$^{\varphi}$	No difference in total number of burst events or frequency of APs within bursts; *Scn1b*$^{+/W}$ mice had longer burst duration compared to *Scn1b*$^{+/+}$ mice			subicular pyramidal neurons of P14-16 mice at 34˚C	(Wimmer et al., 2010); (Reid et al., 2014)
Tonic firing following intrinsic bursts$^{\varphi}$	↑ frequency in *Scn1b*$^{+/W}$ mice and *Scn1b*$^{W/W}$				
AP threshold	-48.74 ± 0.32 mV	-51.43 ± 0.23 mV			(Wimmer et al., 2010)
	-50.91 ± 2.66 mV		-47.01 ± 2.91 mV		(Reid et al., 2014)
Resting membrane potential	-71.69 ± 1.47 mV		-66.64 ± 1.72 mV		
AP frequency (input-output curve)	↑ (left-shift in the curve) in *Scn1b*$^{W/W}$ compared to *Scn1b*$^{+/+}$			cortical layer 2/3 pyramidal neurons	
Proportion of burst firing neurons	56%		81%	subicular pyramidal neurons of P14-16 mice at 34˚C	
Spontaneous PSCs	↓ sPSC inter event interval in *Scn1b*$^{W/W}$ compared to *Scn1b*$^{+/+}$			subiculum, but not CA1	
AP characteristics	No change in amplitude, half-width, rise, threshold, or resting membrane potential between *Scn1b*$^{+/+}$ and *Scn1b*$^{W/W}$			Cortical layer 2/3 pyramidal neurons; CA1 interneurons (@ 22˚C and 34˚C); Cortical layer 5 pyramidal neurons; CA1 pyramidal neurons	(Reid et al., 2014)

	***Scn1b*$^{+/+}$ mice**	***Scn1b*$^{+/W}$ mice**	***Scn1b*$^{W/W}$ mice**	**Tissue**	**Reference**
CA1 oscillations	In *Scn1b*$^{+/W}$ compared to *Scn1b*$^{+/+}$: ↑ number of spikes/oscilation; ↑ event duration; ↓ latency to oscilation onset; ↓ interspike interval			CA1 hippocampal neurons from P16-P21 **at 32˚C**	(Hatch et al., 2014)
	no change in spikes/oscilation; no change in event duration			CA1 hippocampal neurons from P16-P21 **at 28˚C**	
Difference in CA1 oscillations with carbamazepine OR retigabine	↓ number of spikes/oscilation (10μM CBZ) no change in event duration (10μM CBZ) ↓ number of spikes/oscilation (1μM RTG) ↓ event duration (1μM RTG)	↓ number of spikes/oscilation (1μM CBZ) ↓ event duration (10μM CBZ) ↓ number of spikes/oscilation (0.3 μM RTG) ↓ event duration (1μM RTG)		CA1 hippocampal neurons from P16-P21 **at 32˚C**	
Thermal seizure sensitivity	Mean seizure onset ~38.5˚C	↓ 0.44 ± 0.17˚C	↓ 1.2 ± 0.15˚C	P14-16 mice	(Wimmer et al., 2010)
Effect of diazepam on latency to thermal seizure			↑ time to seizure, dose-dependent	P14-17 mice	(Reid et al., 2014)
Effect of stiripentol or lamotrigene on latency to thermal seizure			stiripentol: ↑ time to seizure lamotrigine: no effect	P14-17 mice	
Effect of retigabine on latency to thermal seizure	↑ time to seizure	↑ time to seizure	↑ time to seizure, dose-dependent	P14-17 mice	(Reid et al., 2014); (Hatch et al., 2014)

AIS – axon initial segment; AP – action potential; PSC – postsynaptic current; SPSC – spontaneous postsynaptic current; RTG – retigabine; CBZ - carbamazepine

φ This is an intrinsic property of most subicular pyramidal neurons.

In vivo functional studies of network and neuronal excitability

Studies comparing *Scn1b*$^{+/W}$ and wildtype littermates have only examined subicular pyramidal neurons and CA1 hippocampal neurons (Wimmer et al., 2010; Hatch et al., 2014). A subset of subicular pyramidal neurons respond to current injections with intrinsic burst events followed by tonic firing. *Scn1b*$^{+/W}$ mice had an increased number of burst events, and longer burst duration, as well as an increase frequency of tonic firing compared to *Scn1b*$^{+/+}$ mice (Wimmer et al., 2010). A separate study examined CA1 network oscillations in *Scn1b*$^{+/W}$ and wild-type brain slices. CA1 oscillations were induced by stimulating the stratus oriens and recording extracellular potentials (Hatch et al., 2014). These oscillations could be reduced by pharmacological blockade of AMPA receptors or $GABA_A$ receptors, indicating both excitatory and inhibitory neurons were present in this circuit. In addition, severing connections between CA1 and CA3 did not affect oscillations (Hatch et al., 2014). When CA1 oscillations were measured at 32˚C, *Scn1b*$^{+/W}$ slices had more spikes per oscillation, greater event duration, decreased interspike interval and decreased latency to oscillation onset compared to wild-type controls. However, no differences were seen between *Scn1b*$^{+/W}$ and wild-type slices when measured at 28˚C (Hatch et al., 2014). Both *Scn1b*$^{+/W}$ and wild-type CA1 oscillations decreased in number of spikes per oscillation in response to carbamazepine or retigabine, although *Scn1b*$^{+/W}$ responded at lower doses than wild-type (Hatch et al., 2014). A few patients with *SCN1B-C121W*-associated GEFS+ have hippocampal sclerosis and temporal lobe epilepsy, but this does not describe all *SCN1B-C121W* GEFS+ patients (Table 1.2, (Scheffer et al., 2007)). Therefore, it is unclear whether

these observations in the CA1 contribute to the GEFS+ phenotype for a majority of patients with a *SCN1B-C121W* mutation.

Other studies comparing *Scn1b*$^{W/W}$ mice, which model DS, with wild-type littermates are summarized in Table 1.5. Briefly *Scn1b*$^{W/W}$ subicular pyramidal neurons in brain slices at 34˚C showed a more positive threshold for action potential firing and a more positive resting membrane potential (Reid et al., 2014). Subicular pyramidal neurons in *Scn1b*$^{W/W}$ mice also had decreased spontaneous postsynaptic current inter-event intervals compared to wild-type mice. Both subicular and cortical layer II/III pyramidal neurons showed increased action potential firing frequency in response to current injection, resulting in a leftward shift in the input-output relationship (Reid et al., 2014). No changes in action potential amplitude or threshold were observed in several other brain regions including cortical layer II/III or layer V pyramidal neurons and CA1 interneurons or pyramidal neurons (Reid et al., 2014).

Conclusion

VGSCs are integral to normal neuronal physiology and are important therapeutic targets for treating epilepsy. Understanding how mutations in VGSC genes lead to hyperexcitability in the brain is critical for understanding epilepsy pathophysiology and the identification of novel therapeutic targets. Heterozygous *SCN1B-C121W* mutations are associated with GEFS+. While heterologous over expression studies of this mutation have shown many cell type specific and VGSC α-subunit specific effects, it is unclear how these results translate *in vivo*. The recent generation of a *SCN1B-C121W* knock-in mouse model has made it possible to study the *in vivo* effects of this mutation.

However, studies to date have not yet elucidated whether *SCN1B-C121W* is a loss-of-function or a potential deleterious gain-of-function mutation. In this thesis, I directly compare *Scn1b*$^{+/W}$ and *Scn1b*$^{+/-}$ mice to address this important question.

Chapter 2. β1-C121W is down but not out: Epilepsy-associated *Scn1b-C121W* results in a deleterious gain-of-function

This chapter is in preparation for submission to The Journal of Neuroscience. We plan to submit it prior to my thesis defense on Nov 20th.

Larisa Kruger conducted the majority of data collection and all data analysis for Figure 2.1. Larisa Kruger also completed all data collection and analysis for Figures 2.2-2.5. Heather O'Malley collected and quantified data for Figure 2.6. Jacob Hull performed primary neuronal cultures for Figure 2.3. Amanda Kleeman performed some of the thermal seizure experiments for Figure 2.1. Gustavo Patino developed the modified Racine score and heat-induced seizure protocol and instructed Amanda and Larisa on how to perform this test. Larisa Kruger and Lori Isom wrote the manuscript.

Introduction

Voltage-gated sodium channels (VGSCs), composed of one pore-forming α and two β subunits in brain (Hartshorne and Catterall, 1981), are critical for neuronal excitability, including action potential initiation and conduction. While VGSC β subunits do not form the ion-conducting pore, they are essential for normal excitability *in vivo* through modulation of sodium and potassium currents (Isom et al., 1992, 1995b; Chen et al., 2004; Marionneau et al., 2012). In addition, β subunits are immunoglobulin (Ig) superfamily cell adhesion molecules that play important roles in neuronal proliferation and migration, neurite outgrowth, neuronal pathfinding, and axonal fasciculation *in vitro* and *in vivo* (Davis et al., 2004; Brackenbury and Isom, 2008, 2011; Patino and Isom, 2010; Patino et al., 2011).

Mutations in VGSC genes are associated with multiple genetic epilepsies, including Genetic Epilepsy with Febrile Seizures plus (GEFS+) (Scheffer and Berkovic, 1997; Singh et al., 1999) and Dravet syndrome (Patino et al., 2009). Autosomal dominant mutations in *SCN1B*, encoding VGSC β1 and β1B, are associated with GEFS+ (Wallace et al., 1998, 2002; Scheffer et al., 2007). *SCN1B-C121W,* the first reported GEFS+ mutation, disrupts a critical, intramolecular disulfide bond within the extracellular β1 Ig loop domain (Wallace et al., 1998; Audenaert et al., 2003; Barbieri et al., 2012). The impact of the *SCN1B-C121W* GEFS+ mutation on β1 subunit function is incompletely understood. Wildtype (WT) β1 subunits promote cellular aggregation *in vitro* via *trans*-homophilic cell-cell adhesion (Malhotra et al., 2000). In contrast, while mutant β1-C121W subunits are expressed at the cell surface in heterologous cells, they

do not participate in *trans* homophilic adhesion when tested in a cellular aggregation assay (Meadows et al., 2002). The effects of mutant β1-C121W subunit expression on VGSC function have been extensively investigated in heterologous systems, but results are cell-type and VGSC α-subunit specific (Moran and Conti, 2001; Tammaro et al., 2002; Meadows et al., 2002; Lucas et al., 2005; Aman et al., 2009; Egri et al., 2012; Baroni et al., 2013). *In vivo* studies of the heterozygous *Scn1b*$^{+/W}$ GEFS+ knock-in mouse model showed changes in action potential threshold and brain region-specific changes in AP firing at elevated temperatures (Wimmer et al., 2010; Reid et al., 2014) . In addition, *Scn1b*$^{+/W}$ mice showed differences in dendritic branching in subicular neurons that may be consistent with defects in β1-mediated cell-cell adhesion (Wimmer et al., 2010; Reid et al., 2014). While multiple *in vitro* studies have demonstrated β1-C121W polypeptide expression at the surface of heterologous cells in which β1-C121W cDNA was overexpressed (Tammaro et al., 2002; Meadows et al., 2002; Patino et al., 2011), viral transduction of mouse neurons predicted that β1-C121W may be retained inside the cell and thus non-functional (Wimmer et al., 2010). Finally, studies of homozygous *Scn1b*$^{W/W}$ knock-in mice, which model the epileptic encephalopathy Dravet syndrome, showed that β1-C121W subunits fail to localize to axon initial segments (AIS) of subicular neurons, however, this study did not address whether these mutant β1 polypeptides are expressed at the neuronal cell surface (Wimmer et al., 2015).

Here, we compared *Scn1b-C121W* knock-in GEFS+ mice (*Scn1b*$^{+/W}$) (Wimmer et al., 2010) with mice expressing the *Scn1b* null allele, *Scn1b*$^{+/-}$ mice (Chen et al., 2004), to ask whether the β1-C121W GEFS+ mutation results in simple loss-of-function or

whether it conveys a deleterious gain-of-function. The parents of a Dravet syndrome patient homozygous for the loss-of-function mutation *SCN1B-R125C,* who are each heterozygous for the mutation, did not report seizures (Patino et al., 2009). Furthermore, the Exome Aggregation Consortium (ExAC, http://exac.broadinstitute.org/) database reports several neurologically normal patients with predicted heterozygous loss-of-function *SCN1B* mutations, suggesting that *SCN1B* haploinsufficiency may be tolerated. Here, we report that the thermal seizure phenotype of *Scn1b*$^{+/W}$ GEFS+ mice is more severe than that of *Scn1b*$^{+/-}$ mice. β1-C121W polypeptides are expressed at the cell surface of cultured *Scn1b*$^{W/W}$ mouse neurons, however, they are expressed at lower levels than β1-WT polypeptides in *Scn1b*$^{+/+}$ brain. β1-C121W appears to be incompletely glycosylated compared to WT β1 polypeptides, and its association with VGSC α subunits is disrupted. β1-C121W subunits localize to neuronal cell bodies in *Scn1b*$^{W/W}$ mouse brain cortex and cerebellum, but, unlike WT β1 subunits, are not translocated to specialized axonal subcellular domains, including the AIS and nodes of Ranvier. Taken together, our results suggest that the *Scn1b-C121W* GEFS+ mutation confers deleterious gain-of-function effects *in vivo*.

Methods

Mice

Scn1b$^{+/-}$, *Scn1b*$^{-/-}$, *Scn1b*$^{+/W}$ and *Scn1b*$^{w/w}$ mice of both genders were generated from *Scn1b*$^{+/-}$ and *Scn1b*$^{+/W}$ mice as previously described (Chen et al., 2004; Wimmer et al., 2010). *Scn1b*$^{+/-}$ mice were >N20 on the C57BL/6J background strain. *Scn1b*$^{+/W}$ mice were generated using C57BL/6J mouse embryonic stem cells and maintained on the C57BL/6J strain for >5 generations. Thus, *Scn1b*$^{+/+}$ mice from *Scn1b*$^{+/W}$ x *Scn1b*$^{+/W}$ crossings are congenic C57BL/6J. In spite of this, to be confident that there were no background differences, we compared *Scn1b*$^{+/+}$ mice from *Scn1b*$^{+/W}$ x *Scn1b*$^{+/W}$ litters and *Scn1b*$^{+/-}$ x *Scn1b*$^{+/-W}$ litters in all experiments. No significant differences were observed between *Scn1b*$^{+/+}$ mice generated from either line. Animals were housed in the Unit for Laboratory Animal Medicine at the University of Michigan. All procedures were approved by the University of Michigan Committee on Use and Care of Animals.

Thermal Seizures

Mice were tested for thermal seizure susceptibility at four developmental ages: postnatal day (P)15, P16, P20-21, and P30-33. Seizures were classified according to a modified Racine scale, as reported previously (Racine, 1972; Patino et al., 2009). The scale is as follows: 0, no response; 1, staring or unresponsive; 2, focal or clonic convulsion involving twitches or myoclonic jerk of a single limb, head nods or backing; 3, clonus of both forelimbs; 4, rearing/uncontrolled hind limbs, without loss of posture; 5, loss of upright posture, usually preceded by jumping/rearing; 6, prolonged convulsion (≥ 30 sec of tonic/clonic convulsions with loss of posture) or death. Due to the difficulty in accurately observing level 1 seizures without an EEG, seizures rated as level 1 were

not recorded. Therefore, all seizures used in this analysis were of level 2 or greater. Following a 1 ml intraperitoneal (IP) injection of 0.9% NaCl to prevent dehydration, a rectal thermometer was positioned to monitor body temperature (BT). A heat lamp, connected to the monitor, controlled BT according to the following protocol. Mice were acclimated with set temperature (ST) at 37°C for 30 min. Then, during the observation period, ST was increased by 0.5°C every 2 min. At the 20 min time point, ST was held at 42.5°C for an additional 15 min. When a seizure was observed, the following were recorded: BT, seizure severity (Racine scale), and time elapsed from the beginning of the observation period. After the experiment, all animals were euthanized followed by removal of vital organs. Genotypes were blinded to the observer and experiments were gender-balanced. No significant differences were noted between female and male animals. WT animals from *Scn1b*$^{+/-}$ and *Scn1b*$^{+/W}$ litters were considered separate groups and compared directly during analysis. However, no significant differences were observed between WT genotypes and thus these animals were pooled for final analysis. The numbers of mice used for P15, P16, P20-21, and P30-33 age groups were: *Scn1b*$^{+/+}$ (22, 24, 20, 25); *Scn1b*$^{+/-}$ (16, 16, 18, 23); *Scn1b*$^{+/W}$ (16, 11, 11, 17), respectively.

Behavioral Seizure Analysis

For hyperthermia-induced seizure studies, time and temperature to first seizure were analyzed using the Mantel-Cox test. The most severe seizure for each mouse was analyzed using the Kruskal-Wallis test. Mann-Whitney analysis of these data gave similar results. For all analyses, $P \leq 0.05$ was the threshold for significance. P-values from all analyses are listed in Table 2.1.

Antibodies

Primary antibodies were as follows: rabbit anti-*Scn1b* (directed against an intracellular β1 epitope, Cell Signaling Technology, pre-production serum of D4Z2N, cat #14684, 1:3000 used for Western blotting); rabbit anti-*Scn1b* (directed against an extracellular β1 epitope, Cell Signaling Technology, pre-production serum of D9T5B, cat #13950, 1:25 used for immunofluorescence in optic nerves); rabbit anti-*Scn1b* (directed against an extracellular β1 epitope, Cell Signaling Technology, production version of D9T5B, cat #13950, 1:250 used for immunofluorescence in brains); guinea pig anti-Caspr (gift from Dr. James Salzer, New York University School of Medicine, 1:1000 used for immunofluorescence in optic nerves); mouse anti-PAN VGSC α-subunit (Sigma, S8809, 1:200 used for immunofluorescence in optic nerves and co-immunoprecipitation); goat anti-ankyrinG (recognizing total ankyrinG, gift from Dr. Vann Bennett (He et al., 2014; Jenkins et al., 2015), 1:500 used for immunofluorescence in brains); mouse anti-calbindin (Sigma, C9848, 1:400 used for immunofluorescence in brains); rat anti-Ctip2 (Abcam, ab18465, 1:400 used for immunofluorescence in brains); rabbit anti-PAN VGSC α-subunit (Cell Signaling Technology, D2I9C, 1:1000 used for Western blotting); mouse anti-human α-tubulin (Cedarlane Laboratories, Hornby, ON; CLT9002; 1:5000, used for Western blotting); mouse anti-HSP90 (Enzo Life Sciences, AC88, 1:1000, used for Western blotting). Secondary antibodies for Western blotting were as follows: HRP-conjugated goat anti-mouse (1:500, Thermo Fisher Scientific), HRP-conjugated goat anti-rabbit (1:500, Thermo Fisher Scientific). Secondary antibodies from Thermo Fisher Scientific, used for immunofluorescence at a 1:500 dilution, were as follows: AlexaFluor® goat anti-rabbit 488nm, AlexaFluor® goat anti-mouse 594nm, AlexaFluor®

goat anti-guinea pig 647nm, AlexaFluor® donkey anti-rabbit 488nm, AlexaFluor® donkey anti-goat 594nm, AlexaFluor® donkey anti-rat 594nm, and AlexaFluor® donkey anti-mouse 647nm.

Mouse brain membrane preparation

Mouse brain membrane proteins were prepared as described (Isom et al., 1995a). Complete Protease Inhibitors (Roche Diagnostics) were added to all solutions at 2 times the recommended concentration to minimize protein degradation. Briefly, immediately following anesthetization of the animal by isoflurane, brains were dissected and homogenized in ice-cold Tris EGTA (50 mM Tris, 10 mM EGTA, pH 8.0). A polytron homogenizer was used to mechanically shear the tissue, followed by 20 strokes of homogenization in a chilled glass homogenizer. Homogenates were centrifuged at 2500 x g for 20 min at 4˚C in a swinging bucket rotor to separate homogenized proteins from cell debris and nuclei. The supernatant was then ultracentrifuged (Thermo Fisher Scientific, Sorval WX Ultra 80 ultracentrifuge) at 148,000 x g for 55 min at 4ºC in a fixed-angle rotor (Thermo Fisher, TFT-80.4). The final pellet was resuspended in ice-cold Tris-EGTA and analyzed for protein concentration using the BCA Assay (Thermo Fisher Scientific). Protein sample aliquots were stored at -80˚C.

Western blot analysis

Western blots were performed as described (Malhotra et al., 2000). SDS sample buffer (final concentration 62 mM Tris-HCl, 10% glycerol, 34 mM SDS, 20 mM dithiothreitol, 5% β-mercaptoethanol) was added to protein samples prior to separating on SDS-PAGE gels. Hand-poured 10%, 12%, 15%, and pre-poured 4-15% (Bio-Rad) SDS-

PAGE gels were used as indicated in figure legends. With the exception of experiments using the mouse anti-HSP90 antibody, Western blots were performed using blocking solution containing 5% non-fat dry milk and 1% bovine serum albumin in TBST (0.1 M Tris-Cl, 0.5 M NaCl, pH 7.5, 0.1% Triton X-100), with primary antibodies incubated overnight at 4ºC. For experiments using the mouse anti-HSP90 antibody, a blocking solution of 2% non-fat dry milk in TBST was used and primary antibody was incubated overnight at RT. All secondary antibodies were applied for 1 h at RT. West Femto or West Dura reagent (Thermo Fisher Scientific, 34095 or 34076) was used for detection. Immunoreactive signals were recorded using a Leica Odyssey Fc Imager.

Coimmunoprecipitation

For co-immunoprecipitation experiments, 200 µl of protein-G Sepharose beads (Sigma-Aldrich) were washed three times in PBS and divided equally into 4 microcentrifuge tubes. Beads were incubated overnight with end-over-end mixing at 4ºC with 250 µl of dilution buffer (60 mM Tris/HCl, pH 7.5; 180 mM NaCl; 1.25% Triton X-100; 6 mM EDTA) and 5 µg mouse anti-PAN VGSC antibody (Sigma) or 1.2 µg of mouse IgG (Jackson Immuno Research). Freshly-thawed mouse brain membrane protein preparations (~1.2 mg of *Scn1b*$^{+/+}$ or *Scn1b*$^{W/W}$ for Figure 2.4 A; ~1.2 mg of *Scn1b*$^{+/+}$ or ~2.4 mg of *Scn1b*$^{W/W}$ for Figure 2.4 B) were resuspended in dilution buffer (with Complete Protease Inhibitors at 2X of the recommended concentration) to a concentration of ~2.4 mg/mL. Protein samples were centrifuged at 5000 x g for 5 min. To remove proteins that non-specifically associate with the Sepharose beads, protein supernatants were pre-cleared by incubation with 50 µl protein-G Sepharose beads

(washed three times in PBS, but not incubated with antibody or IgG) for 1 hr at 4°C with end-over-end mixing. The Sepharose beads were pelleted by centrifugation at 3000 x g for 3 min. Protein supernatant was removed and added to protein-G Sepharose beads previously incubated overnight with antibody or IgG. The protein and beads were incubated at 4°C for 4 h with end-over-end mixing. Beads were washed three times with ice-cold wash buffer (50 mM Tris/HCl, pH 7.5; 150 mM NaCl; 0.02% SDS; 5 mM EDTA; 2X Complete Protease Inhibitors) with 0.1% Triton X-100, and then washed once with wash buffer without 0.1% Triton X-100. 25 µl of Western blot sample buffer (see Western blot Methods) was added to beads and heated for 10 min at 85°C to elute proteins from the beads.

Quantification of β1 immunoreactive bands

Quantification of β1 immunoreactive bands on Western blots was performed using ImageJ (version 1.49, Wayne Rasband, NIH). Tissues from 4 animals from each genotype were tested in three replicate experiments. Values were normalized for protein loading using α-tubulin. Protein levels for each experiment were normalized to the mean for *Scn1b*$^{+/+}$. Final analysis was performed using a two-way ANOVA.

PNGaseF digestion

PNGaseF digestion of *Scn1b*$^{+/+}$ and *Scn1b*$^{W/W}$ mouse brain membrane proteins was performed as recommended by the manufacturer (New England BioLabs) with the following changes: Frozen brain membrane protein samples were thawed on ice, 100 µg of protein with 1X Glycoprotein Denaturing Buffer (NEB) in a total volume of 15.6 µl was heated for 10 min at 85°C. Then 2.4 µl G7 buffer (NEB), 2.4 µl NP40 (NEB), and

3.6 µl PNGaseF (or ddH_2O for mock digestion) were added for a total volume of 24 µl. Reactions were incubated at 37°C for 2 h. Western sample buffer was added to each sample and samples were separated by SDS PAGE followed by Western blot. For Western blots, 100 µg of untreated brain membrane protein were loaded as 'input' controls.

Primary Culture of Cortical Neurons

P0-P1 mouse cortices were isolated and digested in unsupplemented Neurobasal medium (Gibco) with 0.25% trypsin for 15 min at 37°C. Cortices were then washed in Hanks Buffered Salt Solution (Gibco) and cells dispersed with fire polished Pasteur pipets. Cells were purified on a 35%/25%/20%/15% Optiprep (Axis-Shield) density gradient. The bottom 2 fractions were collected, washed, and diluted with Neurobasal medium supplemented with 0.5 mM L-glutamine (Gibco), 1% penicillin/streptomycin (Gibco), and 2% B-27 supplement (Gibco). 200 µl of cells were plated on 15 mm diameter poly-d-lysine pre-coated coverslips (Neuvitro) at a density of 250,000 cells/coverslip. After 24 h in a 37°C humidified 5% CO_2 incubator, 2 ml of the above supplemented Neurobasal medium were added. 50% of the medium was replaced every 3rd day and cells were used on the 16th day *in vitro* (DIV).

Surface Biotinylation

Surface biotinylation of primary cultured neurons was performed using the Cell Surface Protein Isolation kit (Thermo Fisher Scientific 89881), with adaptations to the manufacturer's suggested protocol as follows. All solutions were provided in the kit and reactions were performed on ice unless otherwise indicated. Briefly, primary neurons,

cultured as described above, were plated on coverslips and cultured in 6-well plates, with each well containing one coverslip. The culture medium was removed and cells were gently washed twice with ice-cold PBS. 1.5 ml of 0.25 mg/mL Sulfo-NHS-SS-Biotin in ice-cold PBS was added to each well. Plates were rocked gently at 4^{o}C for 30 min to ensure even coverage of the cells with the labeling solution. 150 µl of Quenching solution was added to each well and plates were rocked at RT for 5 min. Contents of each well were then scraped and transferred to 50 mL conical tubes. Each well was washed with 1 ml TBS and wash was added to the corresponding tube of cells. Cells were pelleted at 1000 x g for 10 min in a swinging bucket rotor. The pellet was washed gently with 5 ml of TBS and then re-pelleted. From this point, Complete Protease Inhibitors (Roche Diagnostics) were added to all solutions at 2 times the recommended concentration to minimize protein degradation. Cells were resuspended in 25-50 µl of lysis buffer. Cell lysates were stored at -80˚C. After 4-5 rounds of culture and biotinylation, cell lyses from the same genotypes were thawed on ice and pooled to achieve sufficient protein for detection. Pooled cell lysates were sonicated with a pulse sonicator at 20% power every 5 min on ice for 30 min. Cell lysates were spun at 10,000 x g for 2 min to remove cellular debris. 20 µl of each supernatant was saved for ‘total cell lysate’ sample analysis and used to determine protein concentration. For Figure 2.3, ~40 ug of protein was loaded in the total cell lysate lanes. The remaining supernatant (~450 ug of protein per sample) was added to 100 µl washed NeutrAvidin Agarose beads and rotated end-over-end overnight at 4^{o}C. The following day, beads were washed 3x for 5 min at 4^{o}C with 500 µl ice-cold wash buffer. Beads were then rotated for 1 h at RT with 25 µl of sample buffer containing 50 mM DTT to ensure complete

elution. The entire sample for each genotype was loaded and designated as ‘surface proteins’ for Figure 2.3.

Immunohistochemistry

P15 littermates of the indicated genotypes were anesthetized using isofluorane. Mice were cardioperfused with ~10 ml PBS followed by ~10 ml 4% paraformaldehyde (PFA). Tissues were post-fixed (brains overnight, optic nerves for 15 min) in 4% PFA. Tissues were then cryoprotected in 10% sucrose followed by 30% sucrose overnight, flash frozen in 2-methylbutanol, and stored at -80˚C. Optic nerves were embedded in O.C.T. (Tissue-Tek) prior to freezing. Longitudinal 10 µm optic nerve sections and 20 µm coronal brain sections were cut on a Leica cryostat and stored at -20˚C until processing for immunohistochemistry.

For immunohistochemistry, sections were dried and post-fixed for 10 min with 4% PFA, washed 3 times for 5 min each with 0.05 M phosphate buffer (PB), incubated in blocking buffer (10% goat or donkey serum as appropriate, 0.3% Triton X-100, 0.1% PB) for ≥ 2 h in a humidified chamber. Brain sections were incubated with 1% SDS in PB for 5 min prior to washing steps. Sections were then incubated with primary antibodies (diluted in blocking buffer) overnight in a humidified chamber and washed 3 times for 10 min with 0.1% PB. From this point all steps were performed in the dark to minimize photobleaching of secondary antibodies. Sections were incubated with AlexaFluor-conjugated secondary antibodies (diluted in blocking buffer) for 2 h, washed 3 times for 10 min in 0.1% PB, dried, and coverslips were mounted using ProLong Gold anti-fade

reagent (Life Technologies). Finally, brain sections were incubated with DAPI for 20 min before mounting.

Sections were imaged using a Nikon A1R confocal microscope with Nikon NIS-Elements AR software located in the University of Michigan Department of Pharmacology using either a 60x NA 1.40 oil objective or a 20x NA 0.75 dry objective. Optic nerve sections were imaged using 3.1x digital zoom and Nyquist settings. All other settings were identical for all sections imaged in each experiment. For each optic nerve section, ≥3 single-section images were taken for analysis. Confocal images spanning 3 μm were acquired at 0.15 μm intervals and flattened using maximal signal for presentation in Figure 2.5. Images were analyzed as described below. Cortical and cerebellar confocal images spanning 10 μm were acquired at 0.175 μm intervals (for 60x) or 1.1 μm intervals (for 20x) and flattened using maximum signal for presentation in Figures 2.6 and 2.7.

Quantification of β1 immunofluorescence

For node of Ranvier studies, optic nerves from 4-6 animals per genotype were analyzed. Each animal was stained in at least 3 of 4 total independent immunohistochemistry experiments, with at least 2 sections (4 optic nerves) per animal used in each experiment. Using NIS-Elements Advanced Research software (Nikon), the “region of interest” function was used to outline the area of each complete node in each image. In this step, only anti-PAN VGSC and anti-Caspr signals were made visible, thus blinding the observer to the anti-β1 signal. The software was then used to quantify the average anti-β1 and anti-PAN VGSC signal intensities for each region of

interest. To remove nodes that were out of the plane of focus, nodes with the lowest 20% of anti-PAN VGSC signal were discarded prior to analysis. The average anti-β1 signal intensity per node for each optic nerve sample was used in final analysis (4 optic nerves per animal, per experiment). These values were normalized by setting the mean of all WT animals and the mean for all KO animals for the experiment to 1 and 0, respectively, using the “normalize” function in GraphPad Prism. Normalized values were analyzed using a Linear Mixed Model analysis performed using SPSS Statistics software (IBM) to account for variation between experiments as well as for variation between genotypes. The four comparisons indicated in Figure 2.5 B were determined using this analysis and then correcting for multiple comparisons by multiplying each p-value by the number of comparisons.

For AIS experiments, 3-4 animals per genotype were used, and 2-3 brain sections per animal per region were imaged for analysis. In all cases, sections obtained from the same locations relative to Bregma were chosen. For cortex, imaging was done in the same region in both layer 2/3 and layer 5/6 of the somatosensory cortex, with one image per section per region for each animal. For cerebellum, 3 images per section for each animal were obtained from the same regions of the simple lobule of the cerebellum. Images were imported into NIH ImageJ using the BioFormats plugin and flattened as described above. For each image, AISs were first identified as regions of linear ankyrinG immunolabeling and then evaluated for coincident linear β1 immunolabeling using the Colocalization Finder plugin for ImageJ, followed by visual reassessment of each identified AIS for confirmation. AISs positive for β1 were counted

and results expressed as percent of positive AISs per field of view. Due to unequal number of animals per genotype, statistical Analysis of Variance was not appropriate. Therefore the percent of positive AISs per field of view was analyzed using a Linear Mixed Model Analysis performed using SPSS Statistics software (IBM). P-values were corrected for multiple comparisons by multiplying by the number of comparisons.

Statistics

All statistical analyses were performed using GraphPad Prism, unless otherwise indicated, with significance defined as $P < 0.05$.

Results

Scn1b$^{+/W}$ mice are more susceptible to thermal seizures than *Scn1b*$^{+/-}$ mice

To ask whether the *SCN1B-C121W* GEFS+ mutation results in simple loss-of-function or whether it confers a deleterious gain-of-function *in vivo*, we compared mice expressing the *Scn1b* null allele (Chen et al., 2004) with mice expressing the human *SCN1B-C121W* GEFS+ knockin allele (Wimmer et al., 2010), both congenic on the C57Bl/6 strain. Throughout the manuscript, the heterozygous and homozygous animals from these strains are indicated as *Scn1b*$^{+/-}$, *Scn1b*$^{-/-}$, *Scn1b*$^{+/W}$, and *Scn1b*$^{W/W}$, respectively. Previous work has shown that *Scn1b*$^{+/W}$ GEFS+ mice seize at lower body temperatures than their WT littermates (Wimmer et al., 2010). We compared the thermal seizure susceptibility of the two mouse lines at time points between postnatal day (P)15 and 33 (P15, P16, P20-21, and P30-33) using a previously published protocol (Oakley et al., 2009). To evaluate potential genetic background effects between models, we tested WT littermates from both mouse lines for all thermal seizure, protein analysis, and immunostaining experiments presented in the manuscript. We observed no significant differences between *Scn1b*$^{+/+}$ mice derived from *Scn1b*$^{+/-}$ x *Scn1b*$^{+/-}$ litters, and *Scn1b*$^{+/+}$ mice derived from *Scn1b*$^{+/W}$ x *Scn1b*$^{+/W}$ litters. Thus, for analyses presented in the manuscript, results from these two WT groups were pooled, allowing a direct comparison of *Scn1b*$^{+/W}$ with *Scn1b*$^{+/-}$ mice. Overall, for both genotypes, younger mice had more severe seizures, seized at lower body temperatures, and had a shorter latency to first seizure compared to older mice of the same genotype (Figure 2.1 A, Table 2.1), suggesting that seizure susceptibility using this model is age-dependent, similar to other models of pediatric febrile seizures (Oakley et al., 2009).

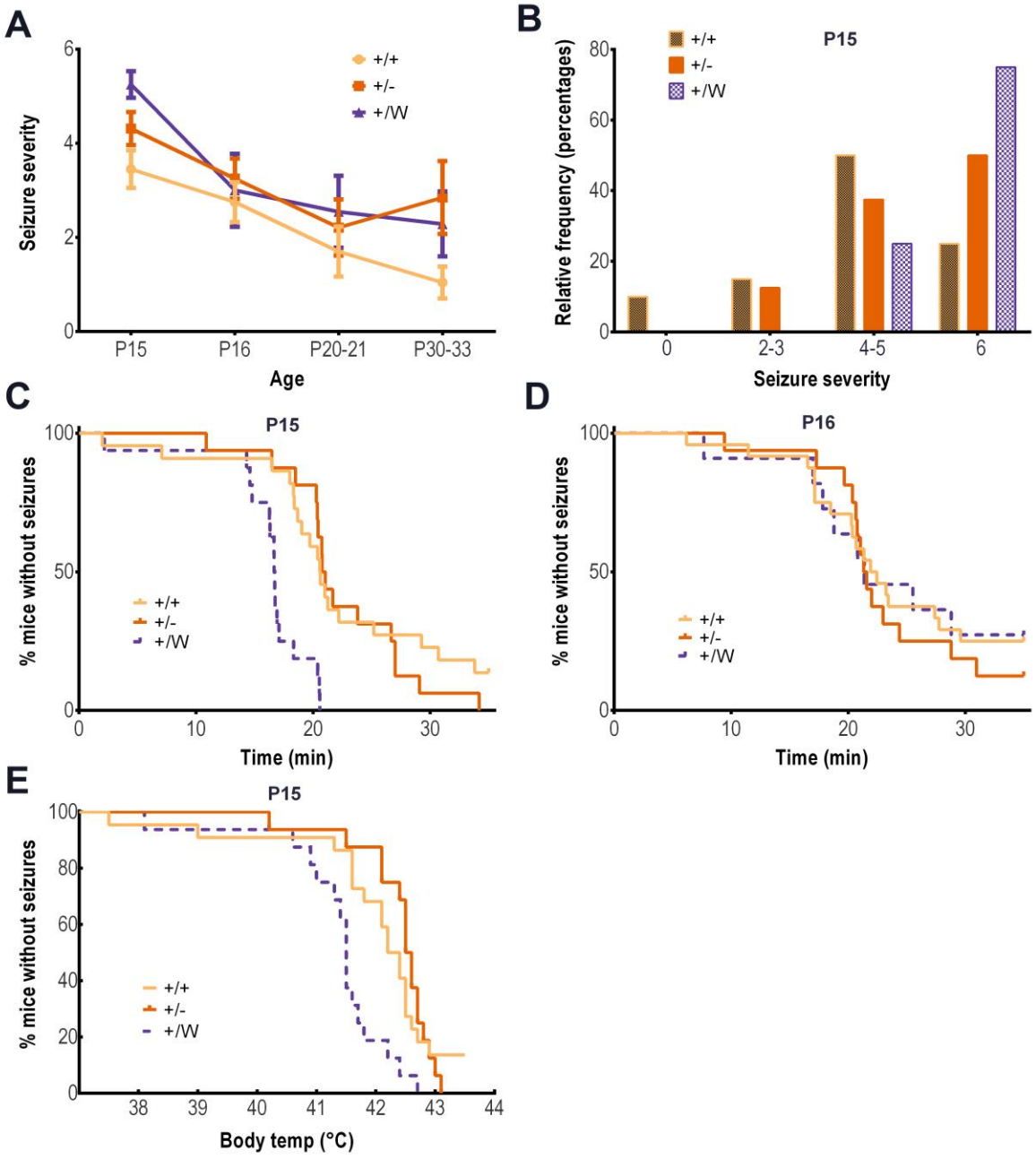

Figure 2.1 *Scn1b*$^{+/W}$ GEFS+ mice are more susceptible to heat-induced seizures than *Scn1b*$^{+/-}$ and *Scn1b*$^{+/+}$ mice.

Behavioral seizures were observed by an investigator blinded to genotype while using a heat lamp to incrementally increase body temperature. A. Seizure severity recorded for each animal, measured according to the modified Racine scale (mean ±SEM). Genotypes were compared at the same age. (Kruskal-Wallis; P<0.001, *Scn1b*$^{+/W}$ vs.

Scn1b$^{+/+}$; P<0.05 *Scn1b*$^{+/W}$ versus *Scn1b*$^{+/-}$). B. Histogram of the most severe seizures at P15 showing that 75% of *Scn1b*$^{+/W}$ GEFS+ mice experienced a seizure of Racine score 6, compared with 25% or 50% of *Scn1b*$^{+/+}$ or *Scn1b*$^{+/-}$, respectively. C - E. Survival curves to first observed seizure for P15 (C, E) and P16 (D) mice in relation to time (C, D) or body temperature (E). C. At P15, *Scn1b*$^{+/W}$ GEFS+ mice experienced seizures sooner in the observation period than the other genotypes (Mantel-Cox; P<0.0001, *Scn1b*$^{+/W}$ versus *Scn1b*$^{+/+}$; P<0.0001, *Scn1b*$^{+/W}$ versus *Scn1b*$^{+/-}$ mice). D. The difference in C was not observed at P16. E. *Scn1b*$^{+/W}$ GEFS+ mice seized at lower body temperatures than *Scn1b*$^{+/+}$ or *Scn1b*$^{+/-}$ mice (Mantel-Cox; P<0.0001, P<0.01, respectively). Number of animals for P15, P16, P20-21, and P30-33 groups were: *Scn1b*$^{+/+}$ (22, 24, 20, 25), *Scn1b*$^{+/-}$ (16, 16, 18, 23), *Scn1b*$^{+/W}$ (16, 11, 11, 17), respectively.

						P-values		
Time to First Seizure		WT	+/-	C/W		WT vs +/-	WT vs. CW	CW vs. +/-
P15	Median Survival	20.6'	20.91'	16.69'		0.605	****<0.0001	****<0.0001
P16		22.18'	21.45'	21.37'		0.5785	0.9288	0.583
P15 vs. P16	P-value	0.3877	0.4453	***0.0004	Mantel-Cox			
P20-21	Median Survival	undefined	undefined	26.05'			0.3818	
P30-33		undefined	undefined	undefined			0.3101	
Temp (˚C) at First Seizure								
P15	Median Survival	42.3	>42.5	41.5		0.7113	**0.0022	***0.0001
P16		42.55	42.6	42.5		0.199	0.6065	0.1677
P15 vs. P16	P-value	0.2643	0.7768	*0.019	Mantel-Cox			
P20-21	Median Survival	>42.5	>42.5	>42.5			0.5851	
P30-33		>42.5	>42.5	>42.5			0.4667	
Most Severe Seizure								
P15	Mean +/- SD (n)	3.45±0.40 (22)	4.313±0.35 (16)	5.250±0.28 (16)		ns	**	ns
P16		2.75±0.42 (24)	3.25±0.42 (11)	3.00±0.77 (16)	Kruskal-Wallis		ns	
P20-21		1.70±0.53 (20)	2.211±0.60 (19)	2.545±0.77 (11)			ns	
P30-33		1.042±0.34 (25)	2.846±0.78 (23)	2.286±0.69 (17)			ns	

Table 2.1 Statistical values for thermal seizure experiments.

Time and temperature to first seizure comparisons were made using Mann Whitney Comparison, median survival is given. For most severe seizure, mean ±SD is given. For the P20-21 and P30-33 groups, there is no significant difference between all groups for temperature to first seizure (P=0.3574, 0.1518) or time to first seizure (P=0.6382, 0.2517). All groups have >11 mice, see methods for descriptions of statistical analysis.

We observed a significant difference in seizure phenotype between *Scn1b*$^{+/W}$ GEFS+ and *Scn1b*$^{+/-}$ mice at P15. At this time point, *Scn1b*$^{+/W}$ mice seized more severely than either WT or *Scn1b*$^{+/-}$ mice (P = 0.0141, 0.0443, respectively; Figure 2.1 A,B). 75% of *Scn1b*$^{+/W}$ GEFS+ mice experienced prolonged convulsions (with or without death) during the experimental period (recorded as Racine score 6) compared to 50% of *Scn1b*$^{+/-}$ mice and 25% of *Scn1b*$^{+/+}$ mice (Figure 2.1 B). Furthermore, latency to first seizure and body temperature at first seizure, as represented by time-to-event curves, were both significantly reduced in *Scn1b*$^{+/W}$ GEFS+ mice compared to *Scn1b*$^{+/-}$ mice (P<0.0001, 0.01, respectively; Figure 2.1 C and E). Taken together, these data indicate that *Scn1b*$^{+/W}$ GEFS+ mice, but not *Scn1b*$^{+/-}$ mice, are significantly more susceptible to heat-induced seizures than WT. In comparison, at P16 and at older ages (P20-21 and P30-33), there were no significant differences in any thermal seizure parameters between *Scn1b*$^{+/W}$, *Scn1b*$^{+/-}$, or *Scn1b*$^{+/+}$ mice (Figure 2.1 A and D, Table 2.1). As discussed above, it is unlikely that the observed differences between *Scn1b*$^{+/W}$ and *Scn1b*$^{+/-}$ mice are the result of residual genetic background differences between the mouse lines. The observation that *Scn1b*$^{+/W}$ GEFS+ and *Scn1b*$^{+/-}$ mice are different in terms of thermal seizure susceptibility is strong evidence that the human *SCN1B-C121W* GEFS+ mutation is not a simple, loss-of-function allele and suggests instead that it confers a deleterious gain-of-function.

<u>β1-C121W protein is expressed at lower levels in brain and may be incompletely glycosylated compared to WT</u>

We next compared levels of β1-WT and β1-C121W polypeptide expression in brain membrane preparations from *Scn1b*$^{+/+}$ and *Scn1b*$^{W/W}$ mice, respectively. Separation of

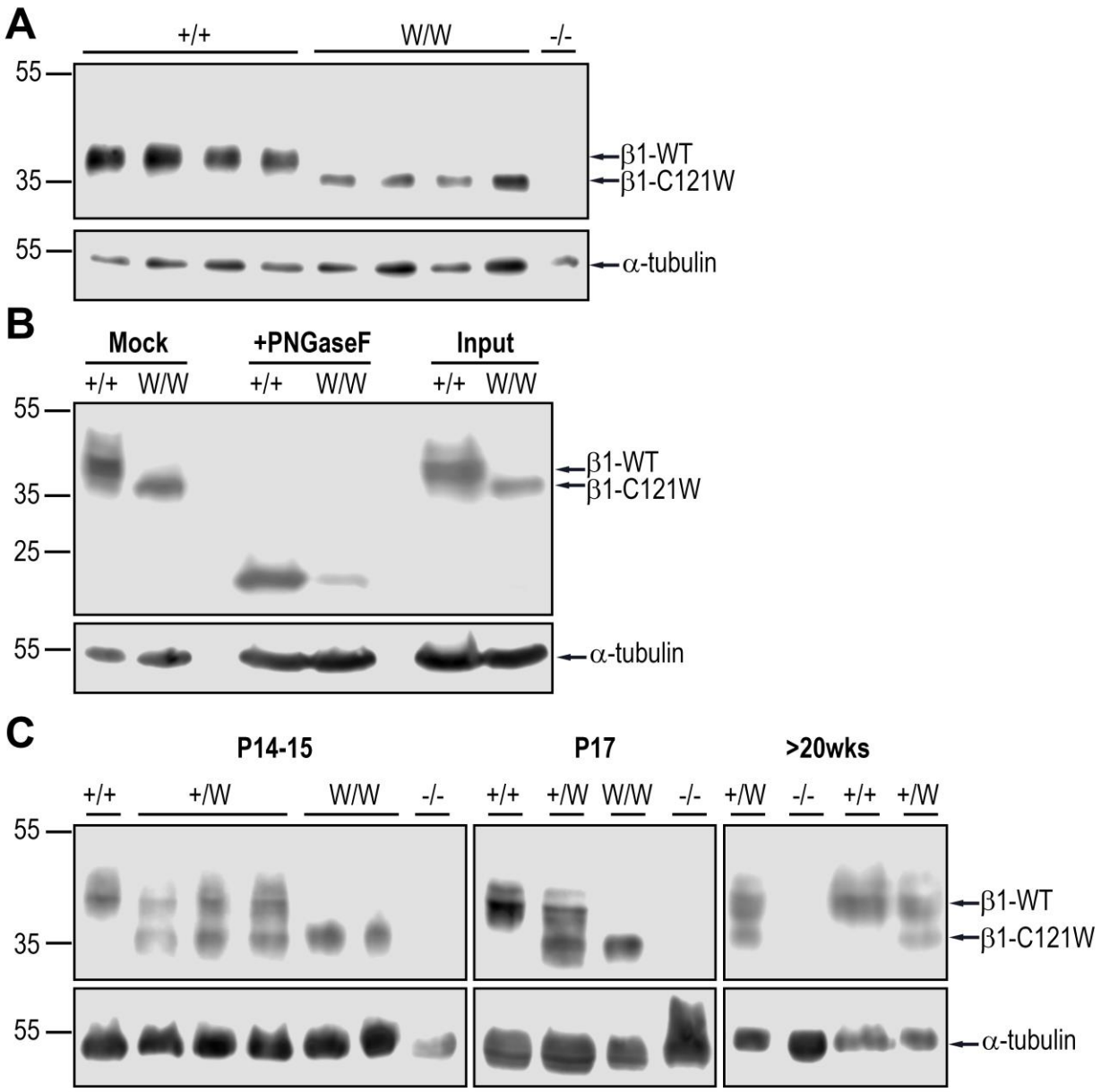

Figure 2.2 Comparison of β1-C121W and β1-WT protein expression.

Representative Western blots comparing β1 immunoreactivity in *Scn1b*$^{+/+}$ and *Scn1b*$^{W/W}$ mouse brain membrane preparations. β1-C121W polypeptides migrate at a lower apparent molecular weight than β1-WT separated on a 10% SDS-PAGE gel. Immunoreactive bands were quantified using densitometry. Each band density was first normalized to its corresponding α-tubulin signal, and β1 levels in *Scn1b*$^{W/W}$ mice were expressed as a percentage of β1 in *Scn1b*$^{+/+}$ mice. *Scn1b*$^{W/W}$ mice had 45±10% of

Scn1b$^{+/+}$ β1 expression (two-way ANOVA; P = 0.0001; three replicate experiments with 4 animals of each genotype). B. Representative Western blots showing mock digested, PNGaseF digested, and control brain membrane inputs from *Scn1b*$^{+/+}$ and *Scn1b*$^{W/W}$ brain separated on a 12% SDS-PAGE gel. β1-WT and β1-C121W polypeptides migrate at similar molecular weights following removal of N-linked glycosylation by PNGaseF (N=3). C. Representative Western blots, separated on a 15% SDS-PAGE gel, comparing levels of β1-WT and β1-C121W polypeptides in P14-15, P17, and >20wk old *Scn1b*$^{+/+}$, *Scn1b*$^{+/W}$, and *Scn1b*$^{W/W}$ mice. α-tubulin is shown as a loading control. Every *Scn1b*$^{W/W}$ mouse tested showed the lower molecular band only (P14-15, N=5; P17, N=5). Every *Scn1b*$^{+/W}$ sample tested showed both bands (P14-15, N=11; P17, N=6; >20 wks, N=4).

equivalent amounts of total protein on 10% SDS-PAGE gels followed by Western blotting with anti-β1 antibody showed that the level of β1-C121W expression in brain was approximately 50% of β1-WT (Figure 2.2 A). In addition, the β1-C121W immunoreactive band migrated at a lower apparent molecular weight compared to β1-WT (Figure 2.2 A). This molecular weight difference was not observed in our previous heterologous expression studies (Meadows et al., 2002) and thus may be tissue or species specific. PNGaseF digestion of brain membrane preparations prior to SDS-PAGE analysis, to remove N-linked glycosylation, abrogated this apparent molecular weight difference (Figure 2.2 B), suggesting differences in post-translational modification between β1-WT and β1-C121W proteins in brain *in vivo*. Finally, the absence of anti-β1 immunoreactive signal in the *Scn1b*$^{-/-}$ lane confirmed antibody specificity (Figure 2.2 A).

Because aberrant post-translational modification can alter protein targeting for degradation (Ellgaard and Helenius, 2003), we tested brain membrane preparations from mice at different ages for the presence of the β1-C121W lower molecular weight band. SDS-PAGE analysis of β1 polypeptides from *Scn1b*$^{+/+}$, *Scn1b*$^{+/W}$, and *Scn1b*$^{W/W}$ mice showed evidence for β1-C121W expression in all mice tested, even at > 20 weeks of age (Figure 2.2 C). Thus, β1-C121W polypeptide expression is maintained throughout mouse brain development and does not appear to decrease with age.

<u>β1-C121W polypeptides localize to the neuronal cell surface in vivo</u>

Cell surface expression is required for VGSC subunit function. Although viral expression of a GFP-tagged β1-C121W construct in mouse neurons predicted intracellular retention

(Wimmer et al., 2010), other studies of β1-C121W heterologous expression showed cell surface localization (Meadows et al., 2002; Patino et al., 2011). In addition, heterologous co-expression studies of β1-C121W and VGSC α subunits reported increased channel expression at the cell surface and/or increased sodium current compared to α subunits alone, predicting that β1-C121W localizes to the cell surface and retains the channel chaperone functions of β1 (Tammaro et al., 2002; Meadows et al., 2002; Rusconi et al., 2007; Baroni et al., 2013). To determine whether β1-C121W localizes to the cell surface of neurons *in vivo*, we performed surface biotinylation of cultured *Scn1b*$^{+/+}$ and *Scn1b*$^{W/W}$ cortical neurons. We detected β1 and β1-C121W polypeptides in both total cell lysate and biotinylated cell surface protein samples from *Scn1b*$^{+/+}$ and *Scn1b*$^{W/W}$ neurons, respectively (Figure 2.3). As a control, the cytosolic protein, HSP90, was detected in the cell lysate but not in the biotinylated samples, confirming the enrichment of cell surface proteins in the biotinylated fraction. These data suggest that endogenously expressed β1-C121W polypeptides are localized to the cell surface of cortical neurons *in vivo*.

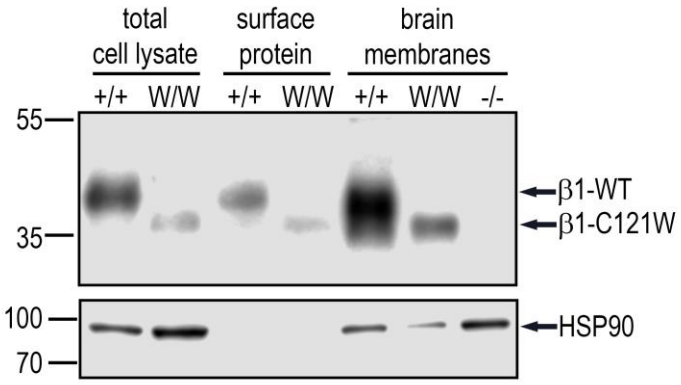

Figure 2.3 β1-WT and β1-C121W are expressed at the neuronal cell surface in cultured mouse cortical neurons.

Primary cortical neurons were cultured from *Scn1b*$^{+/+}$ and *Scn1b*$^{W/W}$ mice. At 16 DIV, surface proteins were labeled with biotin as described in Methods. An aliquot of total cell lysate was reserved prior to performing immunoprecipitation with streptavidin beads to enrich for cell surface proteins. Total cell lysate for *Scn1b*$^{+/+}$ and *Scn1b*$^{W/W}$, along with control brain membrane samples were separated on a 10% SDS-PAGE gel and immunoblotted with anti-β1 and anti-HSP90 antibodies. Anti-HSP90 immunoreactivity was used as an internal control to ensure enrichment of surface proteins in the biotinylated fraction. N=2

β1-C121W association with VGSC α-subunits is not detectable

A critical role for β1 subunits in brain is sodium current modulation via association with VGSC α-subunits (Chen et al., 2004; Brackenbury et al., 2010). Previous studies showed that overexpressed, recombinant β1-C121W protein could be co-immunoprecipitated with $Na_v1.1$, $Na_v1.2$, or $Na_v1.3$ α-subunits from solubilized, transfected cell lines (Meadows et al., 2002; Aman et al., 2009). However, these results may not reflect *in vivo* association of these subunits due to artifacts of heterologous overexpression. We therefore performed co-immunoprecipitation assays from mouse brain membrane preparations using anti-PAN-VGSC antibody followed by anti-β1 antibody to assess α-β1 association. We detected α–β1 but not α–β1-C121W association in these samples, suggesting that β1-C121W does not associate with brain VGSC α subunits *in vivo* (Figure 2.4 A). Because the level of β1-C121W polypeptide expression is approximately 50% of the level of β1-WT in mouse brain (Figure 2.2 A), we repeated the co-immunoprecipitation experiment using twice the amount of *Scn1b*$^{W/W}$ starting material. In spite of this increase, we did not detect β1-C121W and VGSC α-subunit association by co-immunoprecipitation (Figure 2.4 B). Thus, while the *Scn1b*-C121W mutation does not affect β1 cell surface expression *in vivo*, it does appear to weaken or disrupt VGSC α-β1 association.

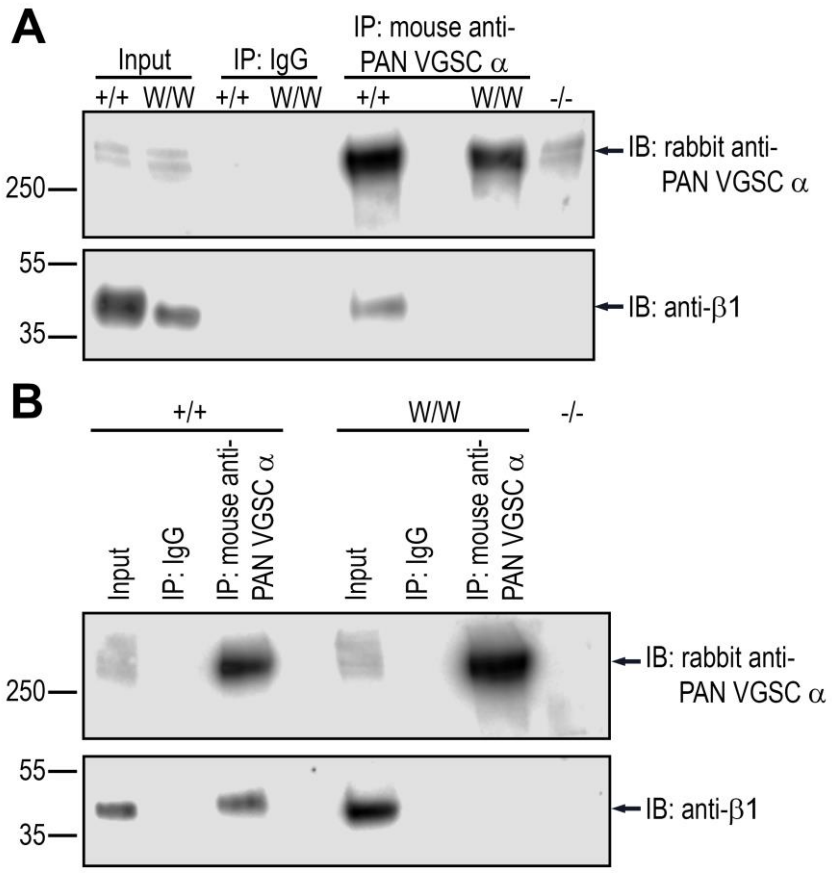

Figure 2.4 β1-C121W association with VGSC α-subunits is not detectable.

Brain membrane proteins from P15 *Scn1b*$^{+/+}$ and *Scn1b*$^{W/W}$ animals were immunoprecipitated (IP) with either mouse IgG or mouse antibody against PAN VGSC α subunit. Input samples, IP samples for each genotype, and a control *Scn1b*$^{-/-}$ membrane sample were separated on a 4-15% SDS-PAGE gel and immunoblotted with rabbit anti-PAN VGSC and anti-β1 antibodies. A. Representative Western blot of PAN VGSC-β1 co-immunoprecipitation using equivalent amounts of membrane proteins for each genotype. N=3. B. Representative Western blot of PAN VGSC-β1 co-immunoprecipitation using twice as much *Scn1b*$^{W/W}$ as *Scn1b*$^{+/+}$ membrane protein, to have equivalent amounts of β1 protein in the samples (see Figure 2.2). Input samples were loaded in the same ratio to reflect the difference in starting protein. N=1.

β1-C121W polypeptides differentially localize to neuronal subcellular domains

VGSC β1 subunits co-localize with VGSC α subunits at the AIS and nodes of Ranvier *in vivo* (Chen et al., 2004; Brackenbury et al., 2010; Wimmer et al., 2015). β1-mediated cell adhesive interactions may be particularly important at the nodes of Ranvier, as *Scn1b* null mice exhibit dysmyelination, reduced numbers of nodes, and disruption of axo-glial cell-cell contact in a subset of neurons (Chen et al., 2004). Thus, we asked whether β1-C121W is localized to these axonal subcellular domains *in vivo*.

We performed fluorescence immunohistochemistry of longitudinally sectioned WT and mutant mouse optic nerve. We found the level of β1 immunofluorescence was significantly decreased at nodes of Ranvier in *Scn1b*$^{W/W}$ mice compared to WT, and similar to that observed in *Scn1b*$^{-/-}$ mice (Figure 2.5 A and B). Quantification of anti-β1 optic nerve nodal immunofluorescence signal across genotypes showed that *Scn1b*$^{+/W}$ levels were lower than *Scn1b*$^{+/+}$, but higher than *Scn1b*$^{+/-}$ (Figure 2.5 B).

We next examined β1-WT and β1-C121W immunofluorescence localization to the AIS in multiple brain regions. Anti-β1 immunofluorescence staining revealed a high percentage of β1 positive AIS domains in cortical layer II and VI neurons and in cerebellar Purkinje neurons in *Scn1b*$^{+/+}$, *Scn1b*$^{+/-}$, and *Scn1b*$^{+/W}$ mice (Figure 2.6 A-C, J-L, D-F). The anti-β1 antibody used for these experiments was directed against an extracellular *Scn1b* epitope and specifically detected both β1-WT and β1-C121W polypeptides on Western blots (Figure 2.6 Q). In Figure 2.6, the left micrograph in the panel for each cortical region is a merged image showing staining for the AIS marker

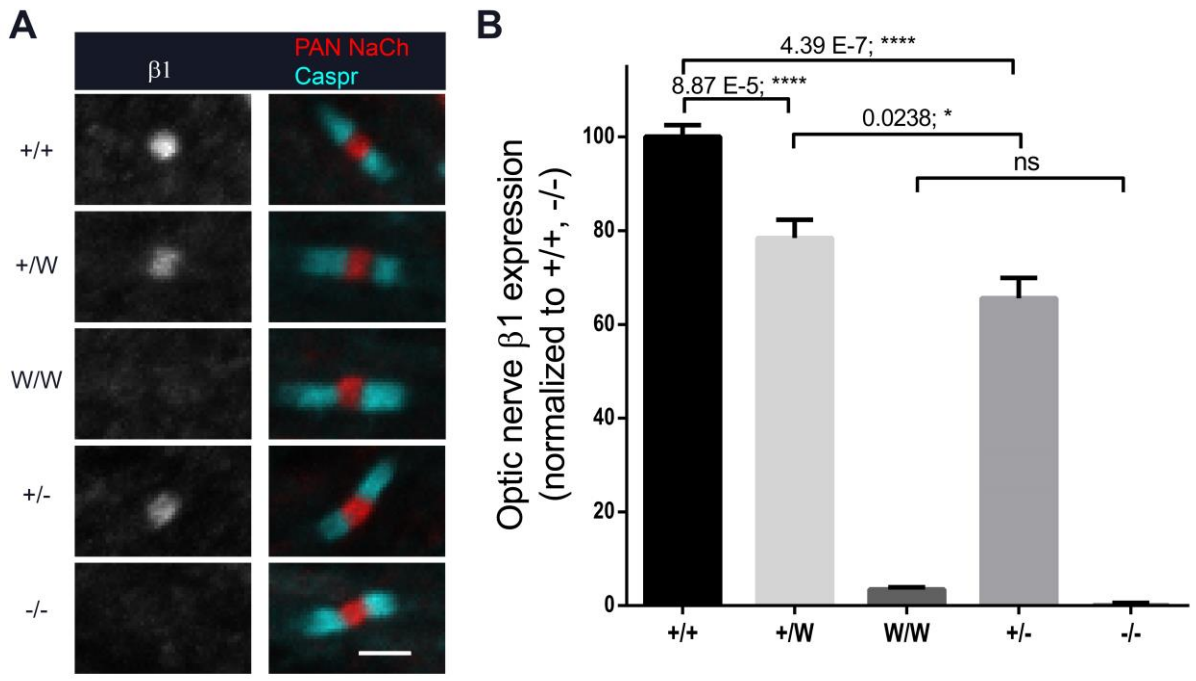

Figure 2.5 β1-C121W is not expressed at optic nerve nodes of Ranvier.

A. Representative images showing that *Scn1b*$^{+/W}$ and *Scn1b*$^{+/-}$ mice have decreased anti-β1 immunofluorescence compared to WT. β1 immunofluorescence in *Scn1b*$^{W/W}$ optic nerve sections is not significantly different from *Scn1b*$^{-/-}$. B. Quantification, as described in Methods, of anti-β1 immunofluorescence at optic nerve nodes of Ranvier. Data represent 4 independent immunohistochemistry experiments, with 4-6 animals per genotype in total. Each animal was tested in at least 3 experiments. Linear Mixed Model analysis was used to make comparisons between genotypes, see Methods for further details. Scale bar: 2 μm.

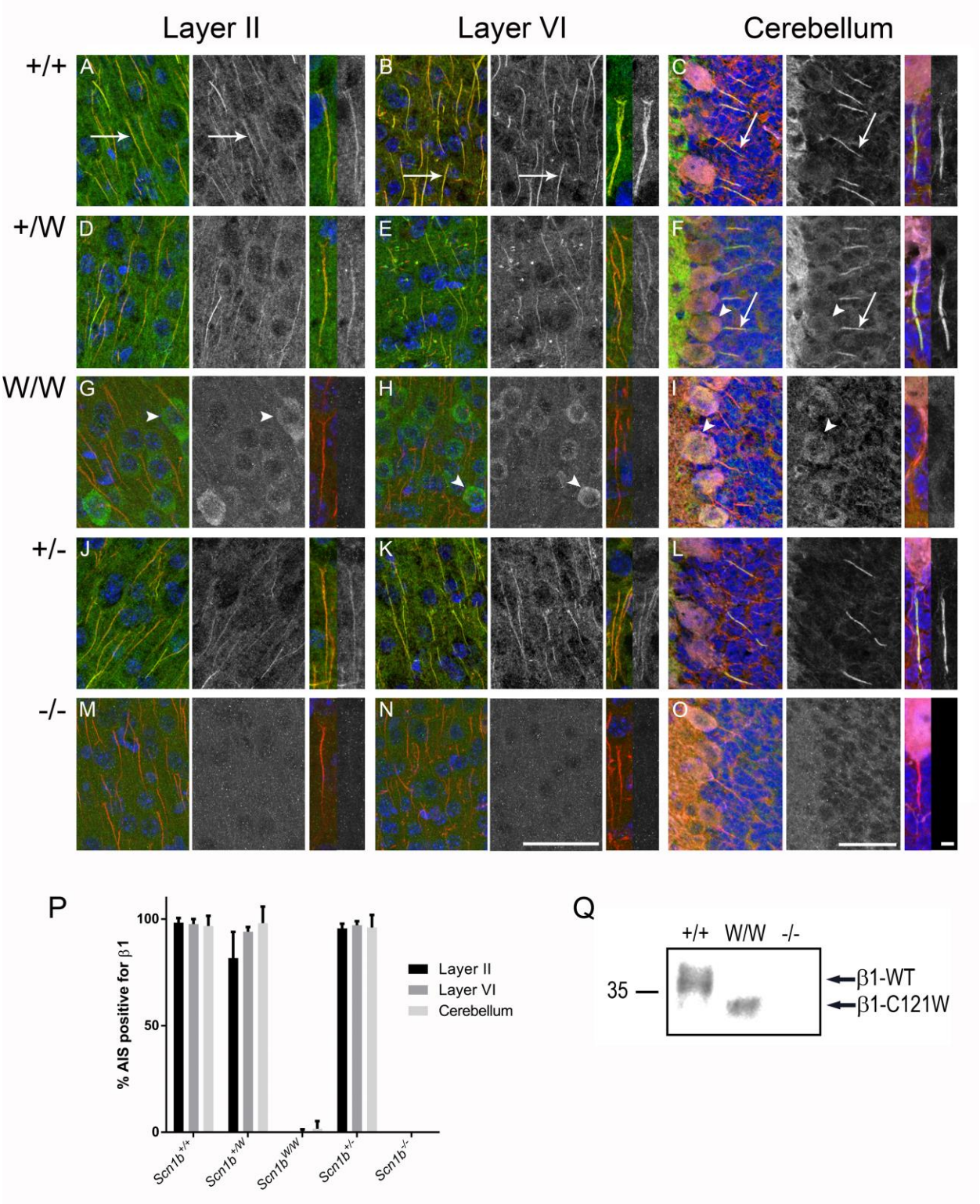

Figure 2.6 β1-C121W is not expressed at cerebellar or cortical axon initial segments.

Representative confocal images of cortical layers II (A, D, G, J, M) and VI (B, E, H, K,

N) and Purkinje cells in the cerebellum (C, F, I, L, O) of *Scn1b*$^{+/+}$ (A-C), *Scn1b*$^{+/W}$ (D-F), *Scn1b*$^{W/W}$ (G-I), *Scn1b*$^{+/-}$ (J-L), and *Scn1b*$^{-/-}$ (M-O) mice. For each genotype and cortical region, the left panel is a merged image of anti-ankyrinG (red), DAPI (blue), and anti-β1 (green) staining; the middle panel is anti-β1 (white) staining; and the right panel is a higher magnification image of a single AIS with the merged image on the left and β1 staining alone on the right. For cerebellum, merged images show anti-AnkG (red)/β1 (green)/calbindin (magenta)/DAPI (blue) staining. Arrows (A, B, C, F) indicate examples of ankyrinG-positive, β1-positive AISs. Arrowheads (F, G, H, I) indicate examples of β1-positive soma in *Scn1b*$^{+/W}$ and *Scn1b*$^{W/W}$ mice. *Scn1b*$^{W/W}$ and *Scn1b*$^{-/-}$ mice showed no β1 immunofluorescence at the AIS. Scale bars: large = 50 μm, small = 10 μm. Three mice of each genotype were tested. (P) Quantification of AISs positive for β1 immunofluorescence. For all regions observed, *Scn1b*$^{W/W}$ mice were comparable to *Scn1b*$^{-/-}$ mice and had a >95% reduction in β1+ AISs compared to *Scn1b*$^{+/+}$ mice ($P<0.0001$). In layer II and VI, *Scn1b*$^{+/W}$ mice had slightly fewer β1+ AISs compared to *Scn1b*$^{+/+}$ and *Scn1b*$^{+/-}$ mice (layer II: 16.6±2.0%, $P<0.0001$, 14.0±2.3%, $P<0.0001$; layer VI: 3.7±0.8%, $P<0.0001$, 3.1±0.9%, $P=0.007$, respectively). (q) Western blot showing β1 immunoreactivity in brain membranes from *Scn1b*$^{+/+}$, *Scn1b*$^{W/W}$, and *Scn1b*$^{-/-}$ mice using the D9T5B anti-β1 antibody used for immunofluorescence in Figure 2.6 and Figure 2.7.

ankyrinG (red, arrows in Figure 2.6 A and B), β1 (green), and DAPI (blue), the center micrograph shows anti-β1 staining alone (white), and the right micrograph shows side-by-side zoomed images of a single AIS showing merged anti-AnkG/β1/DAPI and anti-β1 staining, respectively. In panels showing cerebella, anti-calbindin staining (magenta) was used as a marker of Purkinje neurons, with the leftmost micrograph showing merged anti-AnkG (red, arrows in Figure 2.6 C and F)/β1 (green)/calbindin (magenta)/DAPI (blue) staining, followed by anti-β1 staining alone (white) and side-by-side zoomed images of a single AIS showing merged anti-AnkG/β1/calbindin/DAPI and anti-β1 staining, respectively. In *Scn1b*$^{W/W}$ cortical and Purkinje neurons, anti-β1 staining was observed at the soma (arrow heads) but not at the AIS (Figure 2.6 G-I). Both somal (arrowhead) and AIS (arrow) anti-β1 staining were observed in *Scn1b*$^{+/W}$ sections (Figure 2.6, D-F). These results suggest that mutant β1-C121W subunits do not prevent the translocation of WT β1 subunits to the axon. Anti-β1 staining was absent in *Scn1b*$^{-/-}$ brain sections, as expected, demonstrating antibody specificity (Figure 2.6, M-O). Quantification showed an absence of β1-positive AISs in layer II, VI, and cerebellar *Scn1b*$^{W/W}$ sections compared to *Scn1b*$^{+/+}$ and *Scn1b*$^{+/W}$ mice (Figure 2.6 P). There was also a slight, but significant, reduction in β1-positive AISs in layer II and VI *Scn1b*$^{+/W}$ sections compared to *Scn1b*$^{+/+}$ and *Scn1b*$^{+/-}$. Staining of cortical brain sections with a different anti-β1 antibody(Oyama et al., 2006) (used in (Wimmer et al., 2015)) also showed β1-positive AISs in *Scn1b*$^{+/+}$ neurons in layers II and VI, similar to those in Figure 2.6 A-B (data not shown). However, the large amount of non-specific nuclear staining observed with this antibody precluded detection of cell body staining in *Scn1b*$^{+/W}$ and *Scn1b*$^{W/W}$ mice (data not shown) and explains why this was not reported

previously (Wimmer et al., 2015). Anti-β1 staining observed in neuronal cell bodies in *Scn1b*$^{W/W}$ cortical neurons was layer specific. Figure 2.6 G-I shows limited cell body staining in layers II and VI. In contrast, a much higher proportion of β1-positive cell bodies were Ctip2-positive neurons in layer V (Figure 2.7, B, C, G, H), suggesting that β1-C121W localization may be neuronal cell type specific.

Taken together, our immunofluorescence and cell surface biotinylation results suggest that β1-C121W reaches the neuronal cell surface *in vivo*, but is not translocated to axonal subcellular domains and instead remains localized to neuronal soma.

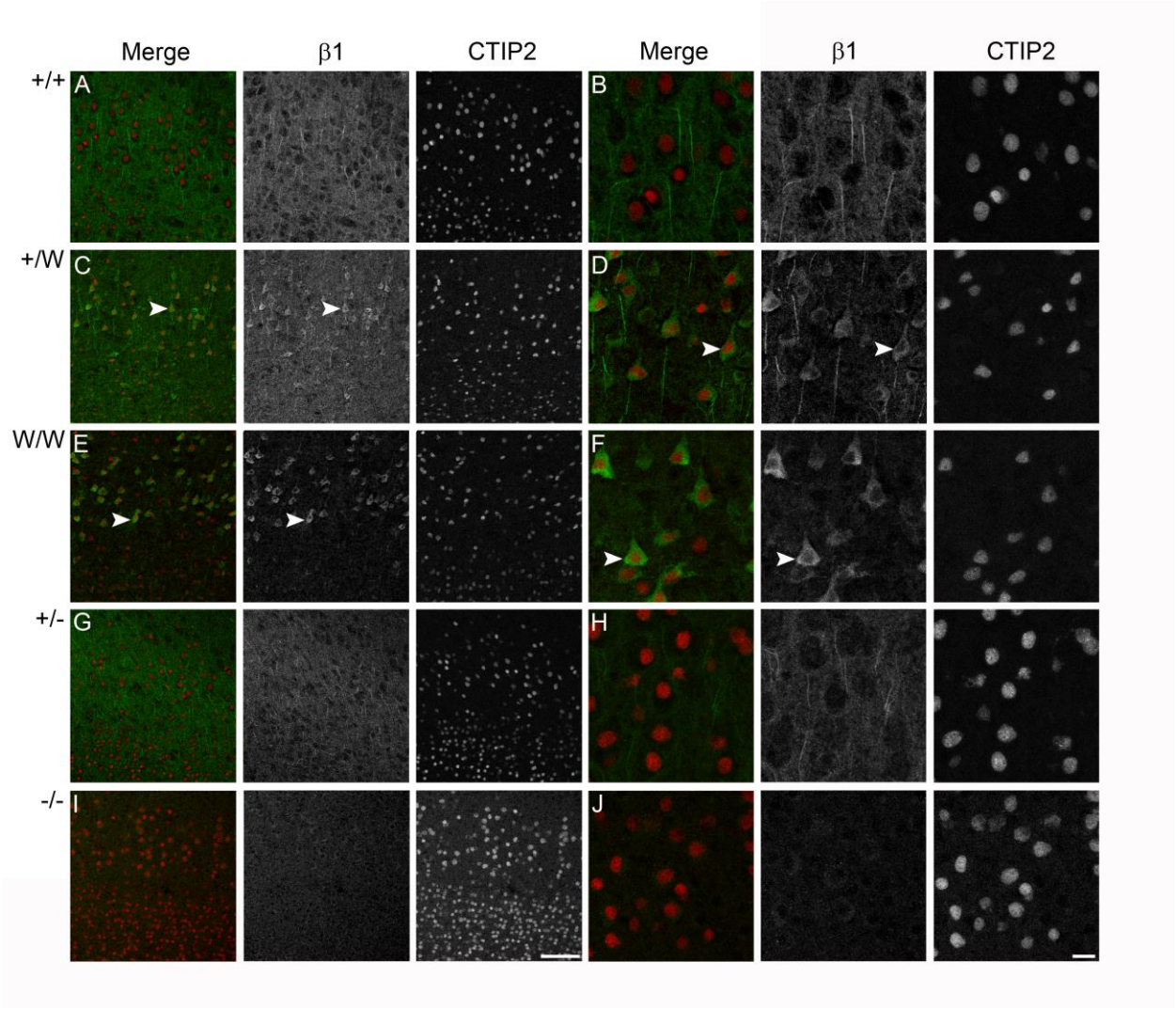

Figure 2.7 β1-C121W is localized at the soma of layer V cortical neurons

Representative confocal images of cortical layer V from *Scn1b*$^{+/+}$ (A, B), *Scn1b*$^{+/W}$ (C, D), *Scn1b*$^{W/W}$ (E, F), *Scn1b*$^{+/-}$ (G, H), and *Scn1b*$^{-/-}$ (I, J) mice. The left panel for each genotype is a merged image of anti-Ctip2 (red), and anti-β1 (green) staining, and the following two panels show anti-β1 (white) followed by anti-Ctip2 (white) staining. Arrowheads indicate examples of β1-positive soma in *Scn1b*$^{+/W}$ and *Scn1b*$^{W/W}$ mice. Lower magnification images (A, C, E, G, I) show the layer specificity of β1-positive soma. Higher magnification images (B, D, F, H, J) showing Ctip2-positive layer V neurons are also presented. Scale bar (A, C, E, G, I): 100 μm. Scale bar (B, D, F, H, J): 20μm. Three mice of each genotype were tested.

Discussion

The objective of this study was to determine the mechanism of how the *SCN1B-C121W* GEFS+ mutation alters VGSC β1 function *in vivo*. To address this question, we used a multi-disciplinary approach that included behavioral, biochemical, and immunofluorescence analysis of transgenic mouse models. We report that *Scn1b*$^{+/W}$ GEFS+ mice are more susceptible to thermally induced seizures than *Scn1b*$^{+/-}$ or *Scn1b*$^{+/+}$ mice. Biochemically, β1-C121W polypeptides are expressed at lower levels than β1-WT in brain and migrate at a lower apparent molecular weight on SDS-PAGE gels. PNGase digestion followed by Western blot analysis shows that this molecular weight difference is likely due to incomplete glycosylation of the mutant β1 polypeptide *in vivo*. Surface biotinylation assays showed that β1-C121W polypeptides are expressed at the cell surface of cultured *Scn1b*$^{W/W}$ cortical neurons. Immunofluorescence confocal microscopy demonstrates that β1-C121W localizes to the neuronal cell body in *Scn1b*$^{W/W}$ brain sections, however, the subcellular localization of these mutant β1 subunits is limited to the soma and precluded from the axon. Our available model and tools do not allow us to distinguish between WT and mutant β1 subunits by immunofluorescence in *Scn1b*$^{+/W}$ mice and thus to determine whether mutant β1 subunits also translocate to the axon in the presence of WT subunits. The observation that the level of anti-β1 immunofluorescence at optic nerve nodes of Ranvier is higher in *Scn1b*$^{+/W}$ GEFS+ compared to *Scn1b*$^{+/-}$ mice may suggest that WT and mutant β1 subunits may be present together in axonal domains. Alternatively, however, the observation of a small, but significant, reduction in β1-positive AISs in layer II and VI *Scn1b*$^{+/W}$ sections compared to *Scn1b*$^{+/+}$ and *Scn1b*$^{+/-}$ may suggest that

mutant β subunits may prevent a portion of WT β subunits from entering the axon. Finally, even though β1-C121W is expressed at the cell surface in *Scn1b*$^{W/W}$ neurons, its association with VGSC α subunits is disrupted as assessed by co-immunoprecipitation.

The crystal structure of the VGSC β1 Ig loop has not yet been solved. However, important information can be gleaned from the crystal structure of a VGSC β4 Ig loop containing a C to W mutation at residue 131, corresponding to β1-C121W (Gilchrist et al., 2013). Importantly, introducing this mutation in the disulfide cysteine bridge of β4, which is conserved in all five VGSC β subunits, did not disrupt protein folding or plasma membrane trafficking compared to β4-WT as assessed in *Xenopus* oocytes. However, the C to W mutation did disrupt the ability of β4 to modulate sodium current expressed by $Na_v1.2$ as well as result in potential alterations in β4 glycosylation (Gilchrist et al., 2013), similar to our present results for β1-C121W.

Our results, taken together with our previous data showing that β1-C121W cannot participate in *trans* homophilic cell-cell adhesion (Meadows et al., 2002), suggest that the *SCN1B-C121W* GEFS+ mutation confers a deleterious gain-of-function. We propose that in *Scn1b*$^{+/W}$ GEFS+ mice, non-functional β1-C121W subunits are expressed together with β1-WT subunits at the plasma membrane and thus effectively reduce the level of β1 function in neurons by diluting the density of WT subunits. β1-mediated *trans* homophilic cell-cell adhesion may be particularly disrupted by this mechanism, as WT-mutant or mutant-mutant β1 subunit pairs may be aligned, but not

associate, in *trans* on adjacent axons, resulting in areas of aberrant adhesion and fasciculation. In addition, we propose that mutant β1B subunits, which are normally soluble ligands for cell adhesion (Patino et al., 2011), are co-secreted with WT β1B subunit in *Scn1b*$^{+/W}$ developing brain, yet are non-functional and effectively change the functionality of secreted WT β1B subunits. This scenario is different than in *Scn1b*$^{+/-}$ neurons, in which only WT β1 and β1B subunits are expressed. In *Scn1b*$^{W/W}$ mice, which model the severe epileptic encephalopathy Dravet syndrome (Wimmer et al., 2010; Ogiwara et al., 2012) , all expressed β1 subunits are mutant and thus fail to associate with VGSC α subunits, fail to participate in cell-cell adhesion, and fail to translocate from the cell body to axonal subcellular domains. Thus, we propose that, while mutant β1 subunits are expressed at the neuronal cell surface in *Scn1b*$^{W/W}$ mice, this model is functionally similar to *Scn1b* null mice, which also model Dravet syndrome (Patino et al., 2011).

In our previous work we showed that covalent VGSC α-β2 association, via formation of an extracellular disulfide bond, is required for β2, but not α, subunit translocation to nodes of Ranvier (Chen et al., 2012). Our present results suggest that association with VGSC α subunits, although non-covalent (Hartshorne and Catterall, 1981), may be required for β1 translocation to axonal domains: We were unable to detect association between β1-C121W and VGSC α subunits and we did not detect β1-C121W at the AIS or nodes of Ranvier in *Scn1b*$^{W/W}$ mice. Thus, in a mechanism similar to α–β2 association, α–β1 association through extracellular domains may be required for proper

β subunit localization in neurons. We have previously proposed that β1 and β4 have opposing actions on neuronal excitability with β1 acting as a 'brake' via promotion of VGSC inactivation (Aman et al., 2009). We showed that β1-C121W was unable to exert these modulatory effects (Aman et al., 2009). Our results here suggest that the absence of mutant β1 subunit association with VGSC α subunits may partially explain hyperexcitability in *SCN1B-C121W*-linked epilepsies.

In addition to modulating VGSCs, β1 subunits are known to associate with voltage-gated potassium channels that express A-type current in neurons (Marionneau et al., 2012). An important future experiment will be to assess the effect of the *SCN1B-C121W* mutation on β1 association with $K_v4.2$ in *Scn1b*$^{W/W}$ brain. While we attempted these experiments, the solubilization conditions for immunoprecipitation of VGSCs and $K_v4.2$ channels using available antibodies were incompatible. Thus we were unable to determine whether β1-C121W subunits maintain their association with $K_v4.2$. In the future, with higher quality antibodies, we may be able to assess whether aberrant β1-Kv association also contributes to the GEFS+ phenotype.

Taken together, our studies provide evidence for a complex molecular mechanism leading to changes in excitability and thermal seizure susceptibility in *Scn1b*$^{+/W}$ GEFS+ mice compared to *Scn1b*$^{+/-}$ mice. Unlike other epilepsy-associated *SCN1B* mutations (Patino et al., 2009), *SCN1B-C121W* does not appear to cause intracellular retention and instead confers deleterious gain-of-function. Therefore, the mechanisms underlying *SCN1B*-linked epilepsy may be diverse, requiring the generation of specific animal

models of *SCN1B* epilepsy mutations to better understand β1 and β1B physiology. To date, 9 unique *SCN1B* mutations in epilepsy patients have been reported (O'Malley and Isom, 2015). Using transgenic mouse and human patient-derived induced pluripotent stem cell models and strategies similar to the present study, a better understanding of the affected molecular pathways may lead to the development of novel therapeutics for patients with *SCN1B*-linked epilepsy. Moreover, because *SCN1B* epilepsy mutations are largely inherited, rather than *de novo*, effective genetic counseling strategies can be developed.

Chapter 3. New avenues of discovery for *SCN1B-C121W* and β1 physiology

My thesis work emphasizes the importance of studying sodium channels in their native environment *in vivo*, with endogenous levels of expression and native channelome components. However, there are many questions that need to be addressed in future work. Based on my work, which builds on the work of others, *SCN1B-C121W* could alter normal physiology through a number of possible mechanisms as follows:

1. Disruption of β1/β1B-mediated homophilic cell adhesion. Heterologous expression studies have demonstrated that the C121W mutation disrupts β1-mediated *trans* homophilic adhesion (Meadows et al., 2002). As depicted in Figure 3.1, there are a number of other possible configurations for β1 and β1-C121W cell adhesive interactions in *Scn1b*$^{+/W}$ mice (or GEFS+ patients), including *cis* adhesion, which have not been explored

2. Aberrant neurite outgrowth and neuronal pathfinding. My data suggest that there are increased levels of β1 localization at optic nerve nodes of Ranvier *Scn1b*$^{+/W}$ mice compared to *Scn1b*$^{+/-}$. One possible explanation for this is that β1-WT can chaperone β1-C121W, as depicted in Figure 3.1 D, such that β1-C121W may be present in axonal subcellular domains such as the AIS, which are critical for b1-mediated neurite outgrowth (Brackenbury et al., 2008). In this scenario, non-functional β1-C121W subunits may dilute the density of β1-WT subunits at the

plasma membrane and thus effectively reduce the level of β1 function at the AIS. β1-mediated *trans* homophilic cell-cell adhesion may be particularly disrupted in this mechanism, as WT-mutant or mutant-mutant β1 subunit pairs may be aligned in *trans* on adjacent axons, resulting in areas of aberrant fasciculation.

3. Altered modulation of sodium and/or potassium current. My results show that β1-C121W does not associate with VGSC α subunits in brain membranes. This absence of association may open the door, so to speak, for modulation of I_{Na} by other β subunits or other compensatory mechanisms. As discussed in Chapter 2, our available tools precluded the investigation of β1-C121W association with K^+ channels, e.g. $K_v4.2$. Here, altered association would also be predicted to affect the excitation-inhibition balance.

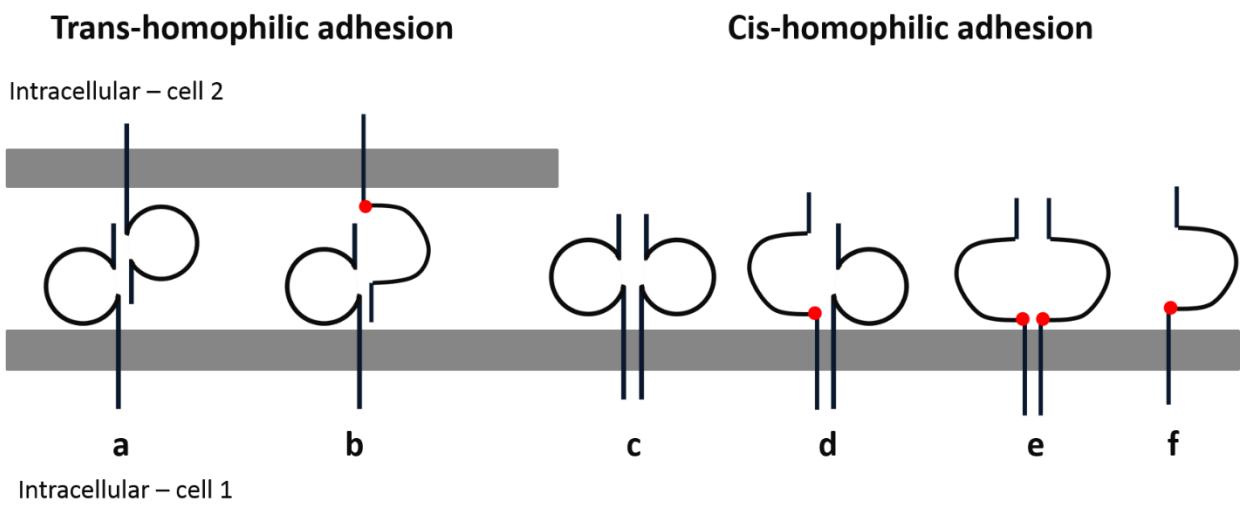

Figure 3.1 Possible homophilic β1 associations in Scn1b+/W mice.

All β1 trans- and cis-homophilic adhesion complexes which may occur in Scn1b+/W mice. Red circles indicate W121. A. β1-WT/β1-WT trans-homophilic adhesion is known to promote neurite outgrowth, as we have shown (Davis et al., 2004). B. It is unknown whether the β1-WT/β1-C121W trans-homophilic adhesion complex occurs, but this dimer could disrupt homophilic adhesion if β1-C121W is unable to stimulate the neurite outgrowth pathway. Similarly, complex d could make less β1-WT available to bind with VGSC α subunits, K+ channels, and cell adhesion partners. Complex C has been proposed, but it is difficult to show that this complex is present. If β1-C121W cis-dimers (E) or β1-C121W monomers (F) exist, our data suggests they do not bind VGSC α subunits.

Before discussing how each of these mechanisms might be tested, I would like to describe some of the available tools that could be used or developed to better answer these questions.

A difficult challenge in studying *Scn1b* is differentiating the physiological effects of β1 vs. β1B *in vivo*. *In vitro,* β1B has cell adhesive and channel specific VGSC α subunit modulatory functions, similar to β1 (Qin et al., 2003; Patino et al., 2011). However, the impact of these functions *in vivo* has yet to be explored. β1B in *Scn1b-C121W* mice also contains the C121W mutation and the role of β1B-C121W in *SCN1B-C121W* -associated epilepsy will also need to be investigated. This presents a complex, multi-faceted problem. There is no one approach that can address all of the complexities. Despite several attempts, currently available β1B antibodies recognize human but not mouse β1B and thus cannot be used to study β1B in mouse models *in vivo*. The anti-*Scn1b* antibodies used in my thesis, which we developed in collaboration with Cell Signaling Technology, are directed against extracellular or intracellular epitopes. To date, we have not observed differential staining patterns in mouse brain using these two antibodies. It is possible that β1 and β1B have identical sub-cellular localization patterns in brain. However, it is more likely that, because β1B is predominantly expressed in embryonic brain, the low levels of β1B protein in postnatal brain are undetectable. In a first attempt to address the functional roles of β1B, other members of our lab generated a BAC transgenic mouse expressing β1B, but not β1. When bred back onto the *Scn1b*$^{-/-}$ mice such that β1B but not β1 is expressed, mice have a phenotype that is indistinguishable from *Scn1b*$^{-/-}$ mice (paper in preparation). Therefore, β1B is not

sufficient to rescue *Scn1b* null epilepsy. It may be that the in vivo cell adhesive partner of β1B is β1 and thus expression of both gene products is essential for normal excitability. The next step will be to generate a β1B-specific knockout mouse line (that expresses β1 but not β1B) to further dissect the respective roles of each splice variant in normal physiology. One method by which splice-variant selective knockout mice have been successfully generated is to insert a preterm translational stop codon preceded by an ER-retention signal (KDEL) (Dours-Zimmermann and Zimmermann, 2012). In this study, placement of this sequence ablated synthesis of the splice variants containing the targeted exon, likely by KDEL-promoted intracellular degradation of the mutant fragment. To generate a β1B splice-variant specific knockout, we could insert a KDEL-stop codon after the end of exon 3, but prior to the stop codon for β1B, as indicated in Figure 3.2. The biggest challenge with this type of transgenic mouse is that we would need to ensure that splicing of β1 mRNA and regulation of β1 expression are not disrupted. To accomplish this, we would need to use a combination of *in situ* hybridization, RT-PCR, and immunofluorescence throughout early development to ensure that β1 is still expressed in the same developmental manner as *Scn1b*$^{+/+}$ mice.

Another challenge of studying β1 subunits is antibody sensitivity. Although the current antibodies we have are specific for β1, their affinity is such that we can only detect β1 *in vivo* in subcellular locations where β1 density is high. To solve this issue, we are generating a C-terminal V5 epitope-tagged β1 mouse using a CRISPR/Cas strategy in collaboration with the University of Michigan Transgenic Core. Testing will be essential to ensure similar developmental expression patterns and functionality of β1-V5

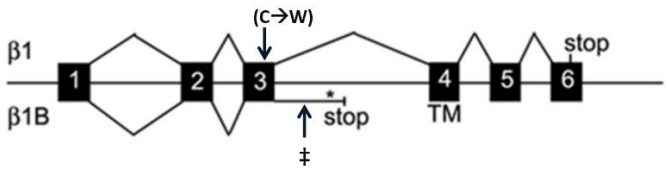

Figure 3.2 Topology of *Scn1b*.

The C121W mutation is located in exon 3, as indicated. ‡ indicates the proposed location for a premature translational stop codon preceded by an ER-retention signal (KDEL). This region is only included in β1B.

compared to β1-WT. Furthermore, we would need to ensure that β1B expression is not disrupted. With this mouse in hand, we will again use a CRISPR/Cas strategy to insert epilepsy mutations, including *SCN1B-C121W*, into this mouse. Because anti-V5 antibodies are very clean, have high sensitivity, and can be used for complex methodologies like immune-electron microscopy, this would allow us to understand *SCN1B*-linked epilepsy mutations *in vivo* with greater resolution and reliability. For example, we have shown evidence *in vitro* that β1 localizes to the axonal growth cone in cultured neurons (Brackenbury et al., 2008). Unfortunately, this cannot be detected *in vivo,* either because it does not occur or, more likely, because of insufficient antibody sensitivity.

All future mouse models will need to be thoroughly tested to ensure similar temporal and spatial expression of β1 and β1B compared to *Scn1b*$^{+/+}$ mice. Nevertheless, the advantages of studying sodium channel physiology *in vivo* are clear based on the cell-type specificity of heterologous cell assay results and the fact that generation of

transgenic mouse models has become much less time-consuming and expensive. It is accepted in our field that heterologous cell lines cannot replicate the neuronal channelome.

While mouse models have many advantages for studying epilepsy, mice are not small humans! Related GEFS+ patients with the same *SCN1B* mutation exhibit a wide variety of epileptic phenotypes (Table 1.2). This suggests that genetic background affects the epileptic phenotype. To account for this, we have generated human induced pluripotent stem cells (hiPSCs), derived from fibroblasts from a GEFS+ patient with p.C121W. This work was done in collaboration with Dr. Jack Parent and patient samples were provided by our collaborator, Dr. Ingrid Scheffer (Wallace et al., 1998). This powerful method allows us to study human GEFS+ neurons, with p.C121W in the presence of potential interacting proteins. We have previously used this technique in our laboratory, in a collaboration with Dr. Jack Parent and Dr. Miriam Meisler to study forebrain neurons derived from DS patients with *SCN1A* mutations (Liu et al., 2013). This approach will allow us to study the C121W mutation in native, human neurons in the presence of the patient's genetic background. By using mouse models and iPSC-derived neurons, we can directly compare the mouse and human disease models and uncover possible species-or mouse strain-dependent effects. Our hope is that by comparing both models we can identify common pathogenic mechanisms that lead to GEFS+ as well as understand which specific classes of neurons are represented by the iPSC neuronal cultures.

The models proposed above will help us address the following critical questions.

Does *SCN1B-C121W* disrupt β1/β1B homophilic interactions?

The differences we observed in β1 vs. β1-C121W glycosylation may impact homophilic and heterophilic β1/β1B cell adhesion. The structure of the β1 Ig loop is very similar to that of myelin P0 (McCormick). Homophilic interactions of myelin P0 require glycosylation of the P0 pair (Filbin and Tennekoon, 1993). Thus, changes in β1 glycosylation may underlie abrogation of β1-C121W/β1-C121W *trans*-homophilic interactions that we have previously reported (Malhotra et al., 2000; Meadows et al., 2002). However, what has not been explored is the remaining possible combinations of β1-WT and β1-C121W that could have aberrant function. β1-C121W/β1-WT *trans*-or *cis*-homophilic adhesion complexes also could decrease the amount of β1-WT available to modulate neuronal pathfinding or associate and modulate sodium or potassium channels (Figure 3.1). For example, it is known that VGSC complexes are very tightly packed at the AIS and nodes of Ranvier. If β1-C121W associates in *cis* with β1-WT associated with VGSC α subunits (Figure 3.1 D), the slight conformational difference of the β1-C121W domain could disrupt the packing. Similarly, it is hypothesized that at points of cell-cell adhesion, such as paranodal domains, cell adhesion molecules are packed in a 'zipper-like' configuration, where molecules are in *cis* and *trans* configurations at the same time. Models suggest that this arrangement increases adhesion strength (Kunz et al., 2002). Therefore, if β1-C121W can associate in *cis* or *trans* with β1-WT, this tight adhesion pattern could be disrupted.

The first step in understanding whether these mechanisms are occurring in *Scn1b*$^{+/W}$ mice is to determine whether β1-C121W and β1-WT associate in *trans*. We could assay this using two populations of *Drosophila* S2 cells: one transfected with EGFP and β1-

C121W and the other transfected with RFP and β1-WT. If β1-C121W and β1-WT can associate in *trans*, mixing of the two cell lines would result in aggregates containing green and yellow fluorescence. In contrast, if β1-WT associates with itself but not with β1-C121W, then cell aggregates will contain only red fluorescence and green fluorescent cells will remain in suspension. A caveat here is that the absence of mixed cell aggregation in this experiment would only eliminate the possibility of WT-mutant *trans*-homophilic adhesion and does not test the possibility of *cis*-homophilic adhesion between these two molecules (Figure 3.1 B vs. D). Next, we would need to determine where β1-C121W and β1-WT co-localize in *Scn1b*$^{+/W}$ mouse brain and are thus available to associate *in vivo*. My data show increased anti-β1 staining at the nodes of Ranvier in *Scn1b*$^{+/W}$ mice compared to *Scn1b*$^{+/-}$ mice. However, *Scn1b*$^{W/W}$ mice showed no specific anti-β1 staining at nodes. These data suggest that translocation to nodes β1-C121W may be facilitated by β1-WT in *Scn1b*$^{+/W}$ mice and that these two subunits may associate in *cis*. Alternatively, it is also possible that β1 localization at the nodes of Ranvier is upregulated in *Scn1b*$^{+/W}$ by some other compensatory mechanism not present in *Scn1b*$^{+/-}$ mice. Therefore, to distinguish these possibilities, we could use the proposed β1-C121W-V5 mice, and using the same method to generate β1-HA mice. By crossing these two lines we would generate mice which express β1-C121W-V5 and β1-WT-HA. Similar to Figures 2.5 – 2.7, we could use immunohistochemistry to determine whether V5-tagged β1-C121W and HA-tagged β1-WT is present at AISs and nodes of Ranvier. We could also immunoprecipitate using a V5 antibody to specifically pull down β1-C121W-Fc and immunoblot for HA to determine whether β1-C121W associates with β1-WT in vivo. Together these experiments would help elucidate the effect of p.C121W

on β1 trans- and cis-homophilic adhesion, which would help interpret the results from electrophysiology and neurite outgrowth experiments. For example, if β1-C121W does not traffick to nodes of Ranvier or AISs, but does associate with β1-WT, then current or action potential changes are likely due to having less β1-WT available.

Does *Scn1b-C121W* result in aberrant neurite outgrowth, neuronal pathfinding, or fasciculation defects?

Scn1b deletion results in increased numbers of dentate granule cells (DGCs) and newborn DGCs in the hilus of the dentate gyrus at P5, prior to seizure onset and observation of spontaneous firing (Brackenbury et al., 2013). At P14, electrophysiological recordings show increased spontaneous firing and neuronal excitability in *Scn1b*$^{-/-}$ cortical and hippocampal slices compared to WT (Patino et al., 2009) (Brackenbury et al., 2013). By this age, *Scn1b* null mice have defects in cerebellar granule neuron (CGN) migration and fasciculation, corticospinal tract (CST) pathfinding abnormalities, and increased proliferation of the external granular layer (EGL) of the cerebellum (Brackenbury et al., 2008). These developmental changes may be due in part to the loss of β1 trans-homophilic adhesion in *Scn1b* null mice, which is required for CGN β1-mediated neurite outgrowth (Davis et al., 2004). Based on these data, we have hypothesized that the developmental defects precede epileptiform activity (Brackenbury et al., 2013) and may contribute to the initiation of the seizure phenotype. This may be a common epileptogenic mechanism in epilepsies caused by *SCN1B* mutations.

Although β1-C121W is incapable of trans-homophilic adhesion *in vitro* (Meadows et al., 2002), my data suggest that β1-C121W may confer a deleterious gain of function. As discussed above, β1-C121W may associate with and therefore alter localization of β1-WT. Furthermore, it is unknown whether β1-C121W can associate with other known β1 cell adhesion partners, e.g. neurofascin-186, contactin, NrCAM, N-cadherin, or tenascin-R. We have shown that β1-mediated neurite outgrowth requires contactin and Fyn kinase (Brackenbury et al., 2008). Therefore, I hypothesize that if we were to compare *Scn1b*$^{+/W}$ mice to *Scn1b*$^{+/-}$ and wildtype mice they may have different extents of defective neurite outgrowth, CGN migration and fasciculation, and CST pathfinding and fasciculation. It would be interesting to also determine whether neurite outgrowth is defective in iPSC-derived GEFS+ patient neurons compared to controls in culture. Finally, it may be possible to inject EGFP-labeled GEFS+ or control patient iPSC-derived neurons into the developing mouse brain and compare migration and degree of neuronal arborization *in situ*.

To test this I would use our previously established methods to investigate whether *Scn1b*$^{+/W}$ mice have aberrant neuronal migration, proliferation, and/or neuronal pathfinding compared to *Scn1b*$^{+/-}$ mice (Brackenbury et al., 2008, 2013). As we have done previously (Brackenbury et al., 2013), I would stain sections from P5 hippocampus of *Scn1b*$^{+/W}$ mice to determine whether the migration and proliferation of neuronal subtypes are altered. Newborn dentate granule cells (DGCs), interphase (proliferating) cells, and DGCs can be identified using Prox1, Ki67, and Nissl respectively. Nissl staining will identify whether there is a decrease in cell density in the dentate gyrus, as we see in *Scn1b*$^{-/-}$ mice. If differences are seen, then we can investigate whether there

are increased Ki67 positive proliferating cells and/or increased post-mitotic dentate granule cells, labeled by Prox1, in the hilus. This could indicate altered regulation of proliferation in the hilus and defective migration of the dentate granule cells. Differences in neuronal migration could lead to changes in network excitability. In *Scn1b*$^{-/-}$ mice we found that some of the aberrant neurons in the dentate gyrus were parvalbumin-positive GABAergic interneurons (Brackenbury et al., 2013). Prox1-positive hilar ectopic DGCs are known to arise from progenitors following status epilepticus (Kron et al., 2010), but can also be seen prior to seizure onset (Brackenbury et al., 2013). Therefore, there may be a minimum level of spontaneous activity required, or a particular pathway that needs to be hyperexcitable, for the appearance of ectopic DGCs. If *Scn1b*$^{+/W}$ mice have less spontaneous activity or different active pathways, we may not see this change.

To determine if p.C121W affects β1-mediated neurite outgrowth, we could use our previously established assay (Davis et al., 2004; Brackenbury et al., 2008). Briefly, acutely dissociated CGNs or iPSC-derived neural progenitors are plated on a monolayer of Chinese hamster lung (CHL) 1610 cells ± expression of β1. Cultures are grown in the absence of FGF, to prevent FGF-dependent neurite outgrowth, which is independent of β1-mediated neurite outgrowth in CGNs (Brackenbury et al., 2008). Using WT littermates and *Scn1b*$^{-/-}$ mice as positive and negative controls, respectively, we then fix the cells 24 hours after culture, stained for Tuj1 (a neuronal β-tubulin), and imaged using confocal microscopy. The longest neurite for each neuron is measured, as previously described (Davis et al., 2004). By combining 1610 cells expressing β1 with *Scn1b*$^{W/W}$ neurons and 1610 cells expressing β1-C121W with *Scn1b*$^{+/+}$ neurons, we can determine whether β1-C121W can interact trans-homophilically with β1-WT to

stimulate neurite outgrowth. It is possible that when β1-WT is expressed in the neuron, it may still be able to induce neurite outgrowth in response to β1-C121W adhesion, but the reverse may not be true because β1-C121W may be incapable of inducing intracellular signal transduction. In this way, we could specifically test the functional output of β1-C121W/β1-WT trans-homophilic cell adhesion, if it occurs.

Regarding injection of GFP-labeled patient-derived iPSC-derived neurons into developing WT or GEFS+ mouse brain, brain slices could be stained for Tuj1 (to indicate neurons), and MAP2 (which will not stain axons). GFP-positive neurons would then be imaged using confocal microscopy with the resulting images re-constructed in three-dimensions. We could compare neuronal branching complexity using Scholl analysis, total neurite length, longest neurite length, and axonal length of iPSC neurons vs. the surrounding mouse neurons. If the brain region the neuron ends up in seems to affect neurite outgrowth, we could transplant patient and control iPSC-derived neurons with different fluorescent markers and inject them both into the same brain. Then we could select matched pairs of control and patient neurons to compare. This may be particularly important when injecting into *Scn1b* null animals, to control for differences in seizure activity(Brackenbury et al., 2013)(Brackenbury et al., 2013) . Both of these approaches would allow us to examine the effect of *SCN1B-C121W* on iPSC-derived GEFS+ patient neurite outgrowth.

Finally, we could also examine changes in fasciculation of the CST. *Scn1b*$^{-/-}$ mice have significant CST fasciculation and pathfinding abnormalities (Brackenbury et al., 2008). We have observed these defects by implanting a DiI crystal into one side of the primary

motor cortex in P9-10 mice. Six days after surgery, we anesthetized and fixed the brain and spinal cord of the same mice. Brain and spinal cord sections were then examined and scored for various types of defasciculations, as described previously (Brackenbury et al., 2008).

We anticipate that mice expressing β1-C121W will have neuronal migration defects, similar, or less severe than *Scn1b*$^{-/-}$ mice, with *Scn1b*$^{+/W}$ mice having a milder (or absence) of some phenotypes compared to the *Scn1b*$^{W/W}$ mice, which are expected to be similar to *Scn1b*$^{-/-}$ mice. Overall, we anticipate that p.C121W expression will result in an increase in proliferating and Prox1+ DGCs in the hilus of the DG, accompanied by an overall dispersion of DGCs in the GCL (seen as a decrease in the density of Nissl+ DGCs in the GCL and an increase in the thickness of the GCL). Finally we expect to see some abberant CST fasciculation, although not as dramatic as that observed in null mice. Collectively, these data will determine the effect of p.C121W on neuronal development.

It may be that we will see no differences in neuronal migration, proliferation, or neurite extension in *Scn1b*$^{+/W}$ mice or GEFS+ patient-derived iPSC neurons. This would suggest that p.C121W expression does not result in changes in neuronal migration or overall brain morphology, and that the GEFS+ phenotype stems mainly from changes in neuronal excitability at the cellular level. However, it could also be the case that β1 mediates migration of other key populations of neurons, such as other sub-populations of interneurons, pyramidal cells, and basket cells, and we may detect variations there.

How does p.C121W affect sodium and potassium channel function and neuronal excitability in mice compared to patient neurons?

Our data suggest that β1-C121W does not associate with VGSC α subunits. However, preliminary data collected by Dr. Luis Lopez-Santiago in our laboratory, indicate that *SCN1B*$^{+/W}$ hiPSC-derived neurons have increased I_{Na} density compared to controls (mean ± SE, -167 ± 31 pA/pF; -72.9 ± 5.2 pA/pF). The peak sodium current from the I-V curve was similarly increased (mean ± SE, -177 ± 31 pA/pF; -86.7 ± 9.6 pA/pF). This could be due to compensatory upregulation of sodium channels. We reported a similar result in iPSC-derived DS patient neurons (Liu et al., 2013). β1 also associates with and modulates $K_v4.2$ *in vivo* (Marionneau et al., 2012). In this study, $K_v4.2$ was immunoprecipitated from 40 mg of wild-type or $K_v4.2^{-/-}$ mouse brain protein. Mass spectroscopy proteomic analysis detected a β1 peptide in wild-type but not $K_v4.2^{-/-}$ samples. In addition, heterologously-expressed $K_v4.2$ was shown to associate with β1-EYFP, detected using anti-YFP antibody (Marionneau et al., 2012). Following shRNA knockdown of *Scn1b* in this heterologous system, A-type current, the majority of which is mediated by $K_v4.2$, was specifically decreased in amplitude (Marionneau et al., 2012). As discussed in chapter 1, β1 has been shown to modulate K_v1 and K_v3 channels in heterologous overexpression systems *in vitro*. Thus, p.C121W expression may result in altered potassium and/or sodium current *in vivo* through altered β1 modulation or other compensatory mechanisms. Overall, this could contribute to an altered balance between excitation and inhibition leading to increased seizure susceptibility.

I tested whether β1-C121W could co-immunoprecipitate with $K_v4.2$. I tried two different anti-$K_v4.2$ antibodies from NeuroMab (K57 and L28) that were recommended by our

collaborator, Dr. Jeanne Nerbonne, whose group performed the initial K_v4.2-β1 coimmunoprecipitation (Marionneau et al., 2012). The L28, but not the K57, antibody gave a consistent immunoreactive signal on a control Western blot. Because L28 is not rated by NeuroMab for immunoprecipitation, I decided to immunoprecipitate using anti-β1 and immunoblot for K_v4.2 using the L28 antibody. Using an anti-β1 antibody targeted against an intracellular β1 epitope (Cell Signaling Technologies), I optimized β1 pulldown by testing different dilution buffers. In order to get clean immunoprecipitation of β1, I had to add either CHAPS (3-[(3-cholamidopropyl)dimethylammonio]-1-propanesulfonate) detergent or β-octyl glucoside to the dilution buffer. Without the addition of one of these detergents, there was very little β1 protein detected in the immunoprecipitated samples. However, even with optimized β1 immunoprecipitation, there was no K_v4.2 signal observed in wild-type brain membrane proteins. After further discussion with Dr. Nerbonne, we decided that β1-K_v4.2 association may not be strong enough to detect biochemically. However, this does not mean that β1 modulation of K_v4.2 does not have physiological relevance. Measuring K+ currents, especially A-type current, in *Scn1b*$^{+/W}$ and *Scn1b*$^{W/W}$ mice may inform the mechanism of increased seizure susceptibility. Using the β1-V5 mice that are in progress, we could easily detect or coimmunoprecipitate even small levels of β1, due to the high affinity of V5 antibodies. This would make detecting an association between K_v4.2 and β1-C121W more feasible. If electrophysiological studies suggested β1-C121W modulation of A-type K+ current, it would also be reasonable to try to immunoprecipitate K_v4.2 from *Scn1b*$^{W/W}$ mice and use mass spectroscopy to detect β1-C121W as in (Marionneau et al., 2012).

In future experiments, it will be critical to verify our preliminary hiPSC neuron results and determine the mechanism of increased sodium current. In addition, it will be important to determine which neuronal population has these properties in *Scn1b*$^{+/W}$ mice. This would require a complex computational neuroscience approach involving electrophysiology and modeling to analyze changes in current and network excitability. The knowledge gained from these experiments would help identify the mechanism(s) by which p.C121W alters β1 function(s), and how this affects VGSC function and neuronal excitability.

While research of some misfolded-protein diseases, including cystic fibrosis, has prompted the development of chaperone protein therapies, my proposed mechanism suggests that this may not be an effective approach for *SCN1B-C121W* –linked epilepsy. β1-C121W is expressed at the cell surface, and therefore does not need a chaperone protein to assist in trafficking to the cell surface. Rather, the problem seems to lie in the incomplete glycosylation and misfolding of β1-C121W. Furthermore, the evidence from *Scn1b*$^{+/-}$ mice suggests that the increased seizure susceptibility of *Scn1b*$^{+/W}$ mice is not due to lower β1 expression. Therefore, based on the data presented here, a potential treatment to target and remove the detrimental β1-C121W may ameliorate some of the detrimental effects of the mutant protein. This would need to be done without significant toxicity to the neurons and other cells containing β1-C121W. One possible approach would be to use recently developed “ubiquibodies” (Portnoff et al., 2014). These are targeted ubiquitin ligases linked to an antibody against a protein of interest. Portnoff et al. have shown specific targeting and depletion of an

otherwise stable protein *in vitro*. These “ubiquibodies” would need further development to test efficacy *in vivo* and in the central nervous system and a β1-C121W-specific antibody would need to be developed, which would be challenging considering the difficulty creating β1-specific antibodies. However, a β1-C121W-targeted “ubiquibody” could provide a means of removing the deleterious β1-C121W protein from the system. Further functional testing of sodium and potassium currents *in vivo* in *Scn1b-C121W* mice and in *SCN1B-C121W* patient-derived iPSCs could also reveal further insights into which anti-epileptic therapeutics might be most effective for this set of patients.

Overall, as with many scientific pursuits, we are left with many questions and a few answers. The data I have presented here suggest that *Scn1b-C121W* confers a deleterious gain-of-function. β1-C121W localizes to the neuronal cell surface but does not associate with VGSC α subunits and does not localize to axon initial segments or nodes of Ranvier. Our previous results showed that, in addition to what I have found, β1-C121W does not participate in *trans* homophilic adhesion. Therefore, we have proposed that the increased seizure susceptibility observed in *Scn1b*$^{+/W}$ mice compared to *Scn1b*$^{+/-}$ mice may be explained by disrupted hemophilic cell adhesive interactions resulting in altered neuronal migration and pathfinding, as well as altered sodium and/or potassium current modulation. Further investigation of these mechanisms will help us to understand *SCN1B*-linked epilepsies and hopefully identify potential pathways for developing better therapeutic targets.

References

Abdelsayed M., Sokolov S., Ruben PC. 2013. A thermosensitive mutation alters the effects of lacosamide on slow inactivation in neuronal voltage-gated sodium channels, NaV1.2. *Frontiers in Pharmacology* 4:1–10.

Adsit GS., Vaidyanathan R., Galler CM., Kyle JW., Makielski JC. 2013. Channelopathies from mutations in the cardiac sodium channel protein complex. *Journal of molecular and cellular cardiology* 61:34–43.

Aman TK., Grieco-Calub TM., Chen C., Rusconi R., Slat E a., Isom LL., Raman IM. 2009. Regulation of persistent Na current by interactions between beta subunits of voltage-gated Na channels. *The Journal of neuroscience : the official journal of the Society for Neuroscience* 29:2027–42.

Armstrong CM., Bezanilla F. 1973. Currents related to movement of the gating particles of the sodium channels. *Nature* 242:459–461.

Armstrong CM., Bezanilla F. 1974. Charge movement associated with the opening and closing of the activation gates of the Na channels. *The Journal of general physiology* 63:533–552.

Audenaert D., Claes L., Ceulemans B., Löfgren A., Van Broeckhoven C., De Jonghe P. 2003. A deletion in SCN1B is associated with febrile seizures and early-onset absence epilepsy. *Neurology* 61:854–6.

Auerbach DS., Jones J., Clawson BC., Offord J., Lenk GM., Ogiwara I., Yamakawa K., Meisler MH., Parent JM., Isom LL. 2013. Altered Cardiac Electrophysiology and SUDEP in a Model of Dravet Syndrome. *PLoS ONE* 8:1–15.

Auld VJ., Goldin AL., Krafte DS., Marshall J., Dunn JM., Catterall WA., Lester HA., Davidson N., Dunn RJ. 1988. A rat brain na+ channel α subunit with novel gating properties. *Neuron* 1:449–461.

Bant JS., Raman IM. 2010. Control of transient, resurgent, and persistent current by open-channel block by Na channel beta4 in cultured cerebellar granule neurons. *Proceedings of the National Academy of Sciences of the United States of America* 107:12357–62.

Bao Y., Isom LL. 2014. Nav1.5 and Regulatory Beta Subunits in Cardiac Sodium Channelopathies. *Card Electrophysiol Clin* 6:679–694.

Baraban SC., Dinday MT., Hortopan G a. 2013. Drug screening in Scn1a zebrafish mutant identifies clemizole as a potential Dravet syndrome treatment. *Nature communications* 4:2410.

Barbieri R., Baroni D., Moran O. 2012. Identification of an intra-molecular disulfide bond

in the sodium channel β1-subunit. *Biochemical and biophysical research communications* 420:364–7.

Barchi RL. 1983. Protein components of the purified sodium channel from rat skeletal muscle sarcolemma. *Journal of neurochemistry* 40:1377–1385.

Baroni D., Barbieri R., Picco C., Moran O. 2013. Functional modulation of voltage-dependent sodium channel expression by wild type and mutated C121W-β1 subunit. *Journal of bioenergetics and biomembranes* 45:353–68.

Beneski DA., Catterall WA. 1980. Covalent labeling of protein components of the sodium channel with a photoactivable derivative of scorpion toxin. *Proceedings of the National Academy of Sciences* 77:639–643.

Bennett E., Urcan MS., Tinkle SS., Koszowski a G., Levinson SR. 1997. Contribution of sialic acid to the voltage dependence of sodium channel gating. A possible electrostatic mechanism. *The Journal of general physiology* 109:327–43.

Bennett ES. 2002. Isoform-specific effects of sialic acid on voltage-dependent Na+ channel gating: functional sialic acids are localized to the S5-S6 loop of domain I. *The Journal of physiology* 538:675–90.

Binstock L., Lecar H. 1969. Ammonium ion currents in the squid giant axon. *The Journal of general physiology* 53:342–361.

Brackenbury WJ., Davis TH., Chen C., Slat E a., Detrow MJ., Dickendesher TL., Ranscht B., Isom LL. 2008. Voltage-gated Na+ channel beta1 subunit-mediated neurite outgrowth requires Fyn kinase and contributes to postnatal CNS development in vivo. *The Journal of neuroscience : the official journal of the Society for Neuroscience* 28:3246–56.

Brackenbury WJ., Calhoun JD., Chen C., Miyazaki H., Nukina N., Oyama F., Ranscht B., Isom LL. 2010. Functional reciprocity between Na+ channel Nav1.6 and beta1 subunits in the coordinated regulation of excitability and neurite outgrowth. *Proceedings of the National Academy of Sciences of the United States of America* 107:2283–8.

Brackenbury WJ. 2012. Voltage-gated sodium channels and metastatic disease. *Channels* 6:352–361.

Brackenbury WJ., Yuan Y., O'Malley HA., Parent JM., Isom LL. 2013. Abnormal neuronal patterning occurs during early postnatal brain development of Scn1b-null mice and precedes hyperexcitability. *Proceedings of the National Academy of Sciences of the United States of America* 110:1089–94.

Brackenbury WJ., Isom LL. 2008. Voltage-gated Na+ channels: potential for beta subunits as therapeutic targets. *Expert opinion on therapeutic targets* 12:1191–203.

Brackenbury WJ., Isom LL. 2011. Na Channel β Subunits: Overachievers of the Ion Channel Family. *Frontiers in pharmacology* 2:53.

Brunklaus A., Ellis R., Reavey E., Semsarian C., Zuberi SM. 2014. Genotype phenotype associations across the voltage-gated sodium channel family. *Journal of medical*

genetics 51:650–8.

Calhoun JD., Isom LL. 2014. The Role of Non-pore-forming beta Subunits in Physiology and Pathophysiology of Voltage-Gated Sodium Channels. In: Ruben PC ed. *Voltage-Gated Sodium Channels*. Handbook of Experimental Pharmacology. Springer Berlin Heidelberg, Berlin, Heidelberg.

Carvill GL., Weckhuysen S., McMahon JM., Hartmann C., Møller RS., Hjalgrim H., Cook J., Geraghty E., O'Roak BJ., Petrou S. et al. 2014. GABRA1 and STXBP1: Novel genetic causes of Dravet syndrome. *Neurology* 82:1245–1253.

Catterall WA. 1986a. Molecular properties of voltage-sensitive sodium channels. *Annual review of biochemistry* 55:953–985.

Catterall W a. 1986b. Voltage-dependent gating of sodium channels: correlating structure and function. *Trends in Neurosciences* 9:7–10.

Catterall W a. 1992. Cellular and molecular biology of voltage-gated sodium channels. *Physiological reviews* 72:S15–48.

Catterall WA., Goldin AL., Waxman SG. 2005. International Union of Pharmacology. XLVII. Nomenclature and structure-function relationships of voltage-gated sodium channels. *Pharmacological reviews* 57:397–409.

Catterall W a. 2012. Voltage-gated sodium channels at 60: structure, function and pathophysiology. *The Journal of physiology* 590:2577–89.

Chang N., Sun C., Gao L., Zhu D., Xu X., Zhu X., Xiong J-W., Xi JJ. 2013. Genome editing with RNA-guided Cas9 nuclease in zebrafish embryos. *Cell research* 23:465–72.

Chen C., Bharucha V., Chen Y., Westenbroek RE., Brown A., Malhotra JD., Jones D., Avery C., Gillespie PJ., Kazen-Gillespie K a. et al. 2002. Reduced sodium channel density, altered voltage dependence of inactivation, and increased susceptibility to seizures in mice lacking sodium channel beta 2-subunits. *Proceedings of the National Academy of Sciences of the United States of America* 99:17072–7.

Chen C., Westenbroek RE., Xu X., Edwards C a., Sorenson DR., Chen Y., McEwen DP., O'Malley H a., Bharucha V., Meadows LS. et al. 2004. Mice lacking sodium channel beta1 subunits display defects in neuronal excitability, sodium channel expression, and nodal architecture. *The Journal of neuroscience : the official journal of the Society for Neuroscience* 24:4030–42.

Chen C., Calhoun JD., Zhang Y., Lopez-Santiago L., Zhou N., Davis TH., Salzer JL., Isom LL. 2012. Identification of the cysteine residue responsible for disulfide linkage of Na+ channel α and β2 subunits. *Journal of Biological Chemistry* 287:39061–39069.

Chioni A-MM., Brackenbury WJ., Calhoun JD., Isom LL., Djamgoz MB a. 2009. A novel adhesion molecule in human breast cancer cells: voltage-gated Na+ channel beta1 subunit. *The international journal of biochemistry & cell biology* 41:1216–27.

Chopra R., Isom LL. 2014. Untangling the dravet syndrome seizure network: The

changing face of a rare genetic epilepsy. *Epilepsy Currents* 14:86–89.

Coombs J., Eccles J., Fatt P. 1955. The electrical properties of the motoneurone membrane. *The Journal of physiology* 130:291–325.

Davis TH., Chen C., Isom LL. 2004. Sodium channel beta1 subunits promote neurite outgrowth in cerebellar granule neurons. *The Journal of biological chemistry* 279:51424–32.

Deveau H., Garneau JE., Moineau S. 2010. CRISPR/Cas system and its role in phage-bacteria interactions. *Annual review of microbiology* 64:475–93.

Dibbens LM., Reid CA., Hodgson B., Thomas EA., Phillips AM., Gazina E., Cromer BA., Clarke AL., Baram TZ., Scheffer IE. et al. 2010. Augmented currents of an HCN2 variant in patients with febrile seizure syndromes. *Annals of Neurology* 67:542–546.

Dib-Hajj SD., Cummins TR., Black J a., Waxman SG. 2010. Sodium channels in normal and pathological pain. *Annual review of neuroscience* 33:325–47.

Diss JKJ., Fraser SP., Walker MM., Patel A., Latchman DS., Djamgoz MBA. 2008. Beta-subunits of voltage-gated sodium channels in human prostate cancer: quantitative in vitro and in vivo analyses of mRNA expression. *Prostate cancer and prostatic diseases* 11:325–333.

Dours-Zimmermann MT., Zimmermann DR. 2012. A novel strategy for a splice-variant selective gene ablation: the example of the versican V0/V2 knockout. *Methods in molecular biology (Clifton, N.J.)* 836:63–85.

Doyle D a., Morais Cabral J., Pfuetzner R a., Kuo a., Gulbis JM., Cohen SL., Chait BT., MacKinnon R. 1998. The structure of the potassium channel: molecular basis of K+ conduction and selectivity. *Science (New York, N.Y.)* 280:69–77.

Egri C., Vilin YY., Ruben PC. 2012. A thermoprotective role of the sodium channel β1 subunit is lost with the β1 (C121W) mutation. *Epilepsia* 53:494–505.

Ellgaard L., Helenius A. 2003. Quality control in the endoplasmic reticulum. *Nature reviews. Molecular cell biology* 4:181–91.

Epi4K Consortium. 2012. Epi4K: gene discovery in 4,000 genomes. *Epilepsia* 53:1457–67.

Escayg A., MacDonald BT., Meisler MH., Baulac S., Huberfeld G., An-Gourfinkel I., Brice A., LeGuern E., Moulard B., Chaigne D. et al. 2000. Mutations of SCN1A, encoding a neuronal sodium channel, in two families with GEFS+2. *Nature genetics* 24:343–5.

Filbin MT., Tennekoon GI. 1993. Homophilic adhesion of the myelin Po protein requires glycosylation of both molecules in the homophilic pair. *Journal of Cell Biology* 122:451–459.

Fraser S., Diss J., Chioni A., Mycielska M., Pan H., Yamaci R., Pani F., Siwy Z., Krasowska M., Grzywna Z. et al. 2005. Voltage-gated sodium channel expression and potentiation of human breast cancer metastasis. 11.

Gao R., Shen Y., Cai J., Lei M., Wang Z. 2010. Expression of voltage-gated sodium channel alpha subunit in human ovarian cancer. *Oncology reports* 23:1293–9.

Gilchrist J., Das S., Van Petegem F., Bosmans F. 2013. Crystallographic insights into sodium-channel modulation by the β4 subunit. *Proceedings of the National Academy of Sciences of the United States of America* 110:E5016–24.

Gilchrist J., Olivera BM., Bosmans F. 2014. Animal toxins influence voltage-gated sodium channel function. *Handbook of experimental pharmacology* 221:203–29.

Grieco TM., Malhotra JD., Chen C., Isom LL., Raman IM. 2005. Open-channel block by the cytoplasmic tail of sodium channel beta4 as a mechanism for resurgent sodium current. *Neuron* 45:233–44.

Grimes JA., Fraser SP., Stephens GJ., Downing JE., Laniado ME., Foster CS., Abel PD., Djamgoz MB. 1995. Differential expression of voltage-activated Na+ currents in two prostatic tumour cell lines: contribution to invasiveness in vitro. *FEBS letters* 369:290–4.

Haider MZ., Habeeb Y., Al-Nakkas E., Al-Anzi H., Zaki M., Al-Tawari a., Al-Bloushi M. 2005. Lack of an association between candidate gene loci and idiopathic generalized epilepsy in Kuwaiti Arab children. *Journal of Biomedical Science* 12:815–818.

Hartshorne RP., Messner DJ., Coppersmith JC., Catterall WA. 1982. The saxitoxin receptor of the sodium channel from rat brain. Evidence for two nonidentical beta subunits. *The Journal of biological chemistry* 257:13888–13891.

Hartshorne RP., Keller BU., Talvenheimo J a., Catterall W a., Montal M. 1985. Functional reconstitution of the purified brain sodium channel in planar lipid bilayers. *Proceedings of the National Academy of Sciences of the United States of America* 82:240–4.

Hartshorne RP., Catterall W a. 1981. Purification of the saxitoxin receptor of the sodium channel from rat brain. *Proceedings of the National Academy of Sciences of the United States of America* 78:4620–4.

Hartshorne RP., Catterall WA. 1984. The sodium channel from rat brain. Purification and subunit composition. *Journal of Biological Chemistry* 259:1667–1675.

Hatch RJ., Reid C a., Petrou S. 2014. Enhanced in vitro CA1 network activity in a sodium channel β1(C121W) subunit model of genetic epilepsy. *Epilepsia* 1:1–8.

He M., Abdi KM., Bennett V. 2014. Ankyrin-G palmitoylation and βII-spectrin binding to phosphoinositide lipids drive lateral membrane assembly. *The Journal of cell biology* 206:273–88.

Heinemann SH., Terlau H., Stühmer W., Imoto K., Numa S. 1992. Calcium channel characteristics conferred on the sodium channel by single mutations. *Nature* 356:441–443.

Hernandez-Plata E., Ortiz CS., Marquina-Castillo B., Medina-Martinez I., Alfaro A., Berumen J., Rivera M., Gomora JC. 2012. Overexpression of NaV 1.6 channels is

associated with the invasion capacity of human cervical cancer. *International journal of cancer. Journal international du cancer* 130:2013–23.

Hille B. 1971. The permeability of the sodium channel to organic cations in myelinated nerve. *The Journal of general physiology* 58:599–619.

Hille B. 1972. The permeability of the sodium channel to metal cations in myelinated nerve. *The Journal of general physiology* 59:637–58.

Hirtz D., Thurman DJ., Gwinn-Hardy K., Mohamed M., Chaudhuri a. R., Zalutsky R. 2007. How common are the "common" neurologic disorders? *Neurology* 68:326–337.

Hodgkin AL., Huxley AF. 1952. A Quantitative Description of Membrane Current and its Application to Conduction and Excitation in Nerves. *J. Physiol.* 117:500–544.

House CD., Vaske CJ., Schwartz AM., Obias V., Frank B., Luu T., Sarvazyan N., Irby R., Strausberg RL., Hales TG. et al. 2010. Voltage-gated Na+ channel SCN5A is a key regulator of a gene transcriptional network that controls colon cancer invasion. *Cancer Research* 70:6957–6967.

Isom LL., De Jongh KS., Patton DE., Reber BF., Offord J., Charbonneau H., Walsh K., Goldin a L., Catterall W a. 1992. Primary structure and functional expression of the beta 1 subunit of the rat brain sodium channel. *Science* 256:839–842.

Isom LL., Scheuer T., Brownstein AB., Ragsdale DS., Murphy BJ., Catterall WA. 1995a. Functional co-expression of the beta 1 and type IIA alpha subunits of sodium channels in a mammalian cell line. *The Journal of biological chemistry* 270:3306–12.

Isom LL., Ragsdale DS., De Jongh KS., Westenbroek RE., Reber BF., Scheuer T., Catterall W a. 1995b. Structure and function of the beta 2 subunit of brain sodium channels, a transmembrane glycoprotein with a CAM motif. *Cell* 83:433–42.

Isom LL. 2014. "It was the interneuron with the parvalbumin in the hippocampus!" "no, it was the pyramidal cell with the glutamate in the cortex!" searching for clues to the mechanism of dravet syndrome - the plot thickens. *Epilepsy currents / American Epilepsy Society* 14:350–2.

Jansson KH., Lynch JE., Lepori-Bui N., Czymmek KJ., Duncan RL., Sikes RA. 2012. Overexpression of the VSSC-associated CAM, beta-2, enhances LNCaP cell metastasis associated behavior. *The Prostate* 72:1080–1092.

Jenkins PM., Kim N., Jones SL., Tseng WC., Svitkina TM., Yin HH., Bennett V. 2015. Giant ankyrin-G: a critical innovation in vertebrate evolution of fast and integrated neuronal signaling. *Proceedings of the National Academy of Sciences of the United States of America* 112:957–64.

Jiang Y., Lee A., Chen J., Ruta V., Cadene M., Chait BT., MacKinnon R. 2003. X-ray structure of a voltage-dependent K+ channel. *Nature* 423:33–41.

Jiao J., Yang Y., Shi Y., Chen J., Gao R., Fan Y., Yao H., Liao W., Sun X-F., Gao S. 2013. Modeling Dravet syndrome using induced pluripotent stem cells (iPSCs) and

directly converted neurons. *Human molecular genetics*:1–12.

Johnson D., Montpetit ML., Stocker PJ., Bennett ES. 2004. The sialic acid component of the beta1 subunit modulates voltage-gated sodium channel function. *The Journal of biological chemistry* 279:44303–10.

Johnson D., Bennett ES. 2006. Isoform-specific effects of the beta2 subunit on voltage-gated sodium channel gating. *The Journal of biological chemistry* 281:25875–81.

Kalume F. 2013. Sudden unexpected death in Dravet syndrome: Respiratory and other physiological dysfunctions. *Respiratory Physiology and Neurobiology* 189:324–328.

Kazarinova-Noyes K., Malhotra JD., McEwen DP., Mattei LN., Berglund EO., Ranscht B., Levinson SR., Schachner M., Shrager P., Isom LL. et al. 2001. Contactin associates with Na+ channels and increases their functional expression. *The Journal of neuroscience : the official journal of the Society for Neuroscience* 21:7517–25.

Kazen-Gillespie KA., Ragsdale DS., D'Andrea MR., Mattei LN., Rogers KE., Isom LL. 2000. Cloning, localization, and functional expression of sodium channel b1A subunits. *Journal of Biological Chemistry* 275:1079–1088.

Kearney JA. 2014. Epi4K Phase I: Gene Discovery in Epileptic Encephalopathies by Exome Sequencing. *Epilepsy currents / American Epilepsy Society* 14:208–10.

Kellenberger S. 1997. Molecular Analysis of the Putative Inactivation Particle in the Inactivation Gate of Brain Type IIA Na+ Channels. *The Journal of General Physiology* 109:589–605.

Kim DY., Ingano L a M., Carey BW., Pettingell WH., Kovacs DM. 2005. Presenilin/gamma-secretase-mediated cleavage of the voltage-gated sodium channel beta2-subunit regulates cell adhesion and migration. *The Journal of biological chemistry* 280:23251–61.

Kim DY., Carey BW., Wang H., Ingano LAM., Binshtok AM., Wertz MH., Pettingell WH., He P., Lee VM-Y., Woolf CJ. et al. 2007. BACE1 regulates voltage-gated sodium channels and neuronal activity. *Nature cell biology* 9:755–64.

Kim DY., Gersbacher MT., Inquimbert P., Kovacs DM. 2011. Reduced sodium channel Na(v)1.1 levels in BACE1-null mice. *The Journal of biological chemistry* 286:8106–16.

Ko H., Gelb BD. 2014. Concise Review: Drug Discovery in the Age of the Induced Pluripotent Stem Cell. *Stem Cells Translational Medicine*:396–402.

Krafte DS. 1990. Inactivation of cloned Na channels expressed in Xenopus oocytes. *The Journal of General Physiology* 96:689–706.

Kraner SD., Tanaka JC., Barchi RL. 1985. Purification and functional reconstitution of the voltage-sensitive sodium channel from rabbit T-tubular membranes. *The Journal of biological chemistry* 260:6341–7.

Kron MM., Zhang H., Parent JM. 2010. The developmental stage of dentate granule

cells dictates their contribution to seizure-induced plasticity. *The Journal of neuroscience : the official journal of the Society for Neuroscience* 30:2051–9.

Kunz B., Lierheimer R., Rader C., Spirig M., Ziegler U., Sonderegger P. 2002. Axonin-1/TAG-1 mediates cell-cell adhesion by a cis-assisted trans-interaction. *The Journal of biological chemistry* 277:4551–7.

Kwan P., Arzimanoglou A., Berg AT., Brodie MJ., Hauser WA., Mathern G., Moshé SL., Perucca E., Wiebe S., French J. 2010. Definition of drug resistant epilepsy: Consensus proposal by the ad hoc Task Force of the ILAE Commission on Therapeutic Strategies. *Epilepsia* 51:1069–1077.

Kwan P., Schacter SC., Brodie MJ. 2011. Drug-resistant epilepsy. *New England Journal …* 365:919–926.

Kwong K., Carr MJ. 2015. Voltage-gated sodium channels. *Current Opinion in Pharmacology* 22:131–139.

Lancaster MA., Renner M., Martin C-A., Wenzel D., Bicknell LS., Hurles ME., Homfray T., Penninger JM., Jackson AP., Knoblich JA. 2013. Cerebral organoids model human brain development and microcephaly. *Nature* 501:373–9.

Laniado ME., Lalani EN., Fraser SP., Grimes JA., Bhangal G., Djamgoz MB., Abel PD. 1997. Expression and functional analysis of voltage-activated Na+ channels in human prostate cancer cell lines and their contribution to invasion in vitro. *The American journal of pathology* 150:1213–21.

Larramendi L., Lorente De No R., Vidal F. 1956. Restoration of sodium-deficient frog nerve fibres by an isotonic solution of guanidinium chloride. *Nature* 178:316–7.

Li D., Qiu Z., Shao Y., Chen Y., Guan Y., Liu M., Li Y., Gao N., Wang L., Lu X. et al. 2013. Heritable gene targeting in the mouse and rat using a CRISPR-Cas system. *Nature Biotechnology* 31:681–683.

Lin X., O'Malley H., Chen C., Auerbach D., Foster M., Shekhar A., Zhang M., Coetzee W., Jalife J., Fishman GI. et al. 2015. Scn1b deletion leads to increased tetrodotoxin-sensitive sodium current, altered intracellular calcium homeostasis and arrhythmias in murine hearts. *The Journal of Physiology* 593:1389–1407.

Liu Y., Lopez-Santiago LF., Yuan Y., Jones JM., Zhang H., O'Malley H a., Patino G a., O'Brien JE., Rusconi R., Gupta A. et al. 2013. Dravet syndrome patient-derived neurons suggest a novel epilepsy mechanism. *Annals of neurology* 74:128–39.

Lombet A., Lazdunski M. 1984. Characterization, solubilization, affinity labeling and purification of the cardiac Na+ channel using Tityus toxin gamma. *European journal of biochemistry / FEBS* 141:651–60.

Lopez-Santiago LF., Pertin M., Morisod X., Chen C., Hong S., Wiley J., Decosterd I., Isom LL. 2006. Sodium channel beta2 subunits regulate tetrodotoxin-sensitive sodium channels in small dorsal root ganglion neurons and modulate the response to pain. *The Journal of neuroscience : the official journal of the Society for Neuroscience* 26:7984–94.

Lopez-Santiago LF., Meadows LS., Ernst SJ., Chen C., Malhotra JD., McEwen DP., Speelman A., Noebels JL., Maier SKG., Lopatin AN. et al. 2007. Sodium channel Scn1b null mice exhibit prolonged QT and RR intervals. *Journal of molecular and cellular cardiology* 43:636–47.

Lopez-Santiago LF., Brackenbury WJ., Chen C., Isom LL. 2011. Na+ channel Scn1b gene regulates dorsal root ganglion nociceptor excitability in vivo. *The Journal of biological chemistry* 286:22913–23.

Lorente De No R., Vidal F., Larramendi L. 1957. Restoration of sodium-deficient frog nerve fibres by onium ions. *Nature* 179:737–8.

Lucas PT., Meadows LS., Nicholls J., Ragsdale DS. 2005. An epilepsy mutation in the beta1 subunit of the voltage-gated sodium channel results in reduced channel sensitivity to phenytoin. *Epilepsy research* 64:77–84.

Maier SKG., Westenbroek RE., McCormick KA., Curtis R., Scheuer T., Catterall WA. 2004. Distinct Subcellular Localization of Different Sodium Channel ?? and ?? Subunits in Single Ventricular Myocytes from Mouse Heart. *Circulation* 109:1421–1427.

Malhotra JD., Kazen-Gillespie K., Hortsch M., Isom LL. 2000. Sodium channel beta subunits mediate homophilic cell adhesion and recruit ankyrin to points of cell-cell contact. *The Journal of biological chemistry* 275:11383–8.

Malhotra JD., Koopmann MC., Kazen-Gillespie K a., Fettman N., Hortsch M., Isom LL. 2002. Structural requirements for interaction of sodium channel beta 1 subunits with ankyrin. *The Journal of biological chemistry* 277:26681–8.

Malhotra JD., Thyagarajan V., Chen C., Isom LL. 2004. Tyrosine-phosphorylated and nonphosphorylated sodium channel beta1 subunits are differentially localized in cardiac myocytes. *The Journal of biological chemistry* 279:40748–54.

Marini C., Scheffer IE., Nabbout R., Suls A., De Jonghe P., Zara F., Guerrini R. 2011. The genetics of Dravet syndrome. *Epilepsia* 52 Suppl 2:24–9.

Marionneau C., Carrasquillo Y., Norris AJ., Townsend RR., Isom LL., Link AJ., Nerbonne JM. 2012. The sodium channel accessory subunit Navβ1 regulates neuronal excitability through modulation of repolarizing voltage-gated K^+ channels. *The Journal of neuroscience : the official journal of the Society for Neuroscience* 32:5716–27.

Massey C a., Sowers LP., Dlouhy BJ., Richerson GB. 2014. Mechanisms of sudden unexpected death in epilepsy: the pathway to prevention. *Nature reviews. Neurology* 10:271–82.

McCormick K a., Isom LL., Ragsdale D., Smith D., Scheuer T., Catterall W a. 1998. Molecular determinants of Na+ channel function in the extracellular domain of the beta1 subunit. *The Journal of biological chemistry* 273:3954–62.

McCusker EC., Bagnéris C., Naylor CE., Cole AR., D'Avanzo N., Nichols CG., Wallace B a. 2012. Structure of a bacterial voltage-gated sodium channel pore reveals

mechanisms of opening and closing. *Nature Communications* 3:1102.

McEwen DP., Chen C., Meadows LS., Lopez-Santiago LF., Isom LL. 2009. The voltage-gated Na+ channel beta3 subunit does not mediate trans homophilic cell adhesion or associate with the cell adhesion molecule contactin. *Neuroscience letters* 462:272–5.

McEwen DP., Isom LL. 2004. Heterophilic interactions of sodium channel beta1 subunits with axonal and glial cell adhesion molecules. *The Journal of biological chemistry* 279:52744–52.

Meadows LS., Malhotra J., Loukas A., Thyagarajan V., Kazen-Gillespie K a., Koopman MC., Kriegler S., Isom LL., Ragsdale DS. 2002. Functional and biochemical analysis of a sodium channel beta1 subunit mutation responsible for generalized epilepsy with febrile seizures plus type 1. *The Journal of neuroscience : the official journal of the Society for Neuroscience* 22:10699–709.

Meng H., Xu H-Q., Yu L., Lin G-W., He N., Su T., Shi Y-W., Li B., Wang J., Liu X-R. et al. 2015. The SCN1A Mutation Database: Updating Information and Analysis of the Relationships among Genotype, Functional Alteration, and Phenotype. *Human Mutation* 36:573–580.

Miller JA., Agnew WS., Levinson SR. 1983. Principal glycopeptide of the tetrodotoxin/saxitoxin binding protein from Electrophorus electricus: isolation and partial chemical and physical characterization. *Biochemistry* 22:462–70.

Miller AR., Hawkins N a., McCollom CE., Kearney J a. 2014. Mapping genetic modifiers of survival in a mouse model of Dravet syndrome. *Genes, brain, and behavior* 13:163–72.

Mistry AM., Thompson CH., Miller AR., Vanoye CG., George AL., Kearney J a. 2014. Strain- and age-dependent hippocampal neuron sodium currents correlate with epilepsy severity in Dravet syndrome mice. *Neurobiology of Disease* 65:1–11.

Moran O., Conti F. 2001. Skeletal muscle sodium channel is affected by an epileptogenic beta1 subunit mutation. *Biochemical and biophysical research communications* 282:55–9.

Morgan K., Stevens EB., Shah B., Cox PJ., Dixon AK., Lee K., Pinnock RD., Hughes J., Richardson PJ., Mizuguchi K. et al. 2000. beta 3: an additional auxiliary subunit of the voltage-sensitive sodium channel that modulates channel gating with distinct kinetics. *Proceedings of the National Academy of Sciences of the United States of America* 97:2308–2313.

Namadurai S., Balasuriya D., Rajappa R., Wiemhöfer M., Stott K., Klingauf J., Edwardson JM., Chirgadze DY., Jackson AP. 2014. Crystal structure and molecular imaging of the Nav channel β3 subunit indicates a trimeric assembly. *The Journal of biological chemistry* 289:10797–811.

Nelson M., Millican-Slater R., Forrest LC., Brackenbury WJ. 2014. The sodium channel β1 subunit mediates outgrowth of neurite-like processes on breast cancer cells and promotes tumour growth and metastasis. *International journal of cancer. Journal*

international du cancer 135:1–14.

Nguyen HM., Miyazaki H., Hoshi N., Smith BJ., Nukina N., Goldin AL., Chandy KG. 2012. Modulation of voltage-gated K+ channels by the sodium channel β1 subunit. *Proceedings of the National Academy of Sciences of the United States of America* 109:18577–82.

Noda M., Shimizu S., Tanabe T., Takai T., Kayano T., Ikeda T., Takahashi H., Nakayama H., Kanaoka Y., Minamino N. et al. 1984. Primary structure of Electrophorus electricus sodium channel deduced from cDNA sequence. *Nature* 312:121–127.

Noda M., Suzuki H., Numa S., Stühmer W. 1989. A single point mutation confers tetrodotoxin and saxitoxin insensitivity on the sodium channel II. *FEBS letters* 259:213–6.

O'Malley H a., Isom LL. 2015. Sodium Channel β Subunits: Emerging Targets in Channelopathies. *Annual Review of Physiology* 77:481–504.

Oakley JC., Kalume F., Yu FH., Scheuer T., Catterall W a. 2009. Temperature- and age-dependent seizures in a mouse model of severe myoclonic epilepsy in infancy. *Proceedings of the National Academy of Sciences of the United States of America* 106:3994–9.

Oakley JC., Kalume F., Catterall WA. 2011. Insights into pathophysiology and therapy from a mouse model of Dravet syndrome. *Epilepsia* 52 Suppl 2:59–61.

Ogiwara I., Miyamoto H., Morita N., Atapour N., Mazaki E., Inoue I., Takeuchi T., Itohara S., Yanagawa Y., Obata K. et al. 2007. Nav1.1 localizes to axons of parvalbumin-positive inhibitory interneurons: a circuit basis for epileptic seizures in mice carrying an Scn1a gene mutation. *The Journal of neuroscience : the official journal of the Society for Neuroscience* 27:5903–14.

Ogiwara I., Nakayama T., Yamagata T., Ohtani H., Mazaki E., Tsuchiya S., Inoue Y., Yamakawa K. 2012. A homozygous mutation of voltage-gated sodium channel β(I) gene SCN1B in a patient with Dravet syndrome. *Epilepsia* 53:e200–3.

Onganer PU., Djamgoz MB a. 2005. Small-cell Lung Cancer (Human): Potentiation of Endocytic Membrane Activity by Voltage-gated Na + Channel Expression in Vitro. 75:67–75.

Oyama F., Miyazaki H., Sakamoto N., Becquet C., Machida Y., Kaneko K., Uchikawa C., Suzuki T., Kurosawa M., Ikeda T. et al. 2006. Sodium channel beta4 subunit: down-regulation and possible involvement in neuritic degeneration in Huntington's disease transgenic mice. *Journal of neurochemistry* 98:518–29.

Parent JM., Anderson S a. 2015. Reprogramming patient-derived cells to study the epilepsies. *Nature neuroscience* 18:360–366.

Patel F., Brackenbury WJ. 2015. Dual roles of voltage-gated sodium channels in development and cancer. *The International Journal of Developmental Biology*.

Patino GA., Claes LRF., Lopez-Santiago LF., Slat E a., Dondeti RSR., Chen C.,

O'Malley H a., Gray CBB., Miyazaki H., Nukina N. et al. 2009. A functional null mutation of SCN1B in a patient with Dravet syndrome. *The Journal of neuroscience : the official journal of the Society for Neuroscience* 29:10764–78.

Patino GA., Brackenbury WJ., Bao Y., Lopez-Santiago LF., O'Malley HA., Chen C., Calhoun JD., Lafrenière RG., Cossette P., Rouleau GA. et al. 2011. Voltage-gated Na+ channel β1B: a secreted cell adhesion molecule involved in human epilepsy. *The Journal of neuroscience : the official journal of the Society for Neuroscience* 31:14577–91.

Patino GA., Isom LL. 2010. Electrophysiology and beyond: multiple roles of Na+ channel β subunits in development and disease. *Neuroscience letters* 486:53–9.

Payandeh J., Scheuer T., Zheng N., Catterall W a. 2011. The crystal structure of a voltage-gated sodium channel. *Nature* 475:353–8.

Portnoff AD., Stephens EA., Varner JD., DeLisa MP. 2014. Ubiquibodies, Synthetic E3 Ubiquitin Ligases Endowed with Unnatural Substrate Specificity for Targeted Protein Silencing. *Journal of Biological Chemistry* 289:7844–7855.

Qin N., D'Andrea MR., Lubin M-L., Shafaee N., Codd EE., Correa AM. 2003. Molecular cloning and functional expression of the human sodium channel beta1B subunit, a novel splicing variant of the beta1 subunit. *The Federation of European Biochemical Societies Journal* 270:4762–4770.

Racine RJ. 1972. Modification of seizure activity by electrical stimulation. II. Motor seizure. *Electroencephalography and clinical neurophysiology* 32:281–94.

Raman IM., Bean BP. 1997. Resurgent sodium current and action potential formation in dissociated cerebellar Purkinje neurons. *The Journal of neuroscience : the official journal of the Society for Neuroscience* 17:4517–4526.

Ratcliffe CF., Qu Y., McCormick K a., Tibbs VC., Dixon JE., Scheuer T., Catterall W a. 2000. A sodium channel signaling complex: modulation by associated receptor protein tyrosine phosphatase beta. *Nature neuroscience* 3:437–44.

Ratcliffe CF., Westenbroek RE., Curtis R., Catterall WA. 2001. Sodium channel beta1 and beta3 subunits associate with neurofascin through their extracellular immunoglobulin-like domain. *The Journal of cell biology* 154:427–34.

Recio-Pinto E., Thornhill WB., Duch DS., Levinson SR., Urban BW. 1990. Neuraminidase treatment modifies the function of electroplax sodium channels in planar lipid bilayers. *Neuron* 5:675–84.

Reid C a., Leaw B., Richards KL., Richardson R., Wimmer V., Yu C., Hill-Yardin EL., Lerche H., Scheffer IE., Berkovic SF. et al. 2014. Reduced dendritic arborization and hyperexcitability of pyramidal neurons in a Scn1b-based model of Dravet syndrome. *Brain : a journal of neurology* 137:1701–15.

Riuró H., Beltran-Alvarez P., Tarradas A., Selga E., Campuzano O., Vergés M., Pagans S., Iglesias A., Brugada J., Brugada P. et al. 2013. A Missense Mutation in the Sodium Channel β2 Subunit Reveals SCN2B as a New Candidate Gene for

Brugada Syndrome. *Human Mutation* 34:961–966.

Roberts RH., Barchi RL. 1987. The voltage-sensitive sodium channel from rabbit skeletal muscle. Chemical characterization of subunits. *The Journal of biological chemistry* 262:2298–303.

Roger S., Rollin J., Barascu A., Besson P., Raynal P-I., Iochmann S., Lei M., Bougnoux P., Gruel Y., Le Guennec J-Y. 2007. Voltage-gated sodium channels potentiate the invasive capacities of human non-small-cell lung cancer cell lines. *The international journal of biochemistry & cell biology* 39:774–786.

Rohl CA., Boeckman FA., Baker C., Scheuer T., Catterall WA., Klevit RE. 1999. Solution structure of the sodium channel inactivation gate. *Biochemistry* 38:855–861.

Rosker C., Lohberger B., Hofer D., Steinecker B., Quasthoff S., Schreibmayer W. 2007. The TTX metabolite 4, 9-anhydro-TTX is a highly specific blocker of the Nav1. 6 voltage-dependent sodium channel. *American Journal of Cell Physiology* 293:783–789.

Rusconi R., Scalmani P., Cassulini RR., Giunti G., Gambardella A., Franceschetti S., Annesi G., Wanke E., Mantegazza M. 2007. Modulatory proteins can rescue a trafficking defective epileptogenic Nav1.1 Na+ channel mutant. *The Journal of neuroscience : the official journal of the Society for Neuroscience* 27:11037–46.

Scheffer IE., Harkin LA., Grinton BE., Dibbens LM., Turner SJ., Zielinski MA., Xu R., Jackson G., Adams J., Connellan M. et al. 2007. Temporal lobe epilepsy and GEFS+ phenotypes associated with SCN1B mutations. *Brain : a journal of neurology* 130:100–9.

Scheffer IE., Berkovic SF. 1997. Generalized epilepsy with febrile seizures plus. A genetic disorder with heterogeneous clinical phenotypes. *Brain* 120 (Pt 3):479–490.

Schmidt J., Rossie S., Catterall W a. 1985. A large intracellular pool of inactive Na channel alpha subunits in developing rat brain. *Proceedings of the National Academy of Sciences of the United States of America* 82:4847–51.

Schmidt JW., Catterall WA. 1986. Biosynthesis and processing of the alpha subunit of the voltage-sensitive sodium channel in rat brain neurons. *Cell* 46:437–444.

Schrey M., Codina C., Kraft R., Beetz C., Kal R., Stefan W., Patt S. 2002. Molecular characterization of voltage-gated sodium channels in human gliomas. 13:20–25.

Shi X., Yasumoto S., Kurahashi H., Nakagawa E., Fukasawa T., Uchiya S., Hirose S. 2012. Clinical spectrum of SCN2A mutations. *Brain and Development* 34:541–545.

Singh R., Scheffer IE., Crossland K., Berkovic SF. 1999. Generalized epilepsy with febrile seizures plus: a common childhood-onset genetic epilepsy syndrome. *Annals of Neurology* 45:75–81.

Siva N. 2015. UK gears up to decode 100 000 genomes from NHS patients. *The Lancet* 385:103–104.

Steinlein OK. 2014. *Mechanisms underlying epilepsies associated with sodium channel mutations*. Elsevier B.V.

Stevens M., Peigneur S., Tytgat J. 2011. Neurotoxins and their binding areas on voltage-gated sodium channels. *Frontiers in pharmacology* 2:71.

Stocker PJ., Bennett ES. 2006. Differential sialylation modulates voltage-gated Na+ channel gating throughout the developing myocardium. *The Journal of general physiology* 127:253–65.

Takahashi K., Tanabe K., Ohnuki M., Narita M., Ichisaka T., Tomoda K., Yamanaka S. 2007. Induction of Pluripotent Stem Cells from Adult Human Fibroblasts by Defined Factors. *Cell* 131:861–872.

Tammaro P., Conti F., Moran O. 2002. Modulation of sodium current in mammalian cells by an epilepsy-correlated beta 1-subunit mutation. *Biochemical and biophysical research communications* 291:1095–101.

Tasaki I., Singer I., Watanabe a. 1965. Excitation of internally perfused squid giant axons in sodium-free media. *Proceedings of the National Academy of Sciences of the United States of America* 54:763–769.

Tasaki I., Singer I., Watanabe a. 1966. Excitation of squid giant axons in sodium-free external media. *The American journal of physiology* 211:746–754.

Tasaki I., Singer I. 1966. Membrane macromolecules and nerve excitability: a physico-chemical interpretation of excitation in squid giant axons. *Annals of the New York Academy of Sciences* 137:792–806.

Terlau H., Heinemann SH., Stühmer W., Pusch M., Conti F., Imoto K., Numa S. 1991. Mapping the site of block by tetrodotoxin and saxitoxin of sodium channel II. *FEBS Letters* 293:93–96.

Theile JW., Cummins TR. 2011. Recent developments regarding voltage-gated sodium channel blockers for the treatment of inherited and acquired neuropathic pain syndromes. *Frontiers in pharmacology* 2:54.

Tyrrell L., Renganathan M., Dib-Hajj SD., Waxman SG. 2001. Glycosylation alters steady-state inactivation of sodium channel Nav1.9/NaN in dorsal root ganglion neurons and is developmentally regulated. *The Journal of neuroscience : the official journal of the Society for Neuroscience* 21:9629–37.

Uebachs M., Opitz T., Royeck M., Dickhof G., Horstmann M-T., Isom LL., Beck H. 2010. Efficacy loss of the anticonvulsant carbamazepine in mice lacking sodium channel beta subunits via paradoxical effects on persistent sodium currents. *The Journal of neuroscience : the official journal of the Society for Neuroscience* 30:8489–501.

Vargas E., Yarov-Yarovoy V., Khalili-Araghi F., Catterall W a., Klein ML., Tarek M., Lindahl E., Schulten K., Perozo E., Bezanilla F. et al. 2012. An emerging consensus on voltage-dependent gating from computational modeling and molecular dynamics simulations. *The Journal of general physiology* 140:587–94.

Vassilev PM., Scheuer T., Catterall WA. 1988. Identification of an intracellular peptide

segment involved in sodium channel inactivation. *Science (New York, N.Y.)* 241:1658–61.

Vassilev P., Scheuer T., Catterall WA. 1989. Inhibition of inactivation of single sodium channels by a site-directed antibody. *Proceedings of the National Academy of Sciences* 86:8147–8151.

Wagnon JL., Meisler MH. 2015. Recurrent and Non-Recurrent Mutations of SCN8A in Epileptic Encephalopathy. *Frontiers in Neurology* 6:1–7.

Wallace RH., Wang DW., Singh R., Scheffer IE., George AL., Phillips HA., Saar K., Reis A., Johnson EW., Sutherland GR. et al. 1998. Febrile seizures and generalized epilepsy associated with a mutation in the Na+-channel beta1 subunit gene SCN1B. *Nature genetics* 19:366–70.

Wallace RH., Scheffer IE., Parasivam G., Barnett S., Wallace GB., Sutherland GR., Berkovic SF., Mulley JC. 2002. Generalized epilepsy with febrile seizures plus: mutation of the sodium channel subunit SCN1B. *Neurology* 58:1426–1429.

West JW., Patton DE., Scheuer T., Wang Y., Goldin AL., Catterall WA. 1992. A cluster of hydrophobic amino acid residues required for fast Na(+)-channel inactivation. *Proceedings of the National Academy of Sciences* 89:10910–10914.

Wimmer VC., Reid CA., Mitchell S., Richards KL., Scaf BB., Leaw BT., Hill EL., Royeck M., Horstmann M., Cromer BA. et al. 2010. Axon initial segment dysfunction in a mouse model of genetic epilepsy with febrile seizures plus. *The Journal of clinical investigation* 120:2661–71.

Wimmer VC., Harty RC., Richards KL., Phillips a M., Miyazaki H., Nukina N., Petrou S. 2015. Sodium channel β1 subunit localizes to axon initial segments of excitatory and inhibitory neurons and shows regional heterogeneity in mouse brain. *The Journal of comparative neurology* 523:814–30.

Wong H-K., Sakurai T., Oyama F., Kaneko K., Wada K., Miyazaki H., Kurosawa M., De Strooper B., Saftig P., Nukina N. 2005. beta Subunits of voltage-gated sodium channels are novel substrates of beta-site amyloid precursor protein-cleaving enzyme (BACE1) and gamma-secretase. *The Journal of biological chemistry* 280:23009–17.

Xiao ZC., Ragsdale DS., Malhotra JD., Mattei LN., Braun PE., Schachner M., Isom LL. 1999. Tenascin-R is a functional modulator of sodium channel β subunits. *Journal of Biological Chemistry* 274:26511–26517.

Xiao Y., Blumenthal K., Cummins TR., Sciences B. 2014. Gating pore currents demonstrate selective and specific modulation of individual sodium channel voltage sensors by biological toxins. *Molecular pharmacology* 46202:159–167.

Yang M., Kozminski DJ., Wold L a., Modak R., Calhoun JD., Isom LL., Brackenbury WJ. 2012. Therapeutic potential for phenytoin: Targeting Nav1.5 sodium channels to reduce migration and invasion in metastatic breast cancer. *Breast Cancer Research and Treatment* 134:603–615.

Yang D., Xu J., Zhu T., Fan J., Lai L., Zhang J., Chen YE. 2014a. Effective gene targeting in rabbits using RNA-guided Cas9 nucleases. *Journal of Molecular Cell Biology* 6:97–99.

Yang H., Wang H., Jaenisch R. 2014b. Generating genetically modified mice using CRISPR/Cas-mediated genome engineering. *Nature Protocols* 9:1956–1968.

Yereddi NR., Cusdin FS., Namadurai S., Packman LC., Monie TP., Slavny P., Clare JJ., Powell AJ., Jackson AP. 2013. The immunoglobulin domain of the sodium channel β3 subunit contains a surface-localized disulfide bond that is required for homophilic binding. *FASEB Journal* 27:568–580.

Yu FH., Westenbroek RE., Silos-Santiago I., McCormick KA., Lawson D., Ge P., Ferriera H., Lilly J., DiStefano PS., Catterall WA. et al. 2003. Sodium channel beta4, a new disulfide-linked auxiliary subunit with similarity to beta2. *The Journal of neuroscience : the official journal of the Society for Neuroscience* 23:7577–7585.

Yu FH., Mantegazza M., Westenbroek RE., Robbins C a., Kalume F., Burton K a., Spain WJ., McKnight GS., Scheuer T., Catterall W a. 2006. Reduced sodium current in GABAergic interneurons in a mouse model of severe myoclonic epilepsy in infancy. *Nature neuroscience* 9:1142–9.

Zhang Y., Hartmann HA., Satin J. 1999. Glycosylation influences voltage-dependent gating of cardiac and skeletal muscle sodium channels. *The Journal of membrane biology* 171:195–207.

Zhang X., Ren W., DeCaen P., Yan C., Tao X., Tang L., Wang J., Hasegawa K., Kumasaka T., He J. et al. 2012. Crystal structure of an orthologue of the NaChBac voltage-gated sodium channel. *Nature* 486:130–134.

Zhang M-M., Wilson MJ., Azam L., Gajewiak J., Rivier JE., Bulaj G., Olivera BM., Yoshikami D. 2013. Co-expression of Na(V)β subunits alters the kinetics of inhibition of voltage-gated sodium channels by pore-blocking μ-conotoxins. *British journal of pharmacology* 168:1597–610.

Zhang Y., Kecskés A., Copmans D., Langlois M., Crawford AD., Ceulemans B., Lagae L., de Witte P a. M., Esguerra C V. 2015. Pharmacological Characterization of an Antisense Knockdown Zebrafish Model of Dravet Syndrome: Inhibition of Epileptic Seizures by the Serotonin Agonist Fenfluramine. *Plos One* 10:e0125898.